BOSE CONDENSATES AND THE ATOM LASER

by

MICHAEL R. ANDREWS

B.S., The University at Stony Brook, New York (December 1992)

SUBMITTED TO THE DEPARTMENT OF PHYSICS
IN PARTIAL FULFILLMENT OF THE REQUIREMENTS FOR THE DEGREE
OF

DOCTOR OF PHILOSOPHY

at the

MASSACHUSETTS INSTITUTE OF TECHNOLOGY

June 1998

Author .....
Department of Physics
April, 1998

Certified by .....
Wolfgang Ketterle
Professor of Physics
Thesis Supervisor

Accepted by .....
Thomas J. Greytak
Associate Department Head for Education

Bose Condensates and the Atom Laser

by

Michael R. Andrews

Submitted to the Department of Physics
April, 1998, in partial fulfillment of the
requirements for the degree of
Doctor of Philosophy

Abstract

In this thesis, I describe four classes of studies of cold, dilute vapors of atomic sodium. The in-situ nondestructive observation of a Bose condensate is presented in the broader context of imaging a cold polarized cloud. Two condensates were made to interfere, and a rudimentary "atom laser" was demonstrated. Excitations of a condensate were imaged in-situ and nondestructively, opening up the field of real-time dynamical studies. A related study attempting (unsuccessfully) to create and detect superfluid currents and vortices is discussed. Lastly, Feshbach resonances were used to modify the interactions in a Bose condensate, and the scattering length was observed to vary by over a factor of ten.

Thesis Supervisor: Wolfgang Ketterle
Title: Professor of Physics

Acknowledgments

What a person thinks on his own, without being stimulated by the thoughts and experiences of other people, is even in the best case rather paltry and monotonous. — ALBERT EINSTEIN 1879–1955

MIT was an excellent experience, and I feel fortunate to have made the admissions cut, and thereafter, fortunate to have made it into a good research group headed up by a fantastic all-around scientist. I thank the whole bunch of students, professionals, and others who worked here over the years, helping to make this work possible. Particularly helpful were physicists in other groups here (Pritchard's and Kleppner's) who always seemed eager to generously share their expertise and equipment; MIT is lucky that together you are too numerous to name individually. Thanks to Wolfgang, Ken, Marc, and Mike for being especially formative and positive influences, and to Carol for being a great support person. Thanks to Gerry for his top-notch attention too. My best regards, however, go to Wolfgang's crew: you're each quite an impressive individual and I'm definitely glad to have gotten to know you. Let's keep in touch! I can testify to the first-class efforts of my collaborators Ananth, Klaasjan, Dallin, Shin, Dan, Hans, Chris, and Jörn, and I thank them for their indispensable contributions to the topic of this thesis. Thanks also to Roberto for a critical reading.

For me Cambridge was a home away from home since at the end of every day I returned either to Boston (1993–1994) or Brookline (1994–1998) across the Charles. Genya, who also lives on the other side of the river, is due much thanks for being a great friend over many years. Thanks to my family Tom and Zelda (parents), Peter (brother), Sylvia and David (grandparents), and my friends for their support, interest, advice, and encouragement. Out of everyone I would have to say that the most important source of my enthusiasm for physics comes from Tom, my father and fellow physicist. He impressed upon me from an early age that everything has a rational physical explanation, and that it's got to be simple.

Contents

List of Figures

List of Tables

Chapter 1

Introduction

Bose condensation is a nexus of physics, having overlap not only with atomic physics, but also with the disparate fields of condensed matter physics, nuclear physics, elementary particles, and astrophysics [1]. The multiple announcements of Bose condensation in dilute atomic alkali vapors in 1995 [2, 3, 4] opened up a whole new era for the field in terms of interest and activity. In contrast to superfluid helium and superconductors, these new atomic condensates are model systems whose properties are regarded as understandable from first principles. Other types of condensates have properties complicated by interactions or their environments and thus are understood rather more phenomenologically than fundamentally.

The history of Bose condensation encompasses low temperature physics, superfluidity, superconductivity, fundamental issues in quantum mechanics, and even laser physics. In addition to perusing reference [1], see also reference [5] and references therein for a recent review of the field. In the next few paragraphs there will be a broad overview of developments in atomic Bose condensate physics.

Thermodynamic properties of atomic condensates were among the first to be studied (see references [6, 7], generally); the condensate fraction, the interaction energy, and the specific heat were found to be in agreement with theory. In contrast to superfluid helium, here the interactions were found not to significantly affect the transition temperature or to 'deplete' the condensate; a single-particle wavefunction (equation (C.1)) describes important aspects of the system. Many experiments have verified that interactions between atoms of a condensate can be understood from first principles; the system is quite dilute from a theoretical perspective. The shape of the ground state and elementary excitations are accurately predicted by a mean-field interaction theory, and pulses of sound were observed to travel across a condensate [8, (5.1)][1]. Condensates consisting of attractive atoms [10] have confirmed predictions of metastability. Dissipation, which always seems

[1] Explicit references to publications copied into the thesis appear, for instance, as [9, (4.3)], indicating that reference [9] is to be found photocopied into section (4.3).

to be present, is still an open area of investigation.

The coherence properties of condensates are beginning to be uncovered [11, 12]. Although its existence was expected, a coherent quantum phase (relative phase) revealed itself through the interference of two condensates [9, (4.3)]. And even though the formation of a condensate requires it, the bosonic stimulation of millions of particles all into the same state has been observed to occur [13]. Coherences between pairs, triplets, and other combinations of particles are also important and have been shown to exhibit nature's disregard for individual identities in a condensate; separate bosons in a condensate are subsumed within a single matter wave. This completes the picture and all the elements are there to call a beam of condensed atoms a rudimentary 'atom laser'.

Many new groups are entering the field right now with their own Bose condensates, and there are still many interesting subjects to study. Indeed, Bose condensates and atom lasers are regarded to naturally become work-horses for atomic physics in the next decade, just as laser-cooled gases and atomic beams were in the last one and will undoubtedly continue to be so in the future.

The work described in this thesis began after developments in laser cooling. It started with efforts to evaporatively cool sodium in 1993 [14], and spans the period until 1998 when Feshbach resonances were used to manipulate the interactions within a Bose condensate [15, (6.1)]. In the intervening time, properties of cold clouds and condensates were studied, and various tools were developed. The incorporated publications (references [16, (3.5)], [9, (4.3)], [8, (5.1)], and [15, (6.1)]) constitute the backbone of this thesis, whereas the rest of the text is to provide additional material and discuss issues and details of particular relevance. The reader is encouraged to read these included publications, rather than to concentrate only on the text of the thesis alone.

The following itemization broadly indicates the contents of chapters to follow. The presentation is somewhat chronological, and parallels the history of the group at MIT which is where this thesis work was done over the last five years in collaboration with others.

- The topic of chapter 2 is the preparation and manipulation of ultracold atoms. Their preparation begins with atoms in an oven and finishes with atoms in a Bose condensate, a reduction in temperature by a factor of a billion. The first step is laser cooling, followed by evaporation in a magnetic trap [14] (thesis work of K. Davis [17] and M. Joffe [18]). Issues relating to magnetic trapping will be discussed here. Optical dipole potentials (focused far-detuned laser beams) have also been used for trapping and manipulating atoms. The insensitivity of optical dipole forces to sodium's hyperfine structure was key for the study of Feshbach resonances (chapter 6) in condensates that were optically trapped in strong-field seeking states [15, (6.1)].

- Chapter 3 is devoted to imaging. All data about ultracold clouds of sodium have so far been obtained through images, and the basic effect is the scattering of light as it propagates through matter. The evaporative cooling of sodium [14] and later, the nondestructive in-

situ observation of a condensate [16, (3.5)], particularly showed how images of clouds provide important information.

- Chapter 4 is devoted to the concept of the 'atom laser', so far rudimentarily realized. Essential to this realization was the demonstration of interference between two condensates [9, (4.3)], and the technique of splitting a coherent matter wave with an 'output coupler' [19] (thesis work of M.-O. Mewes [20]). Later, the observation of bosonic stimulation as an important feature in condensate formation gave additional support to the identification of a Bose condensate as a coherent matter wave [13]. As in an optical laser, stimulated, or 'amplified' processes result in a large population of particles in a single quantum state.

- Dynamical phenomena of ultracold and condensed clouds is the topic of chapter 5. Localized pulses of 'zero sound' were observed to propagate across a condensate [8, (5.1)], and other types of excitations were studied in references [21] (thesis work of M.-O. Mewes [20]) and [22]. An exploratory (and so far unsuccessful) study of vortices and superfluidity will also be discussed.

- The observation of Feshbach resonances [15, (6.1)] is presented in chapter 6. These resonances show that it is possible to vary atomic interactions in a condensate.

Chapter 2

Making and manipulating cold atoms

The topic of this chapter will be the preparation and manipulation of ultracold atoms. The preparation of ultracold atoms begins with atoms in an oven and finishes with atoms in a Bose condensate, a reduction in temperature by a factor of a billion. The first step is laser cooling, followed by evaporation in a magnetic trap [14]. The kinds of traps used so far have been varied. The spherical quadrupole field was first used to demonstrate evaporation, and later was 'optically plugged' to achieve Bose condensation [3]. Thereafter, the 'cloverleaf' magnetic trap [23] was used in the production of condensates for a variety of studies to be discussed in later chapters. Beginning with the optically plugged trap, forces arising from focused laser light were used to mechanically manipulate ultracold matter. Green light was used to produce pairs of condensates that could later interfere [9, (4.3)], and also to create excitations for the study of sound [8, (5.1)]. Infrared light was used to trap atoms outright [24]. The insensitivity of dipole forces to sodium's hyperfine structure was key for the study of Feshbach resonances [15, (6.1)] in condensates that were optically trapped and in strong-field seeking states.

2.1 Cooling towards condensation

The techniques used to cool atoms will be briefly reviewed here. Generally speaking, if the final temperature is low enough a condensate will be present. The criterion for Bose condensation is to have a high enough phase space density $n\Lambda^3$ [25], where n is the number density and Λ is the thermal de Broglie wavelength

$$\Lambda = \left(\frac{2\pi\hbar^2}{mk_BT}\right)^{1/2}, \tag{2.1}$$

where m is the mass of bosons at a temperature T. Specifically, the phase space density must be equal to or greater than

$$n\Lambda^3 = \sum_{s=1}^{\infty} \frac{1}{s^{3/2}} = \zeta_{3/2} \approx 2.612375. \tag{2.2}$$

Phase space density can be usefully thought of as a measure of the occupancy of the lowest quantum state. For example, atmospheric nitrogen has a phase space density of about a part per million [26] and is therefore far from Bose condensing. See appendix B for more details concerning the criteria for condensation.

Atoms are cooled in stages after they emerge in a collimated beam from an oven. The beam is first slowed by bombarding it with resonant photons in a Zeeman slower, and then caught in a magneto-optical 'dark-spot' trap [27] where the number of accumulated atoms saturates in a few seconds. The atoms are then briefly cooled with optical molasses before being transferred to a magnetic trap. At this point right after laser cooling, the phase space density is about six orders of magnitude too small for Bose condensation, which is coincidentally similar to atmospheric nitrogen. The temperature is about 100 μK and the density is about 5×10^{10} cm^{-3}. The final condensation temperature is roughly 100 times lower and the density is over a thousand times higher. See reference [14] for more details.

Laser cooling becomes more difficult as the phase-space density increases because of combined limitations on density (opacity) and temperature (photon recoil). For instance, at low temperature, the energy-momentum conserving recoil from scattered photons heats the cloud at a level comparable to the degree of cooling. This gives a lower limit to attainable temperatures. The cloud also begins to become optically thick, which impedes photons from reaching atoms. These limits are linked through the size of the cloud d and the optical wavelength λ. Assuming that the resonant optical density should be less than unity gives $n\sigma d < 1$, where the resonant cross-section $\sigma = 3\lambda^2/2\pi$ and n is the atomic density. Assuming that the temperature must be greater than a photon recoil gives $k_B T > \hbar^2 k^2/2m$, where $k = 2\pi/\lambda$. Substituting these limits for density and temperature into equation (2.1) then gives a limiting phase space density that scales approximately as λ/d. Even for the dark-spot type of trap where the resonant optical density can be a hundred times higher, such clouds are still far away from Bose condensing without even considering that temperatures are typically limited to many photon recoils and not just a single one. Other cooling techniques, such as 'dark state' and Raman cooling, are governed by different criteria by modification of the assumptions made above. Dark state cooling relies on a stochastic process to populate a zero-momentum state that does not interact with the light, and Raman cooling can effectively lower the Doppler limit by making use of the narrower linewidth of a Raman transition. These techniques are practically more difficult to implement, and still do not reach high enough phase space densities (see reference [14] and refs. therein). Thus, it is natural to switch to a cooling technique that doesn't use light at all.

Evaporation is a technique that doesn't use light, and works by removing the highest energy atoms while the remaining ones rethermalize to higher phase space density. For efficient evaporative cooling, the ratio of rethermalizing elastic collisions ('good collisions') to collisions that lead to trap loss ('bad collisions') has to be large. The tool that enables atoms to be selected in evaporative cooling is radio-frequency (rf) resonance in a magnetic trap, which will be discussed in the next paragraph.

The transfer of laser-cooled atoms to the magnetic trap consists in turning off all the lasers and simultaneously turning on the magnetic fields. Since the trap is turned on suddenly, the strength of the potential (determined by the currents in the trapping coils) is chosen so as to confine the atoms without compressing them or allowing them to expand further. This keeps any increase of entropy to a minimum [20]. Once in the magnetic trap, rf evaporation begins and atoms near the 'surface' of the cloud are spin-flipped to untrapped states. This type of spin-flipping is also called 'electron spin resonance'. The surface atoms are the ones carrying more than the average thermal energy (potential energy in the form of a Zeeman shift in a magnetic field), and so their loss reduces the temperature once rethermalization by elastic collisions takes place. As the cloud cools, the rf is lowered and progressively lower energy atoms are removed. Evaporation proceeds continuously until the cloud reaches the final temperature needed for a particular experiment. The studies in this thesis were primarily concerned with condensates at the lowest attainable temperatures (zero-temperature limit).

2.2 Magnetic trapping

Magnetic trapping is one of the major techniques used for producing Bose condensates, and so the subject is worth some discussion on its own. In this section the principles of magnetic trapping will be laid out, and some of the important issues will be presented. Since magnetic traps provide the environment for atoms being evaporated with rf radiation, the type of trap can directly influence the efficiency of cooling. The design and operation of magnetic traps involve various considerations, technical and otherwise, which will also be discussed.

Sodium atoms in the ground state have a magnetic moment arising from their spinning valence electron, which allows them to be trapped at a spatial minimum of a magnetic field. The trapping forces arise from the energy of a magnetic moment μ in a magnetic field B (both vectors), in the form $V = -\mu \cdot B$. Classically, a spinning magnetic dipole can be trapped if its moment is oriented anti-parallel to the external field. This is the principle behind the Levitron (trademark) device, available commercially as a toy. Without spinning, a magnetic moment is attracted to the strongest field and ultimately, its south pole will find and attach itself to the external magnet's north pole (north/south), or the other way around (south/north). By spinning, however, the orientation of

the magnetic moment can precess about the external field and be gyroscopically stabilized in the 'north/north' relative orientation. In this orientation, the moment is repelled from regions of high field. If the field is large enough, the orientation of the moment can adiabatically follow as it orbits in space [17].

Magnetic traps can only provide a local minimum of the field in free space, and not a maximum. This is because of one of Maxwell's equations, stating that $\nabla \cdot B = 0$. Thus, strong-field seeking states can not be trapped this way, a limitation removed by the introduction of the optical trap as discussed later in section (2.3). The disadvantage to trapping a weak-field seeking state (for an atom with hyperfine structure) is that it can not be the true ground state. The true ground state for such an atom must be strong-field seeking since its energy decreases with the applied field. In particular, one major disadvantage to trapping weak-field seekers is that after inelastic collisions it is sometimes possible for atoms to change their spin orientations and become untrapped. This reaction is made possible by the excess groundstate energy. The weak-field seeking state that was magnetically trapped throughout this thesis work was the $|F = 1, m_F = -1\rangle$ hyperfine ground state of sodium, mainly because it is the one produced in laser cooling.

Tight confinement of atoms is important for efficient evaporative cooling because it results in higher densities. The higher the density, the higher the collisional rethermalization rate (the collision rate scales with density $\times$ velocity), and thus the faster evaporation can proceed and the less important loss processes become for the cloud. Another criterion for efficient cooling is that as the cloud cools, the density should correspondingly increase to keep the rethermalization rate constant or increasing. This is called 'runaway' evaporative cooling. A tight trap is also important for holding atoms against the pull of gravity. These several considerations lead one to desire a configuration of coils producing a gradient of the field about the minimum. For a given set of coils and electrical currents, a gradient field is the most effective in these regards.

The main advantage of a linear trap is how the cloud behaves as it cools. In a linear trap, a cloud's size shrinks in proportion to the temperature and inversely with the gradient. In an harmonic trap, on the other hand, as the cloud cools its size only shrinks in proportion to the square root of the temperature. Thus, for the same temperature decrease the density increases much more in a linear trap, and so does the collision rate. This leads to the evaporation process reaching and remaining in the runaway regime in reference [14] and thereafter in later studies.

The spherical quadrupole trap, in particular, produces a field linear about a zero located at the center. This trap gives strong confinement and is ideal for evaporation up to a point: losses due to the zero of the magnetic field increase as the cloud cools. Atoms that orbit through a region of small field are less able to follow the field orientation adiabatically and can thus become neutral or strong-field seeking instead [17]. Unfortunately, as the cloud cools it shrinks towards this low-field region. This effect of accelerating losses limited the increase in phase space density in reference [14]

to a factor of 190, instead of the factor of about a million needed for Bose condensation after laser cooling. This gives a practical lower limit to temperatures in the spherical quadrupole trap.

By preventing atoms from entering regions of small field, further cooling was enabled and led to the formation of a Bose condensate [3]. The 'optical plug' of focused green laser light which was used for this purpose will be discussed in section (2.3). Also to be discussed there will (mainly) be the use of such light in general for the manipulation of ultracold matter. This will then naturally lead into a discussion on the use of infrared light for trapping atoms without the use of magnetic fields [24].

Currently, Bose condensates are produced in the cloverleaf trap which has a finite bias field [23]. Unlike the spherical quadrupole trap, the cloverleaf trap has no lower limit on the temperature of clouds it can hold. Whereas clouds in the spherical quadrupole trap are oblate spheroids (pancakes) with a fixed aspect ratio of two, clouds in the cloverleaf trap are prolate spheroids (cigars) with a variable aspect ratio typically much greater than one. In the two radial dimensions the cloverleaf trap has strong linear confinement and in the third axial dimension the confinement is weaker and harmonic.

2.2.1 Field optimization

To engineer a strong trap there are several considerations that must be made. One is that the current-carrying elements should be as close as possible to the atoms because magnetic fields decay over space. Another is to optimize the fields while minimizing the resources used. One very important resource is three-dimensional space. Other resources are high current power supplies, the right size wire, and a means of cooling resistive heating. Water is regarded as an excellent coolant because of its easy availability, its convenience in handling, and its high specific heat (as liquid water, not as steam).

To optimize a magnetic trap, one looks at the fields produced in terms of currents:

$$B(r) = \frac{\mu_0}{4\pi} \int \frac{J(r') \times (r - r')}{(r - r')^3} \, d^3r'. \tag{2.3}$$

The spherical quadrupole trap is a 'linear' trap, whereas the cloverleaf trap is linear in two dimensions and has curvature along the third. Thus, one can generally look for either the strongest gradients or curvatures, which are proportional to the coefficients of the power series expansion of the field around its minimum.

For a distance A on axis away from a coil of radius R, the power series expansion for the axial (z) and radial (ρ) field components are [28]:

$$B_z = \left[1 + b_1 z + b_2(z^2 - p^2/2)\right] b_0 \tag{2.4}$$

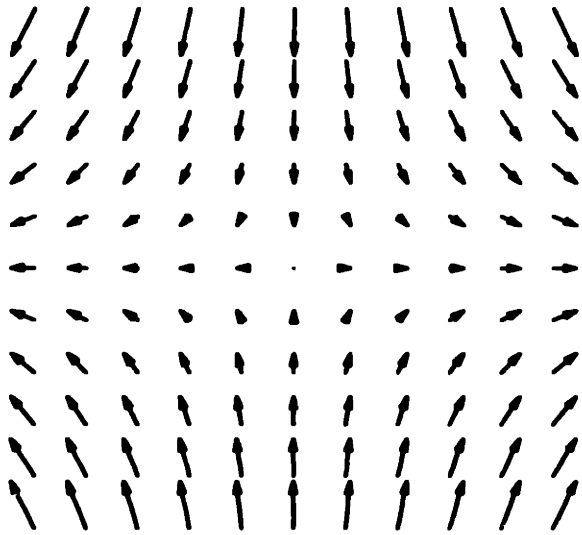

Figure 2-1: Vector structure of spherical quadrupole trap. Shown is the projection of field vectors in the plane having the axis vertically in the center; the coils are at the top and bottom of the image. The atoms are trapped in the central region where the bias fields cancel and the magnitude of the field is smallest.

$$B_p = -[b_1\rho/2 + b_2\rho z]\, b_0 \tag{2.5}$$

where

$$b_0 = \frac{\mu_0 I R^2}{2(A^2+R^2)^{3/2}} \quad \text{(bias)} \tag{2.6}$$

$$b_1 = \frac{3A}{A^2+R^2} \quad \text{(gradient)} \tag{2.7}$$

$$b_2 = \frac{3(4A^2-R^2)}{2(A^2+R^2)^2} \quad \text{(curvature).} \tag{2.8}$$

$\mu_0 = 4\pi/10$ gauss · cm/ampere, or numerically about 5/4 to 1% accuracy using these units. Note that these equations are only for the fields of single coils close to the axis. Further considerations are required for the cloverleaf coil which uses off-axis fields.

A spherical quadrupole trap consists of two coils on axis with opposite-flowing currents. The atoms are trapped at the midway-point between the coils where the bias fields (b_0) from the two coils cancel while the gradient fields ($b_1 \times b_0$) add constructively. The field structure of the spherical quadrupole trap is of the form $\pm B'(x, y, -2z)$ with a gradient B', and is shown in figure (2-1). Since the atoms respond mainly to the magnitude of the field (aside from adiabatically following the vector as they orbit), the potential for atoms is $B'(x^2 + y^2 + 4z^2)^{1/2}$ and is shown in figure (2-2). This assumes that the Zeeman energy of an atom is linear in the field, which is a good assumption when trapping sodium at low fields.

In making a spherical quadrupole trap one optimizes the gradient in Eqs. (2.4–2.7) by varying the placement of wires in space while staying within the limits of the power supply and cooling

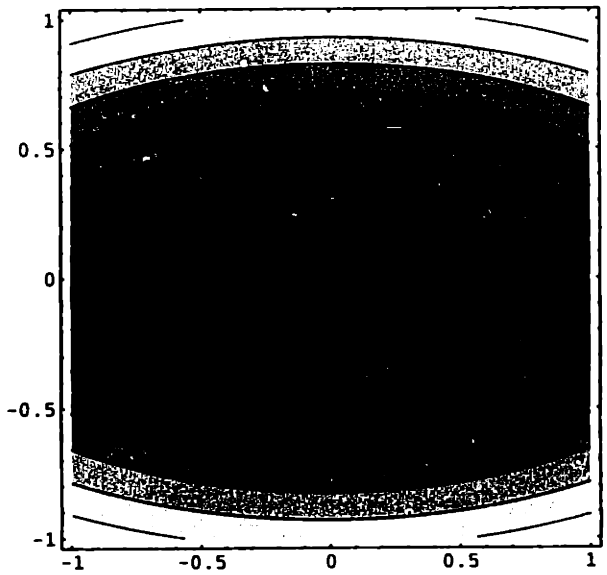

Figure 2-2: Potential in the spherical quadrupole trap. Shown is the potential in the plane having the axis vertically in the center; the coils are at the top and bottom of the image. The atoms are trapped in the central region where the bias fields cancel and the magnitude of the field grows in every direction.

system. Two coils were built, each a matrix of 5 × 7 windings with an inner radius of about 1.4 cm, and separated from each other by about 2.8 cm. Each coil consisted of approximately 5 m of copper refrigerator tubing. Winding the coils was done on a very slow lathe around an aluminum cylinder machined to the desired inner diameter. A custom tool was constructed for a person to hold the copper tubing against the tension without crushing it as the lathe turned. This tool made it possible to hold the tension with one's legs while insulating the tubing being wound with one's hands, or alternately to use one's hands to position the windings in the matrix with a lever. Two specially-built aluminum clamps were positioned on the cylinder to hold the matrix of coils while they were being wound, so that the windings in a lower layer would not spread out on the cylinder as the next layer was tightly wound over it.

Deciding on an insulation material was done with care, since its thickness influences how close the windings can be to one another and thus to the atoms. Kapton polyamide film strips were used for insulation, and were helically wound around the 1/8" copper refrigerator tubing which carried the current. Kapton is thin, withstands hundreds of °C, and is also compatible with ultra-high vacuum.

Even though the coils were compatible with ultra-high vacuum, no gloves were worn to avoid contamination from oils and other materials from the hands. The hands were simply kept clean by washing with Lava-brand soap every hour or oftener; this should come as a relief to most people who take less convenient precautions. Before wrapping with Kapton, the copper tubing was wiped with

a weak (but still dangerous) mixture of acids called 'bright dip' (hydrochloric, sulfuric, nitric) [29] and then with methanol.

The trap was designed to provide 1000 G/cm, and to be driven with a 300 A / 20 V power supply. With about 6 kW power dissipation, forced cooling was essential. The refrigerator tubing allowed chilled water to circulate at nearly 150 pounds per square inch (psi). Flows were measured to be about 120 $\sqrt{p/l}$ ml/min, where the pressure p and length l were measured in psi and meters. This gave about 8 $\sqrt{p/l}$ W of cooling power per °C of the water's rise in temperature, and at full current, the cooling water emerged at nearly boiling temperature. Note that the dependence of the flow on the square-root is common for turbulence.

For the evaporative cooling work, the coils were inside the vacuum system and did not significantly affect the background gas levels. After a number of cycles to atmospheric pressure, however, while at high currents an ion gauge registered a factor of 5–10 rise in pressure above the low 10^{-11} torr levels. All-in-all, having high-current coils within the chamber was inconvenient and currently all coils are outside but still close to the atoms. Recessed ports on a large stainless steel chamber enabled this design. One advantage is that the present chamber has been under vacuum for over two years and the coils (currently the 'cloverleaf' type) are still serviceable. A good bakeout can take at least a man-month including the time to identify leaks and replace all the equipment surrounding the chamber (optics, etc.).

2.3 Optical manipulation and trapping

High intensity gradients of laser light can exert forces on neutral atoms. The oscillating electric field of a light wave induces an oscillating electric dipole moment in the electron cloud of an atom. The closer the laser's frequency is to a resonance of the atom, the larger is the amplitude of the electron's oscillating moment. Below resonance ('red detuned') the oscillating moment is in phase with the laser field, while above resonance ('blue detuned') the oscillating moment is out of phase (180 degree phase shift). Similarly to the principle behind the magnetic trap ($V = -\mu \cdot B$), the optical dipole potential is expressible as $V = -p \cdot E$, where p and E are the oscillating moment and electric field. The oscillating moment is elementary to compute (e.g., reference [30]), and can even be estimated assuming a classical harmonically bound valence electron as $V/\hbar \sim \alpha I/\pi m(\nu^2 - \nu_0^2)$ [17]. Here m is the mass of an electron bound with a resonance frequency ν_0 and driven by an electric field of intensity I and frequency ν ($\alpha \approx 1/137$ is the fine structure constant). The frequency factor $(\nu^2 - \nu_0^2)^{-1}$ varies approximately with the inverse of detuning when close to resonance. Below resonance ($\nu < \nu_0$) the atom is drawn towards higher intensities, whereas above resonance, the atom is repelled from high intensity. The forces due to this effect create a conservative potential field for the atom, either attractive or repulsive. Close to resonance, the atom would scatter light

strongly and be randomly kicked about from the recoil of absorbed and emitted photons; this would correspond to damping in the classical electron oscillator model. Therefore, the choice of laser frequency is a balance between minimizing the heating due to absorption, which decreases as the square of the detuning, and maximizing the strength of the optical force, which increases as the inverse of the detuning. Since red-detuned light draws atoms into the highest intensity, its criterion for minimizing heating is more stringent than for blue-detuned light which pushes atoms towards the lowest intensities.

A single emission line of an argon ion laser at 514 nm (green light) was used to repel atoms. In the first study of Bose condensation at MIT, the so-called 'optically plugged' trap extended the capability of the spherical quadrupole trap towards the low temperature regime. This was done by 'plugging the hole' at the center of the trap caused by the absence of a magnetic bias field at that location. This was discussed previously and is presented in more detail in reference [3]. In that work, 3.5 W of laser power was focussed to a 30 μm beam waist, creating 7 MHz (350 μK) of optical potential energy that repelled atoms from the center of the trap.

The uses of focussed green laser light to manipulate condensates have been varied. Although its first use was as a 'plug', its subsequent uses have largely been to add features to already well-working systems. These 'features' allow one to mechanically manipulate ultracold matter. In the study of interference between two condensates, a focused green laser light sheet of moderate power (tens of mW) was used to create a double well potential in the cloverleaf magnetic trap. At 100 mW power, below about 10 μK two separate clouds formed well before the onset of Bose condensation at about 2 μK [9, (4.3)]. Later, in a study of sound propagation, focussed green laser light was flashed into an existing condensate. The resulting local build-up of density around the laser beam initiated the propagation of a pulse called 'zero sound' [8, (5.1)]. In another study of sound at finite temperatures, a moving sheet of focussed green laser light served either to push a condensed fraction out of the center of the trap, or to modulate the thermal fraction at the periphery of the cloud to study superfluid/normal-fluid interactions [22].

A study looking into the possibility for vortices and persistent currents used green light in a variety of ways. The first use was to mechanically induce rotational motion in a spherical magnetic trap. This beam was envisioned to 'pin' a vortex should one have formed, since the geometry of the combined magnetic and optical potentials was toroidal (see figure (5-2)). Later, a sheet of green light was rotated in a cloud to promote the formation of vortices through 'churning' action. These as-yet unsuccessful attempts will be detailed later in section (5.2).

More recent was the study of Feshbach resonances that used two endcaps of green laser light to hold atoms axially against a repulsive magnetic field curvature [15, (6.1)]. In this case radial confinement was provided by focused infrared laser light, which is the subject of the next paragraphs [24].

A schematic of the optical trap is shown in figure (2-4). A focused beam of infrared laser

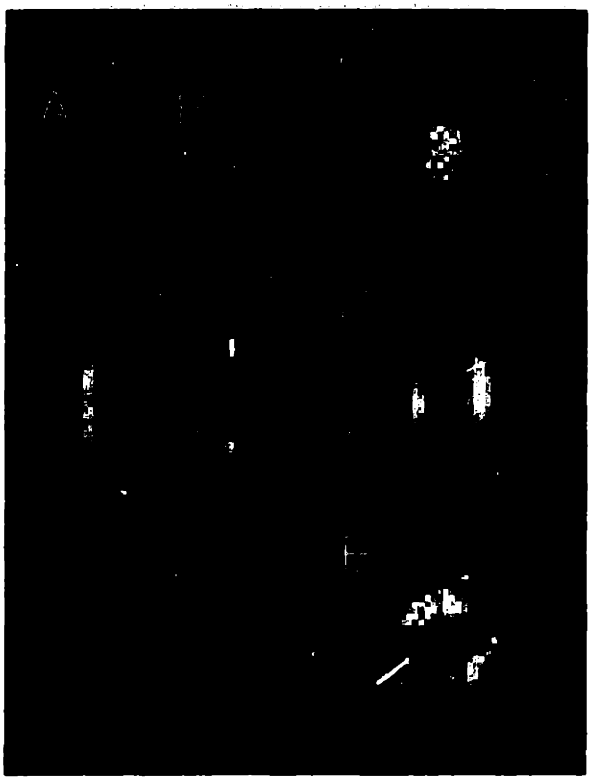

Figure 2-3: A gallery of magnetically trapped clouds. All are in the Thomas-Fermi regime of negligible kinetic energy and large interaction energy. Fig. A shows a condensate in the 'cloverleaf' trap, weakly confined axially ($\sim$ 18 Hz) but strongly confined radially ($\sim$ 250 Hz). Fig. B shows two independent condensates in the same trap but separated by a focused sheet of argon-ion laser light. This light coherently repels atom with the optical dipole force. Fig. C shows a condensate trapped in a cloverleaf trap with large bias field. This cloud is nearly round and about 100 μm wide. Figs. D and E show that same cloud pierced by different geometries of focused argon-ion laser light. (Graphics courtesy of H.-J. Miesner)

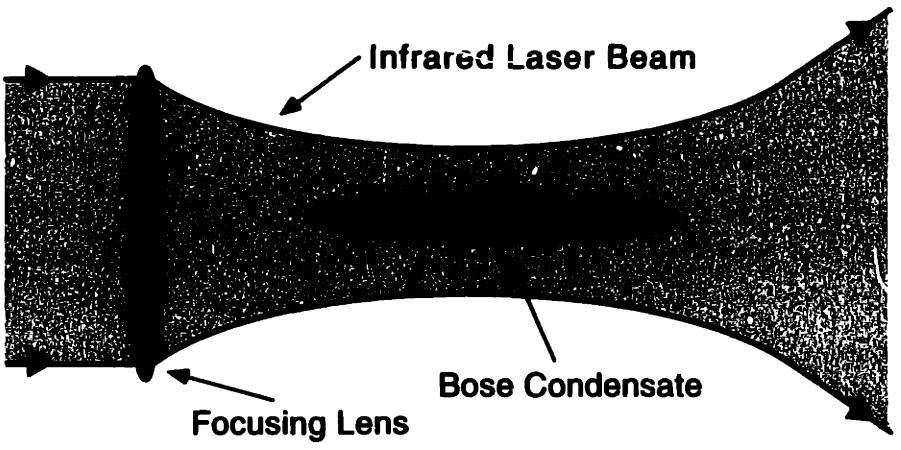

Figure 2-4: Schematic of optical trap. A focused infrared laser beam traps atoms with the optical dipole force.

light draws sodium atoms into the region of highest intensity. On moving away from the focus in any direction, atoms experience a reduction in intensity and are thus trapped. Trapping occurs independently of hyperfine state or magnetic field, which gives added flexibility for the types of experiments that can be performed.

The optical trap was particularly well suited for studying Feshbach resonances. The study of Feshbach resonances required high magnetic fields, which would be difficult to produce while maintaining magnetic trapping. Indeed, the radial trapping frequency in the cloverleaf trap varies inversely with the square root of the bias field. Additionally, Feshbach resonances are predicted for many hyperfine ground states, whereas the magnetic trap is effective for only a subset of all ground states, namely, the weak-field seeking ones. As mentioned, the Feshbach study also integrated the repulsive forces of green laser light. The simultaneous use of two colors illustrates the strength of techniques to manipulate condensates with light. This and more will be discussed further in chapter 6.

The optical trap is described in detail in reference [24], but in the next several paragraphs additional information is given. The basic procedure is to transfer atoms to the optical trap from the magnetic trap. Far less power is needed here than in prior implementations of optical traps because condensates are of such low energy. It is sufficient for the infrared trap to use several mW laser light of 985 nm wavelength to trap ultracold atoms; for a beam waist of 6 μm, the trap depth is given approximately by 1 μK/mW.

The first step in the transfer of atoms to the optical trap is locating the magnetically trapped condensate. An image of atoms in the cloverleaf trap taken from the side shows a round cloud since the long axis is projected into the plane of the image from this vantage point. The next step is to focus the infrared beam to the same point in space as the atoms, using the image on the camera as a guide. Since the image of the condensate is taken with yellow light, the imaging system must be refocused to compensate for chromatic shifts when imaging infrared light. These slight chromatic shifts are present even for so-called 'achromatic' lenses. A test pattern inserted in place of the atoms (using a mirror outside the vacuum chamber) allows one to do this refocusing. The test pattern is illuminated with either yellow or infrared light, depending upon which color is to be imaged properly. There are chromatic shifts for each of the three spatial dimensions.

Astigmatism in the optical trap had to be minimized, since its presence leads to two separated potential minima along the beam. The overriding concern, however, was beam quality in general. For this reason, the laser light was spatially filtered through an optical fiber to achieve close to gaussian beam quality. To address astigmatism directly, each lens in the path of the infrared light was independently tilted, including lenses in the imaging system. The beam was also directed through the centers of all the lenses. Astigmatism was judged negligible when the imaging system was focused along the beam and showed a nearly circular cross-section throughout.

After the infrared beam is aligned, its power is ramped up while an ultracold cloud is in the magnetic trap. The magnetic trap is then suddenly switched off and atoms remain trapped by the infrared beam. Turning off the magnetic trap slowly would be a superior technique, but a more difficult one since large displacements during decompressing would have to be compensated. For now, the slight increase in entropy that results is acceptable.

Chapter 3

Imaging

As pointed out in the introduction, this chapter will be devoted to imaging. All data about ultracold clouds of sodium have so far been obtained through images, and the basic effect is just the scattering of light as it propagates through matter. The evaporative cooling of sodium in reference [14] and later, the nondestructive in-situ observation of a condensate in reference [16, (3.5)], showed how images of clouds provide important information about the system. In particular, the direct observation of a Bose condensate presented a tool that opened up the field for real-time dynamical studies of a spatially condensed system. Previous investigations of Bose condensates, such as those imaging freely expanding clouds [2, 23], established that Bose condensation was an actual phenomenon through observation of a velocity or energy distribution. Atomic Bose condensates form in inhomogeneous potentials, and their direct observation in the trap showed that condensation occurs in space as well as in velocity.

For clouds with a uniform index of refraction throughout (the index describes both absorption and dispersion through a complex number), the atomic density is plainly related to the optical signal in the image. This is usually the case for ultracold clouds, and for instance, was particularly true for clouds in the cloverleaf trap. Images in that trap clearly show shapes in agreement with basic predictions for the distribution of atoms [16, (3.5)]. For clouds with inhomogeneously distributed resonances and polarizations, however, images are more difficult to interpret but still amenable to analysis from the basic principles laid out in this chapter. Difficulties like these were encountered before evaporation in a spherical quadrupole trap [14]. In particular, the analysis of images was complicated by hyperfine spectroscopy in a magnetic field. Ultimately, these images' analysis allowed a determination of the decrease in temperature and increase in density during evaporation to be made. Spherical quadrupole traps are still important for many types of studies, and so it is hoped that use will be made of some of the particular imaging techniques described herein.

3.1 Overview

Resonant or near-resonant imaging of sodium is highly sensitive to few atoms. To give a realistic example, a diffuse cloud of only ten million atoms spread over more than a square millimeter of area can still absorb most of a resonant probe laser beam passing through it (if the intensity is low enough; see discussion of 'bleaching' effect later). That opacity is due to the fact that the cross-section for scattering scales with the square of the optical wavelength (and with the inverse square of the frequency detuning from resonance), rather than with the size of the atom. This resonant enhancement of about eight orders of magnitude for sodium enables one to observe the typical femtomole- or attomole-sized samples of atoms. In this sense, the atom acts like an antenna coupled to a resonant radio circuit.

The trio of atomic density, magnetic field, and probe light determines the strength of signal in an image. Optimally, the magnetic field is homogeneous, and the probe light is properly polarized and detuned to match the orientation and resonance of the atoms. If this is the case, images are manifestly related to the atomic density; what one sees manifestly reflects what is in the vacuum chamber. In several cases there can be exceptions, however. If one images in a magnetic trap, temperature can be a determining factor. Clouds hotter than the 'Doppler cooling' limit ($\sim 240\ \mu$K) have a spatially inhomogeneous resonance frequency due to the Zeeman shift. Doppler broadening can also reduce the cross-section. There can be an inhomogeneous orientation of the field across the cloud, which prevents a uniform match between the polarization of the light and atoms throughout. Most imaging work is done at temperatures low enough for some of these considerations to be irrelevant. And also, the cloverleaf (at low temperatures) and optical traps hold atoms in a rather uniform field environment. Thus, the simple picture of images as directly representing atomic density is appropriate for ultracold clouds and especially so for condensates.

A special problem encountered is when one images clouds in the spherical quadrupole trap, independently of temperature. There, the fundamental nature of the field polarization is inhomogeneous since any orbit in a plane containing the trap's center experiences the full 2π rotation, as shown in figure (2-1). Therefore, images of such clouds are subject to a more sophisticated spectroscopic interpretation, and a simple model for that will be presented in this chapter. Also worth mentioning is the optically plugged trap, which supplanted the bare spherical quadrupole field for the observation of Bose condensation [3]. The addition of a focused green laser beam to repel atoms from the low field region at the center also alleviated problems arising from the inhomogeneous field polarization. The coldest clouds in the oblate quadrupole field separated into two pockets on either side of the focused laser, and therefore no orbits were able to experience a complete 2π rotation of orientation. Thus the atomic polarization becomes more uniform towards the right half of figure (3-1).

Imaging a dense cloud presents yet another problem, which is that it absorbs too strongly. All resonant light can be absorbed, and no information about the density distribution can be inferred

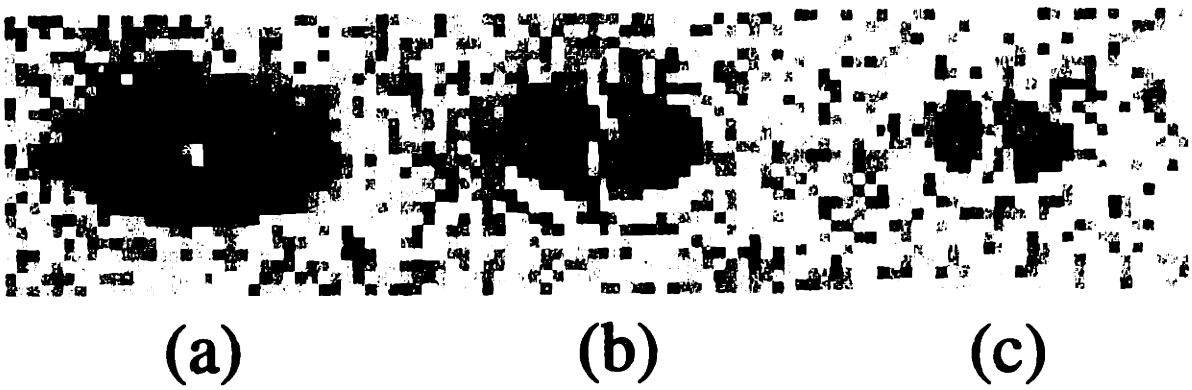

Figure 3-1: Clouds in the optically plugged trap. As the temperature decreases, from left to right or (a) to (c), the oblate cloud in the spherical quadrupole trap separates into two pockets. The atomic polarization in each pocket in (c) is more uniform than the polarization across the entire cloud (a).

— similar to a black hole in that no light escapes to the camera once it enters the cloud. This is resolved by using off-resonant light which is not absorbed. The probability of absorbing a photon off-resonantly is less compared to resonantly by a factor proportional to the square of the frequency detuning from resonance, whereas the index of refraction is less only by the detuning itself. This suggests the use of refraction for imaging instead of absorption, which is what's done in the 'dispersive imaging' techniques such as 'dark ground' or 'phase-contrast' [31, 16, 8], to be discussed later. Choosing the detuning so that the phase shift of the probe light going through a cloud (due to refraction) is about 2π gives a strong signal without significant absorption of photons.

It is useful to consider a unified picture of the scattering of light by trapped samples, and so an understanding based on the work of Politzer [32] and others is presented in this paragraph. Probing resonantly causes atoms to absorb and re-emit photons, whereas the dispersive part of the cross-section represents a coherent process where the phase of the probe light is affected. In a finite sample, coherent scattering gives rise to diffraction, and the photons go off in the forward direction. Quantum-mechanically, coherent scattering does not cause atoms to undergo transitions between quantum motional states in the trap, whereas absorption does. In absorption, random transitions between trap states lead to heating of the sample. In coherent scattering, however, to assess heating the detuning of the light is important and so is the duration of the probe pulse in comparison with the period of oscillation in the trap. For longer pulses of off-resonant light, atoms predominantly return to the same trap state, whereas for shorter pulses there are many frequencies present and atoms can be stimulated to return to different states. Long pulses allow atoms to adiabatically respond to the presence of the light, whereas short pulses do not. The presence of a condensate mainly affects this picture by merely adding a component to the signal corresponding to the condensate density. This is just what is expected for a classical system of particles in a cloud.

The theory of imaging is based on how light propagates through matter and how matter is

affected by light. Politzer's treatment is fully quantum, but for most purposes a semi-classical picture is needed. The parts of imaging having to do with light rely on Maxwell's equations, which are classical, and the parts about matter rely on atomic physics, which have quantum aspects. This basic division is well established, and for instance, described in the theses of [33, 34] and reference [35]. Much of their treatment will be reproduced in the following section, although the inclusion of the phase factors $e^{\pm 2i\phi}$ of equations (3.24) and (3.25) are presented here for the first time. These factors have observable effects in images, as will be discussed.

3.2 The propagation of light

The propagation of light through a dilute gas is modeled by solving Maxwell's equations assuming the gas is a linear polarizable medium. A dilute gas in this context is one where there is on average much less than one atom per photon mode $n \ll k^3$, and each atom responds to the field essentially on its own. A linear medium has polarization $P = \epsilon_0 \chi_e E$ where E is the electric field of the traveling wave. Maxwell's equations in this context are

$$\nabla \cdot E = 0 \tag{3.1}$$

$$\nabla \times E = -\frac{\partial B}{\partial t} \tag{3.2}$$

$$\nabla \cdot B = 0 \tag{3.3}$$

$$\nabla \times B = \frac{1}{c^2}\left(\frac{\epsilon_0}{\epsilon}\right)^2 \frac{\partial E}{\partial t} \tag{3.4}$$

where the permittivity within the cloud is ϵ. Transforming these equations in the standard way to a wave equation, and using that $\epsilon = \epsilon_0(1 + \chi_e)$, one gets

$$\nabla^2 E - \frac{1}{c^2}\frac{\partial^2 E}{\partial t^2} = \frac{1}{\epsilon_0 c^2}\frac{\partial^2 P}{\partial t^2} \tag{3.5}$$

In this representation the polarization of the atoms appears as a source term, indicating that light is scattered. The effect of the cloud on the light is denoted by the complex amplitude $E_0(r,t)$ on a carrier wave $\exp(ikz - iwt)$, and likewise for the induced polarization P:

$$E(r,t) = E_0(r,t)e^{i(kz-wt)} \tag{3.6}$$

$$P(r,t) = P_0(r,t)e^{i(kz-wt)}. \tag{3.7}$$

Making the standard 'slowly varying amplitude' approximation, where all changes in E_0 and P_0 are on larger scales than those in the carrier wave, one gets a simple differential equation governing

propagation of light rays through the cloud:

$$\frac{\partial E_0}{\partial z} = \frac{ik}{2\epsilon_0} P_0 = \frac{ik}{2} \chi_e E_0. \tag{3.8}$$

What is left to discuss is how the atoms respond to the light, which is encapsulated in the susceptibility tensor χ_e in the following way (summation convention):

$$P_0^\alpha = \epsilon_0 \chi_e^{\alpha\beta} E_0^\beta. \tag{3.9}$$

The tensor χ_e can be calculated from known spectroscopic properties, and will be discussed in a moment. Assumed in this relation between spectroscopic properties and the induced polarization is the linearity of the medium (the atomic cloud). For this, the radiation should be applied in a steady-state fashion, or much longer than the excited state lifetime. This is about 16 ns for sodium, and so typical pulses of 50-1000 μs are perfectly satisfactory. Another assumption is that the time-averaged probability of finding a particular atom in the excited state is small. This assumption requires intensities below the level where an atom immediately absorbs a photon after the emission of another, which is just about the 'saturation intensity'. At intensities close to or above this level, however, one also finds an optical degradation of the sample, called 'bleaching'. Photons that could otherwise be absorbed aren't because atoms in the excited state are temporarily transparent.

In the orthogonal basis in which the magnetic field is along one of the axes, the tensor χ_e' can be made diagonal (the 'prime' denotes the diagonal frame). Its elements are just proportional to the transition strengths for left circular (σ_-) right circular (σ_+), and linearly (σ_π) polarized light:

$$\chi_e' = \begin{pmatrix} \chi_+ & 0 & 0 \\ 0 & \chi_- & 0 \\ 0 & 0 & \chi_\pi \end{pmatrix} \tag{3.10}$$

Physically, the $\chi_\pm$ elements give the atomic response to a circularly oscillating electric field polarization perpendicular to the magnetic field, and χ_π gives the response to linear polarization parallel to the field. In particular, χ_+ (and similarly for the other elements) is given by the sum over all possible 'right-circular' atomic transitions $i \rightarrow j$:

$$\chi_+ = \frac{6\pi}{k^3} \sum_{i,j} n_i \frac{S_{ij}}{S_j} \left(\frac{\gamma}{\omega_{ij} - \omega - i\gamma} \right). \tag{3.11}$$

n_i is the atomic density in the ground state i, γ is half the linewidth (same for all the relevant sodium transitions), S_j is the total oscillator strength to the excited state j, S_{ij} is a particular transition's oscillator strength relative to S_j, and ω_{ij} is the resonant frequency of that transition. The relevant frequencies are all yellow light close to 589 nm for sodium. The S's and ω_{ij}'s may be taken from

tables of sodium's spectroscopic lines (for example, as appearing in reference [36]), or calculated as indicated in section (3.4.3).

Equation (3.11) describes a lorentzian frequency response with both absorptive (imaginary) and dispersive (real) parts. In sodium, for instance, probing atoms in the state $|F = 2, m_F = +2\rangle$ with right circular light can resonantly excite a transition to the $|F = 3, m_F = +3\rangle$ state with the full oscillator strength $S_{23}/S_3 = 1$. Resonant light means that $\omega_{ij} - \omega = 0$ for this particular choice of i and j. Therefore, ignoring all other transitions, equation (3.8) would become

$$\frac{\partial E_0}{\partial z} = -\frac{3\pi}{k^2} n(z) E_0, \tag{3.12}$$

and the light decays exponentially in the sample as

$$E_0(z) = \lim_{a \to -\infty} E_0(a) \exp\left(-\frac{\sigma}{2} \int_a^z dx\, n(x)\right) \tag{3.13}$$

when it travels through the cloud due to absorption; z could be the position relative to the center of the cloud. In this case, the absorption cross-section σ would be $6\pi/k^2 = 3\lambda^2/2\pi$.

The phase shift of the light as it travels through the cloud would be zero in this case of $\omega_{ij} - \omega = 0$ (equation (3.13)) since a phase shift is a dispersive effect which requires probing off-resonantly. Calculating the phase shift of the electric field due to probing off-resonantly would proceed analogously to the steps leading to equation (3.13), with the addition of a detuning factor in the cross-section as shown in equation (3.11).

It's worth emphasizing again that the majority of imaging theory needed for the study of ultracold clouds and Bose condensates makes use of these kinds of elementary expressions for the propagation of light. In contrast, for a small subset of tasks the interpretation of images is more difficult, namely for observing clouds in a spherical quadrupole trap. While the next section is a detailed model for the propagation of light through matter, it is mainly of use for this specific task of imaging in that particular trap.

3.3 The atomic polarization

The treatment of this section gives optical cross-sections for arbitrary atomic polarization. Additionally, a basis is provided for interpreting the spectroscopic images of clouds above and below the Doppler temperature in a spherical quadrupole trap.

A complex orthogonal basis that diagonalizes χ_c is given by $\{e_+, e_-, e_\pi\}$, where e_π is parallel to the magnetic field as mentioned previously:

$$e_\pi = B \tag{3.14}$$

$$e_2 = k \times B \tag{3.15}$$

$$e_1 = e_2 \times e_\pi \tag{3.16}$$

$$e_\pm = (e_1 \pm i e_2)/\sqrt{2}, \tag{3.17}$$

where B is the magnetic field vector and k is the wave vector of the light. Three tensor equations determine χ_e because of its diagonal form in equation (3.10), which can be solved in *any* basis:

$$\chi_e^{ij} e_+^j = \chi_+ e_+^i \tag{3.18}$$

$$\chi_e^{ij} e_-^j = \chi_- e_-^i \tag{3.19}$$

$$\chi_e^{ij} e_\pi^j = \chi_\pi e_\pi^i. \tag{3.20}$$

Using a magnetic field expressed in cartesian coordinates as

$$B_0 \times (\sin\theta\cos\phi, \sin\theta\sin\phi, \cos\theta), \tag{3.21}$$

with light propagating along the z-axis such that $k = k_0 \times (0,0,1)$, the following expression can be derived for χ_e using a circular basis for polarizations in the lab frame:

$$\chi_e = \begin{pmatrix} \chi_{++} & \chi_{+-} \\ \chi_{-+} & \chi_{--} \end{pmatrix} \tag{3.22}$$

where

$$\chi_{++} = \chi_+ \cos^4(\theta/2) + \chi_- \sin^4(\theta/2) + (\chi_\pi/2)\sin^2\theta, \tag{3.23}$$

$$\chi_{+-} = (\chi_\pi/2 - \chi_+/4 - \chi_-/4) e^{-2i\phi} \sin^2\theta, \tag{3.24}$$

$$\chi_{-+} = (\chi_\pi/2 - \chi_+/4 - \chi_-/4) e^{+2i\phi} \sin^2\theta, \tag{3.25}$$

and

$$\chi_{--} = \chi_- \cos^4(\theta/2) + \chi_+ \sin^4(\theta/2) + (\chi_\pi/2)\sin^2\theta. \tag{3.26}$$

The matrix for χ_e in equation (3.22) is only 2×2 (rather than 3×3 as in equation (3.10)) because light has transverse polarization. Thus, the 'longitudinal' components of χ_e have no physical effect and are ignored.

One particularly simple situation is when $\theta = 0$ and the light propagates parallel to the magnetic field. In this case one expects only left and right circular transitions, and indeed equation (3.8) and equation (3.22) give

$$\frac{\partial E_{0\pm}}{\partial z} = \frac{ik}{2} \chi_\pm E_{0\pm}, \tag{3.27}$$

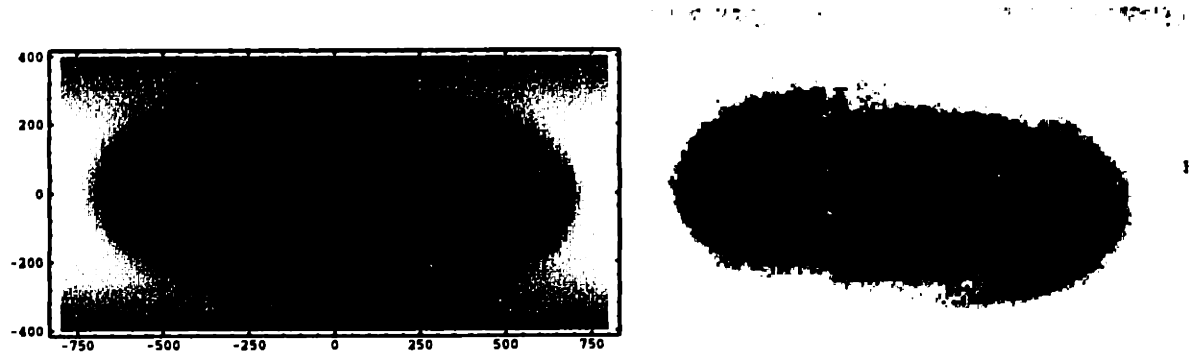

Figure 3-2: Swirly cloud at $\sim$ 1000 G/cm (on right) together with a matching simulation (on left) at a temperature $\sim$ 800 μK and density $\sim$ 0.6 μm^{-3}. Probe frequency is -92 MHz detuned from the $|F = 1\rangle$ to $|F = 2\rangle$ transition with linear polarization. Scale in simulation is in microns.

image. The close correspondence between simulated and experimentally observed clouds shows that the basic understanding of spectroscopic imaging, as explained in this chapter, is sound. But generally, note how the same cloud appears differently when imaged with various probe frequencies.

It's important to note that the clouds in the trap are distributed in space according to the Boltzmann factor $\exp(-g\mu_B B'r/k_B T)$, where B' is the magnetic field gradient and $g\mu_B$ is the Zeeman shift of the atoms. This is a rather isotropic distribution (albeit oblate with an aspect ratio of two), whereas the images shown do not have that character at all. Moreover, most of the clouds appear much larger than they actually are. Especially in figure (3-5) one can see that the highest regions of optical density appear in shells. These shells are due not only to the distribution of atoms, but to the distribution of atoms resonant with the probe light. This is precisely one of the troubles with imaging spectroscopic features, rather than merely density features. The linewidth for optical transitions in sodium is about 10 MHz, and so the 'width' of the shells is about 15 gauss in field (0.7 kHz/mG). 10 MHz corresponds to about 500 μK, which is comparable to the temperature of the cloud (Doppler limit is 240 μK). Therefore, one 'shell' of energy width $\sim k_B T$ is in resonance with the probe light, whereas others are not. The surfaces of these shells are viewed edge-on and appear blacker. Depending on which transitions are in resonance at which field for the particular probe frequency, the shells will either move to the periphery of the cloud as in figure (3-3) and figure (3-4), or move towards the atoms at the lowest field in the center as in figure (3-6) and figure (3-8). In figure (3-9) to figure (3-11) atomic resonances are moving toward the periphery of the cloud as the probe detuning is varied even further.

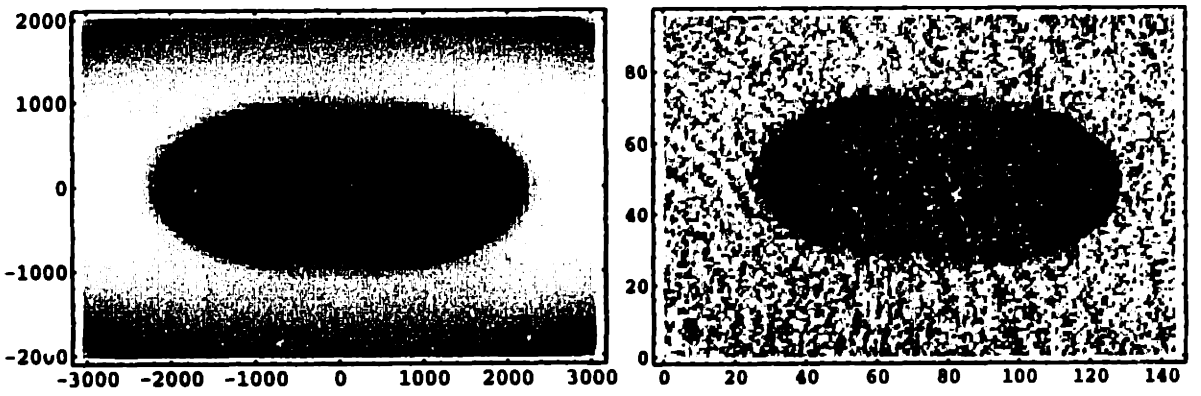

Figure 3-3: ccd image of cloud on right, simulated image on left. Probe frequency is -180 MHz detuned from the $|F = 1\rangle$ to $|F = 2\rangle$ transition with linear polarization. This is a cold cloud of sodium at ~ 500 μK with a peak density of ~ 0.2 μm^{-3} in a spherical quadrupole magnetic trap with gradient ~ 500 G/cm. The field of view on right is labelled in pixels, and on left in μm. On this scale the atoms mainly occupy the central $\sim 1\%$ of image area (an ellipsoid $\sim 10 \times 20$ pixels), but appear to be distributed differently due to imaging effects discussed in the text.

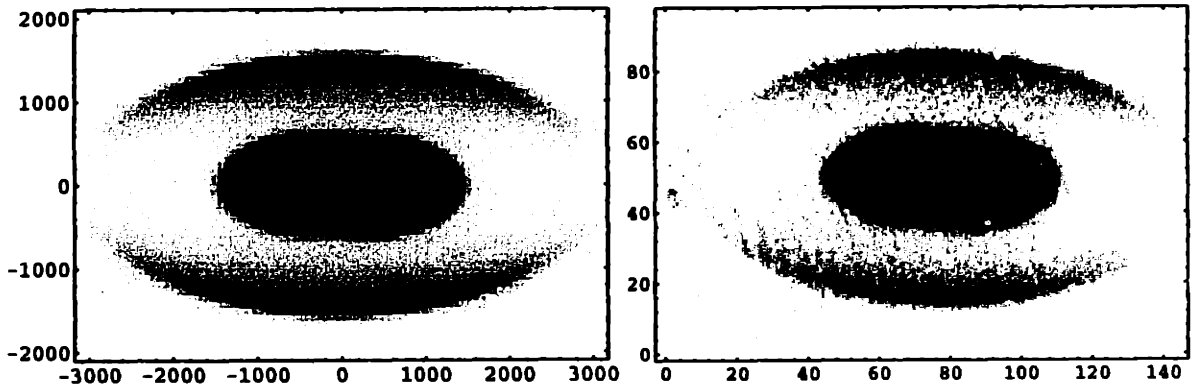

Figure 3-4: ccd image of cloud on right, simulated image on left. Probe frequency is -110 MHz detuned from the $|F = 1\rangle$ to $|F = 2\rangle$ transition with linear polarization. See caption of figure (3-3) for more information.

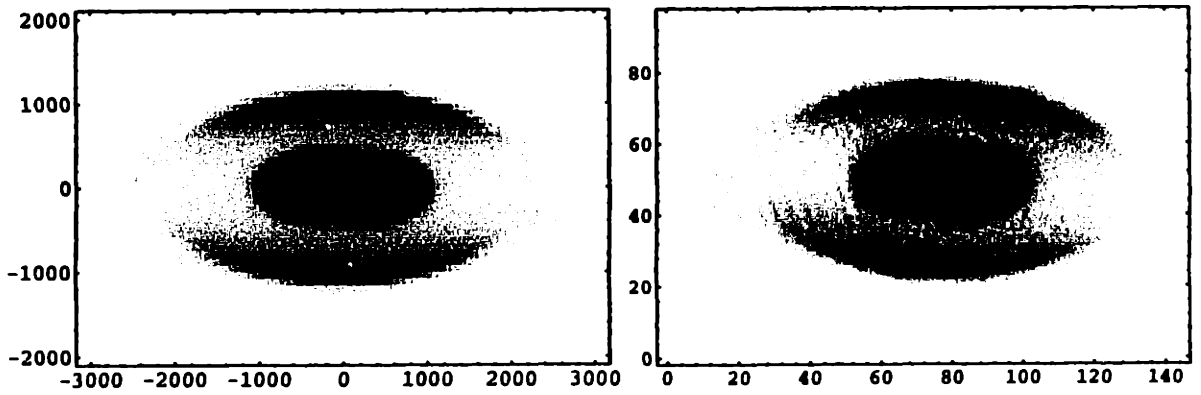

Figure 3-5: ccd image of cloud on right, simulated image on left. Probe frequency is -80 MHz detuned from the $|F = 1\rangle$ to $|F = 2\rangle$ transition with linear polarization. See caption of figure (3-3) for more information.

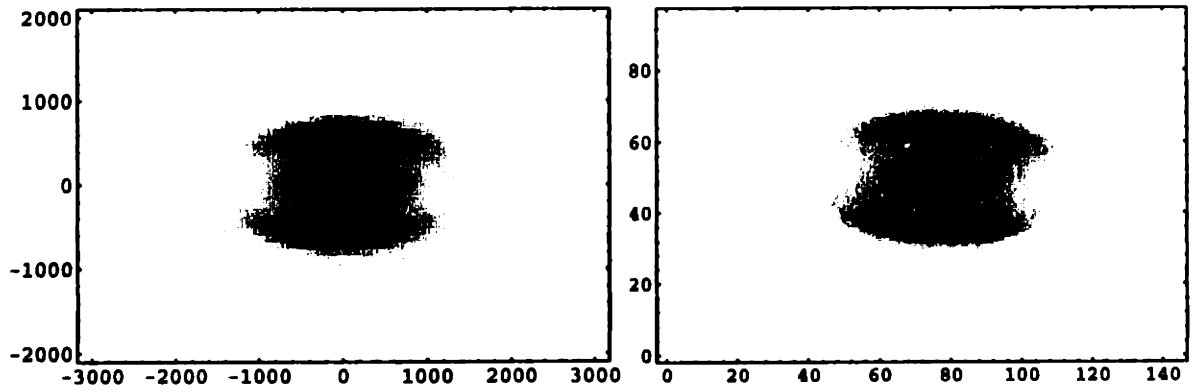

Figure 3-6: ccd image of cloud on right, simulated image on left. Probe frequency is -40 MHz detuned from the $|F=1\rangle$ to $|F=2\rangle$ transition with linear polarization. See caption of figure (3-3) for more information.

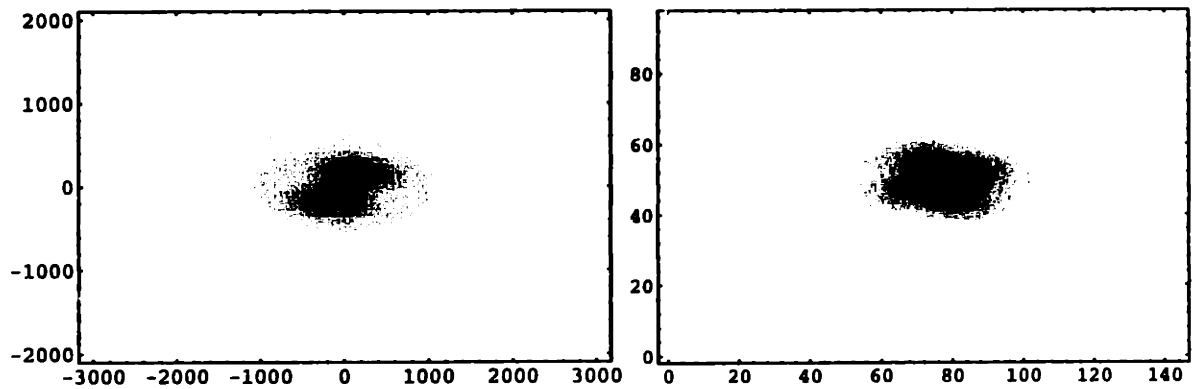

Figure 3-7: ccd image of cloud on right, simulated image on left. Probe frequency is -20 MHz detuned from the $|F=1\rangle$ to $|F=2\rangle$ transition with linear polarization. See caption of figure (3-3) for more information.

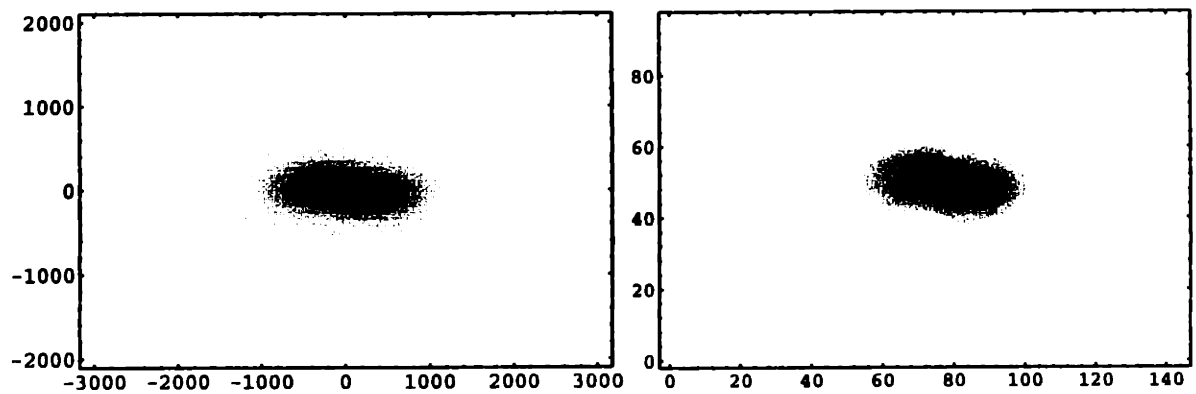

Figure 3-8: ccd image of cloud on right, simulated image on left. Probe frequency is 0 MHz detuned from the $|F=1\rangle$ to $|F=2\rangle$ transition with linear polarization. See caption of figure (3-3) for more information.

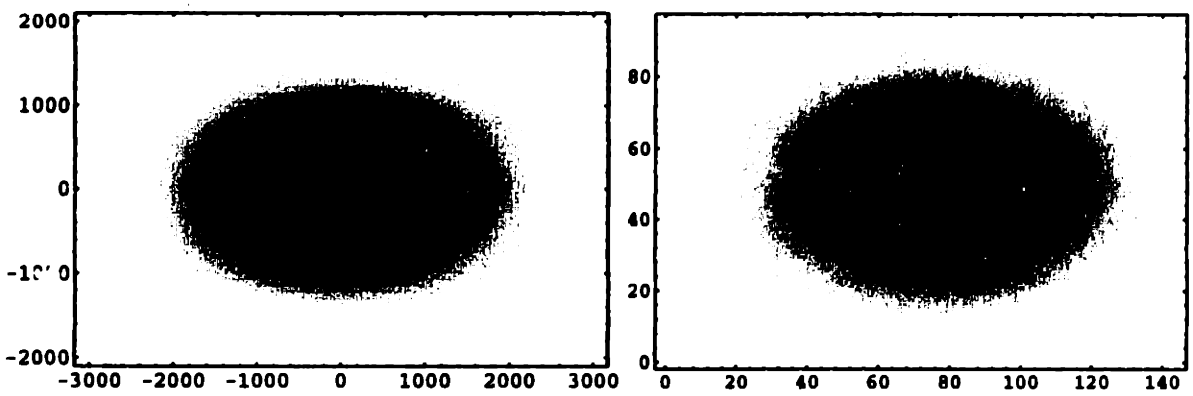

Figure 3-9: ccd image of cloud on right, simulated image on left. Probe frequency is +30 MHz detuned from the $|F=1\rangle$ to $|F=2\rangle$ transition with linear polarization. See caption of figure (3-3) for more information.

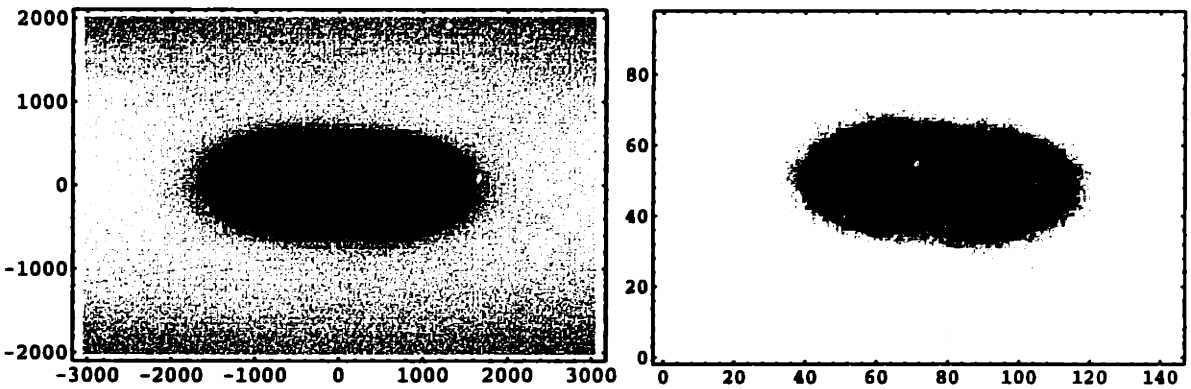

Figure 3-10: ccd image of cloud on right, simulated image on left. Probe frequency is +80 MHz detuned from the $|F=1\rangle$ to $|F=2\rangle$ transition with linear polarization. See caption of figure (3-3) for more information.

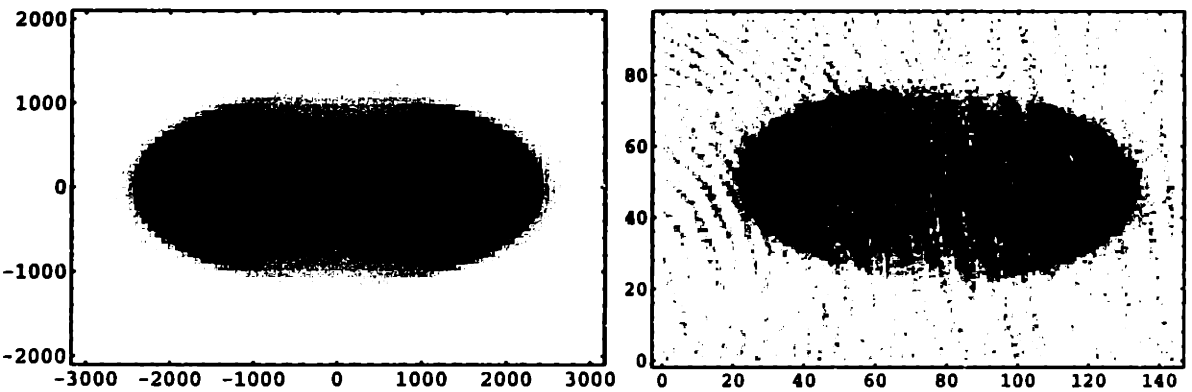

Figure 3-11: ccd image of cloud on right, simulated image on left. Probe frequency is +120 MHz detuned from the $|F=1\rangle$ to $|F=2\rangle$ transition with linear polarization. See caption of figure (3-3) for more information.

3.4 Experimental details

In this section some of the details of how imaging is actually done in the lab will be discussed. This will include issued related to imaging resolution, dispersive imaging techniques, probe illumination, and atomic structure.

The main object of the imaging system is to get the best pictures of the features one is observing. Practically, this means projecting the image onto a ccd camera and having each pixel give as much information as possible. These pictures should have the minimum blurriness, which requires focusing the system properly, and for low f-number and high magnification requires diffraction limited optics. Not only does this entail good quality lenses, but the same quality for mirrors and phase plates (for phase-contrast). In particular, 2" broadband dielectric mirrors and phase plates are used with a surface smooth to $\lambda/10$. More roughness was seen to degrade the ultimate resolution.

For matching the lens and pixel resolutions, a sufficient design is to have a point source imaged onto a circular area at least two pixels wide on the camera. This satisfies Nyquist's theorem for the minimal sampling of a signal, which states that all the information can be recovered if one samples at twice the cutoff frequency for features in the original signal. For the largest magnification $m = 8$ used so far, each pixel on the camera corresponded to about 3 μm in the object. The primary lens had a limiting f-number of $f/d = 250\,\text{mm}/50\,\text{mm} = 5$, and so Nyquist's criterion was close to being matched (the smallest diffraction-limited spot size is $\sim 1.2f\lambda/d$).

The design of the imaging system used pairs of achromatic lenses at infinite conjugate ratio (the light scattered by the cloud was roughly collimated between the two lenses). The primary lens system magnified the object by a factor of two, and consisted of a 250 mm and 500 mm (focal-lengths) pair, each having a 50 mm diameter. For higher magnification, another pair of 100 mm and 400 mm relayed the intermediate image to the camera for a total magnification of eight. The primary lens of 250 mm was the most crucial one in terms of reaching the diffraction limit (having the lowest f-number), and thus was the one that required the most careful positioning and tilting. This type of design is elementary and is covered by basic textbooks such as reference [31].

The illumination should be as uniform as possible to minimize noise in the image, although dividing by an additional image with no atoms (pixel by pixel) normalizes the background inhomogeneities. To start with as uniform an illumination as possible, single-mode polarization preserving fibers carry probe light from the laser room to the experiment. This light is expanded to the desired beam size, typically 1 cm or so, and directed towards the atoms. Before entering the chamber, however, beams of light having different frequencies are multiplexed in such a way that from minute to minute one can be substituted for the other if desired, using 'kinematic mounts'. Additionally, there are similar provisions to direct light vertically or horizontally through the atoms, or both simultaneously. When imaging $|F = 2\rangle$ atoms on the cycling transition $|F = 2, m_F = +2\rangle$ to $|F = 3, m_F = +3\rangle$, $F = 1$ optical pumping light must simultaneously be used (if only to initially

pump to $|F = 2\rangle$), and is usually directed at the atoms from the perpendicular direction. The picture to keep in mind is that any illumination configuration is possible, and almost all of them have been used depending on what was required for a particular experiment.

3.4.1 Dispersive imaging

Dispersive imaging uses diffraction and phase shifts of light to resolve spatial structures, and so this class of techniques is naturally associated with probing far off-resonantly where absorption is less important. Whereas absorption of light is imaged as a shadow on the camera, phase shifts do not affect the intensity and are not visible in the same way. The same holds true for diffracted light which can be focused by the imaging lens back onto the camera along with the undiffracted light. Thus, additional techniques are called for to be able to 'read out' the information encoded in the coherent scattering of photons that doesn't give rise to absorption.

In dark-ground imaging, one simply prevents light which has not been scattered by the cloud from reaching the camera. Thus, the cloud shows up as a bright area (of scattered light) in the image. The technique as implemented for the nondestructive observation of a condensate relies on the fact that the probe laser light is collimated whereas the scattered light has an angular distribution. An imaging system (almost by definition) has a lens, which is all that is needed to angularly select photons — therefore any imaging setup is compatible, in principle, with the dark-ground technique. The unscattered photons are collimated, and come to a focus in the center of the focal plane of the imaging lens. Scattered photons also pass through the focal plane, but do not pass through its center. Thus, one simply blocks the central region in the focal plane. To do this, a wire 0.2 to 1 mm thick was used, and the fact that a small fraction of scattered photons were blocked as well was neglected. Since the condensate was cigar-shaped, most of the scattered light was also cigar-shaped (but with the perpendicular orientation). A 7 mrad rms scattering angle observed in the focal plane was consistent with a 20 μm wide cloud without a condensate at 1.5 μK. Below the phase transition, a 20 mrad rms scattering angle was consistent with the size and shape of a condensate in the Thomas-Fermi regime for the given number of atoms and the trapping potential. The enhanced forward direction of scattering observed in the presence of a condensate reflected the fact that a localized fraction of the gas became denser. A $f = 167$ mm focal length achromatic lens pair (the 250 and 500 mm lens pair used at infinite conjugate ratio) with a 200 μm wire was thus more than adequate to allow most of the scattered light to pass. For a wire of size w, the minimum angle of scattered light that can pass is given by $\sim w/f$, or less than a milliradian in this particular case. Alternatively, the maximum sized object that can be imaged is $\sim \lambda f/w$.

Phase contrast is another interferometric imaging technique, and instead of blocking the unscattered light it is phase-shifted by a quarter-wave. Thus, small phase modulations are converted to amplitude modulations and become visible. This technique was used for all studies of the conden-

sate after its initial observation in the trap with dark-ground imaging [16, (3.5)]. For a realistic imaging system with technical noise sources, the following considerations hold. For a small amount of scattered light, phase contrast is practically better than dark-ground because of the homodyne effect. The small scattered amplitude is mixed with the strong 'carrier', and so the intensity has a term linear in both. In other words, the small scattered signal is amplified by the carrier and is boosted above technical noise sources. In dark-ground, however, the intensity of the scattered light is detected alone, and thus there is no amplification. For large signals, one can also argue that phase-contrast is better, because the dark-ground signal saturates at the incident light intensity whereas in phase-contrast one develops an interferogram having many fringes. There is no loss of information as long as fringes can be counted.

The phase plates were 2" optical flats, each with one of a variety of circular spots 0.1–1.0 mm at the centers. Some spots were of thin films with $\lambda/4$ optical thickness, and others were the lack of same in a broad field of $\lambda/4$ film. These are colloquially called 'positive' and 'negative' phase plates, and they correspondingly lead to opposite phase shifts of the light.

3.4.2 Probe light

The background normalization is a simple yet essential step in taking good images. Three images are taken in sequence, one image with atoms called 'I', one without atoms called the bright field 'B', and one without light called the dark field 'D'. Every pixel in images I and B has the same contribution of dark counts D (aside from random noise), and of light B. Signals in absorption and phase contrast images are naturally scaled to the amount of background light, and so the normalized image can be computed as $(I - D)/(B - D)$. Dark-ground images, however, do not have a bright field and thus are not normalized — yet another disadvantage to this technique. This normalization procedure removes spatial inhomogeneities in the probe light, and corrects for the background light level. If the light level fluctuates between the image and the bright field, then the background level of the normalized image will be different from unity and software can renormalize it. Vibrations in the imaging system often cause shifting fringes between I and B, and give rise to imperfect normalization.

The advantage of imaging atoms in $|F = 2\rangle$ is that there is a cycling transition to $|F = 3\rangle$. Atoms predominantly return to the initial state after absorbing a photon, and thus are available again to absorb. Imaging atoms in $|F = 1\rangle$, however, requires one to use at most a single photon per atom, since the chance of returning to the same state is not very high. Making a determination of the proper illumination intensity during an experiment is straightforward, and is done by looking at the light level in a ccd image. The probability for absorbing a photon is equal to $(1 - e^{-\rho})$ where $\rho \sim n\sigma d$ is the optical density, σ is the absorption cross section, and nd is the number of atoms in the cloud per area of the image. Thus, for less than one absorption per atom on average, each pixel

Figure 3-12: Quadrupole oscillation at $\sqrt{5/2}\omega_z \sim 30$ Hz in a magnetic trap, superimposed on a smaller dipole oscillation. Vertical field of view is about 750 μm, and frames are separated by 5 ms.

should be exposed to A/σ photons in the limit of small optical density, where A is the area of a pixel. For the magnification $m = 2$ at MIT (typically used for time-of-flight imaging), $A \sim 530\ \mu\text{m}^2$ and for $|F = 1\rangle$ atoms $\sigma = 3\lambda^2/4\pi \sim 1/12\ \mu\text{m}^2$. Thus, one typically wants less than 6400 photons. Since the ccd camera gives about one count per ten photons, one limits the probe intensity in this case to 640 counts.

The work on propagation of sound was the first one at MIT where phase-contrast nondestructive movies were taken of an in-situ dynamical phenomenon [8, (5.1)]. For instance, see figure (3-12) for an example of a quadrupole excitation observed using this technique [22]. The important issue is using enough light for acceptable signal levels while at the same time avoiding a significant amount of heating. Heating is due to absorption and spontaneous emission, and decreases with the square of the frequency detuning from resonance. To make a movie nondestructively, one adds up the total number of photons scattered and makes sure that the total energy imparted to the cloud is negligible compared to its temperature, or for a condensate, compared to its energy. In a typical case, the resonant optical density is a few hundred, and so light that excites the $|F = 2, m_F = +2\rangle$ to $|F = 3, m_F = +3\rangle$ transition is about 1.7 GHz or 350 half linewidths detuned for $|F = 1\rangle$ atoms in a magnetic trap. Thus, the probability for the cloud to absorb a photon is less than 1%. A typical light level gives about 1000 counts per pixel in the image, or 10000 photons meaning that 100 photons per pixel are absorbed. But since trapped condensates are typically imaged over an area 1000 μm^2 or 100 square pixels, a total of 10000 absorbed photons is negligible in a cloud containing millions of atoms.

Table 3.1: Sodium hyperfine constants

State	A (MHz)	B (MHz)	g_J
$3S_{1/2}$	885.8130644(5)	—	2.0022960(7)
$3P_{1/2}$	94.3(1)	—	0.66581(12)
$3P_{3/2}$	18.69(9)	2.90(21)	1.3341(3)

3.4.3 Atomic structure

Remaining to be discussed is the atom itself. One needs atomic structure information to plug into the expression for the susceptibility equation (3.10). This information is predominantly determined by the hyperfine interaction, which gives structure to sodium's spectrum near the D-lines at 589 nm. The hyperfine hamiltonian can be written as

$$W = hA\,\mathbf{I}\cdot\mathbf{J} + hB\,\frac{6(\mathbf{I}\cdot\mathbf{J})^2 + 3(\mathbf{I}\cdot\mathbf{J}) - 2I(I+1)J(J+1)}{2I(2I-1)2J(2J-1)} + (g_J J_z + g_I I_z)\mu_B H, \qquad (3.31)$$

where A and B are hyperfine constants [37], h is Planck's constant, $\mathbf{I}$ and $\mathbf{J}$ are the nuclear and electronic angular momenta (boldface for vectors), g_I and g_J are the nuclear and electronic g-factors, and H is the applied field. Recommended values are shown in table 3.1, taken from ref. [37]. The nuclear g-factor $g_I = -0.0008046108(8)$.

Diagonalizing this hamiltonian gives eigenvalues and eigenvectors. The differences in eigenvalues are the transition frequencies ω_{ij}, and the squared overlap of eigenvectors are the relative oscillator strengths S_{ij}. These values are then inserted into equation (3.11).

3.5 'Direct, Nondestructive Observation of a Bose Condensate'

For this section the following paper is presented:

- 'Direct, Nondestructive Observation of a Bose Condensate', by M. R. Andrews, M.-O. Mewes, N. J. van Druten, D. S. Durfee, D. M. Kurn, and W. Ketterle. *Science*, Vol. 273, p. 84, 1996. Reference [16].

Reprint Series
5 July 1996, Volume 273, pp. 84–87

SCIENCE

Direct, Nondestructive Observation of a Bose Condensate

M. R. Andrews, M.-O. Mewes, N. J. van Druten, D. S. Durfee,
D. M. Kurn, and W. Ketterle

Direct, Nondestructive Observation of a Bose Condensate

M. R. Andrews, M.-O. Mewes, N. J. van Druten, D. S. Durfee, D. M. Kurn, W. Ketterle

The spatial observation of a Bose condensate is reported. Dispersive light scattering was used to observe the separation between the condensed and normal components of the Bose gas inside a magnetic trap. This technique is nondestructive, and about a hundred images of the same condensate can be taken. The width of the angular distribution of scattered light increased suddenly at the phase transition.

Bose-Einstein condensation (BEC) is characterized by a macroscopic population of particles in the quantum-mechanical ground state below a critical temperature. It is the origin of macroscopic quantum phenomena such as superfluidity in liquid helium (*1*). For a homogeneous sample, BEC is sometimes called "condensation in momentum space" (*2*) because it does not lead to a spatial separation between the condensate and the normal component. However, in any inhomogeneous potential—for example, in atom traps or even in Earth's gravitational field—the condensate and the normal fraction of a Bose gas are spatially separated (*2*, *3*). So far, BEC has only been seen in momentum space: the condensate fraction of liquid helium was determined by neutron scattering (*4*), the condensation of excitons was deduced from the observed energy distribution of the excitonic particles (*5*), and BEC in dilute atomic gases was detected by observation of the velocity distribution of freely expanding Bose condensates (*6*, *7*). We report the direct and nondestructive observation of the spatially localized condensate in a gas of magnetically trapped sodium atoms.

Bose condensates of dilute atomic gases are a new form of quantum matter. The pioneering work toward BEC in atomic gases was done with spin-polarized hydrogen with the use of magnetic trapping and evaporative cooling (*8*). In work at JILA (*9*) and the Massachusetts Institute of Technology (*10*), these techniques were successfully combined with laser cooling (*11*), which resulted in the observation of BEC in rubidium in June (*6*) and in sodium in September of 1995 (*7*). Lithium has also been cooled to the quantum degenerate regime (*12*). Since these developments, there has been a flurry of both theoretical and experimental activity (*13*).

In atom traps, the condensation phenomenon results in the formation of a dense core of atoms in the ground state of the system surrounded by the normal component—analogous to droplet formation in a saturated vapor. Our earlier attempts to observe the Bose condensate directly by absorption imaging failed because of the high optical density of the atom cloud near the critical temperature. For typical parameters of our experiment, the peak optical density D_0 for resonant light was about 300, corresponding to a transmission coefficient of e^{-300}. Thus, the probe light was completely absorbed, even in the wings of the spatial distribution, preventing direct imaging of the condensate. Detuning of the light, which reduced the absorption, revealed major image distortions caused by dispersive effects: the condensate acted as a lens and strongly deflected the light. However, by using the so-called "dark-ground" imaging technique (*14*), we were able to use the dispersively scattered light to clearly image the condensate.

Dispersive imaging has significant advantages over absorption methods for the imaging of small and dense clouds ($D_0 \gg 1$). To obtain a good absorption signal, one would like to detune the probe light until the off-resonant optical density D is close to unity; D is given by $D = D_0/\Delta^2$, where the detuning Δ from the resonant frequency ω_0 is $\Delta = 2(\omega - \omega_0)/\Gamma$, with Γ being the natural linewidth. The maximum phase shift δ of the transmitted wave is $\delta = D_0/2\Delta$, and thus for $D \sim 1$, the phase shift is $\delta \sim \sqrt{D_0}/2$. Such a large phase shift is caused by lenslike refraction, which bends

Department of Physics and Research Laboratory of Electronics, Massachusetts Institute of Technology, Cambridge, MA 02139, USA.

the incident probe light beyond the cloud's diffractive scattering angle. If the spatial resolution of the imaging system is well matched to the small size of the cloud, this refracted light is not collected by the optics; therefore, absorption images of small and dense clouds are unavoidably degraded. In order to use the imaging system at its nominal resolution, detunings on the order of D_0 are necessary, where absorption signals are negligible, but dispersive phase shifts are close to unity. The signal in dispersive imaging depends on this phase shift, yielding a viable method for probing small and dense clouds.

This argument can be quantified by considering the small, dense cloud to be a lens. A sphere of radius R and index of refraction n acts as a lens having focal length f with $1/f = 2(n - 1)/R$ (*14*). The phase shift δ of light at wavelength λ passing through the center of the lens is $\delta = 4\pi R(n - 1)/\lambda$, yielding $f = 2\pi R^2/\delta\lambda$, and the maximum deflection angle θ for the light is approximately $\theta \approx R/f = (2\delta/\pi) \times (\lambda/4R)$. If $\delta > \pi/2$, light will be deflected as a result of refraction at an angle that exceeds the scattering angle $\lambda/4R$ due to diffraction. As long as the imaging system collects and images the refracted light, quantitative absorption imaging is possible. However, the radius R of the smallest object that can be resolved is usually determined by the collection angle α of the optics to be $R = \lambda/2\alpha$. Additional refraction by the object will scatter light out of the optical system and impede absorption measurements. Therefore, dispersive refraction limits the use of absorption imaging to objects $\approx 2\delta/\pi$ times as large as the diffraction-limited value of $R = \lambda/2\alpha$.

Dispersive scattering is the coherent forward scattering of light. In a homogeneous medium, the scattered light interferes constructively only in the direction collinear with the incident light. Interference with the transmitted beam results in a phase shift and is described by the usual theory for the index of refraction (*14*). In contrast, for an inhomogeneous medium of extension $2R$, such as a trapped cloud of atoms, the coherently scattered light interferes constructively in an angular region $\lambda/2R$. The scattered light can be separated from the incident light in the Fourier transform plane of the imaging system. The incident beam comes to a focus there and can be blocked by a small opaque object. This "dark-ground" method is common in microscopy and is related to Schlieren and phase contrast methods (*14*). In all of these methods, the image is modified in the Fourier plane, enhancing the contrast or the sensitivity for phase objects.

In our experiment, sodium atoms were cooled down to BEC by a combination of laser cooling, magneto-optic trapping, magnetic trapping, and evaporative cooling. The atom cloud was confined in a magnetic trap that uses cloverleaf coils to generate the inhomogeneous magnetic field (*15*). Near the bottom of the trap, the potential was harmonic and axially symmetric, with independently adjustable axial and radial confinement. We controlled the evaporative cooling by continuously reducing the frequency of rf (radio frequency) radiation. The rf field induces spin flips at a specific value of the magnetic field where the condition for electron spin resonance is met. Because the spin flips reverse the sign of the magnetic force on the atoms, the spin-flipped atoms are ejected from the trap (*16*); in this way, the rf frequency determines an effective trap depth. The escape of the hottest atoms from the trap, in combination with rethermalization of the remaining atoms through elastic collisions, cools the sample (evaporative cooling) to a temperature that is about 10% of the effective trap depth.

Typically, we reached the BEC phase transition with 1.5×10^7 atoms in the $F = 1, m_F = -1$ hyperfine state at a temperature of 1.5 μK and a number density of 10^{14} cm^{-3}. Further cooling resulted in the formation of a nearly pure condensate with 5×10^6 atoms (*15*). Temperature and number were determined by a time-of-flight technique in which the trap was suddenly switched off and the cloud expanded ballistically. The expanding cloud became dilute, and quantitative absorption images could be taken. The temperature was derived from the root mean square (rms) velocity of the cloud's normal component, and the number was obtained from the total light absorption.

To image the cloud with the use of dispersive light scattering, we detuned the probe light frequency by 1.71 GHz ($\Delta = -342$) to the red of the $F = 1$ to $F = 2$ optical transition (*17*). The cloud was imaged with a CCD (charge-coupled device) sensor using a lens system with a resolution of 5 μm. A thin wire (0.2 or 1.0 mm) in the Fourier plane of the lens system blocked the transmitted unscattered light (dark-ground imaging). We obtained the images by exposing the trapped atoms to weak probe light for 0.5 s after the loading and cooling procedure. For each image, a new cloud was loaded and cooled to a progressively lower temperature. In this way, we were able to monitor the growth of the condensate fraction within the saturated Bose gas (Fig. 1). The number of atoms in the normal component saturates at $1.202(k_B T/\hbar\bar{\omega})^3$ (*18*), where k_B is Boltzmann's constant, T is the temperature, $\hbar$ is Planck's constant divided by 2π, and $\bar{\omega}$ is the geometric mean of the three harmonic trapping frequencies. Lowering the temperature forces the atoms that exceed this number to condense, similar to droplet formation in a saturated vapor. We measured the effective area of the cloud as observed in dark-ground imaging versus final rf frequency. The sudden decrease in area at the onset of BEC (at an rf frequency of 1200 kHz) (Fig. 2) is a sensitive indicator for the phase transition.

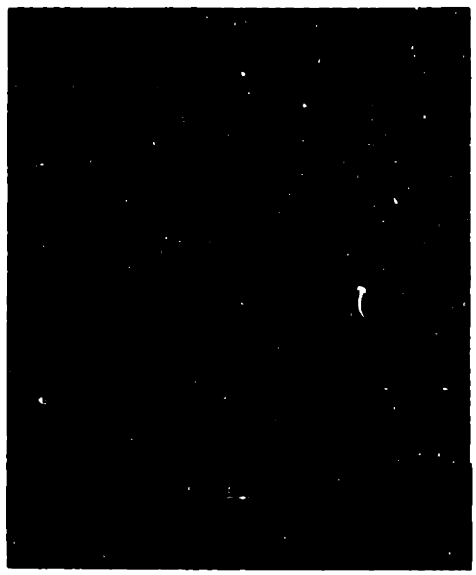

Fig. 1. Direct observation of BEC of magnetically trapped atoms by dispersive light scattering. The probe laser beam propagates along a radial direction of the trap. The clouds have condensate fractions that increase from close to 0% (left) to almost 100% (right). This series was taken at axial and radial field curvatures of 0.1 and 3 kG/cm^2, respectively, resulting in an aspect ratio of the trapped cloud of about 6. The signal for the normal component is rather weak and interferes with the speckle pattern of stray laser light, giving it a patchy appearance.

Dispersive imaging is a nondestructive technique and allows many pictures of the same condensate to be taken. Absorption imaging relies on incoherent large-angle (Rayleigh and Raman) scattering. Each scattering event heats an atom by an aver-

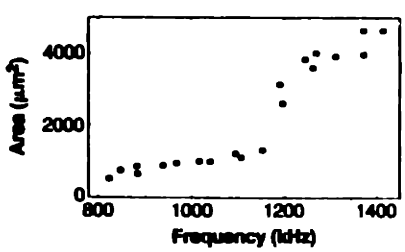

Fig. 2. Effective area of the atom cloud in dark-ground imaging versus final rf frequency, which is approximately linearly related to temperature. The effective area is defined as the total amount of scattered light divided by the peak scattered intensity. The sudden decrease in the effective area indicates the BEC phase transition.

age energy of $(\hbar k)^2/m = 2.3\ \mu K \times k_B$, which is twice the single-photon recoil energy ($\hbar k$ denotes the photon momentum, and m is the atomic mass). In dispersive scattering, the photons are elastically scattered by only a small angle $\lambda/4R$, which was typically 0.02 rad in our experiment. The recoil energy of this process is about 0.5 nK, 1/2000th of the single-photon recoil energy. Furthermore, when the probe pulse duration is much longer than the oscillation period in the trap, the momentum transfer to an individual atom averages out; hence, no heating is associated with the coherent forward scattering of light. This suppression of heating can be regarded as a Mössbauer effect, where the momentum is absorbed by the trap and not by individual atoms. An alternative explanation uses the concept of light forces. For light detuned to the red of the atomic resonance, the incident plane wave is focused (because the index of refraction is greater than one). As a consequence, the light exerts an outward force on the atoms through the stimulated light force (or the optical dipole force). If this force is switched on and off adiabatically, there is no heating.

To test the nondestructive nature of dispersive imaging, we imaged the same condensate twice with a delay time of 1 s: There was no observable reduction in the signal (Fig. 3A). When the incident pulse energy of the probe light was increased to 2 $\mu J/cm^2$, the signal in the second image deteriorated. At this energy, 5×10^6 scattered photons were detected, which is sufficient to allow 100 consecutive images of the same condensate to be taken. We estimate that under these conditions, the probability for off-resonant absorption was about 4%, implying an energy transfer of around 100 nK per atom in the cloud. It is therefore likely that the limit to the probe pulse energy was set by residual absorption and can be further reduced with the use of larger probe-light detunings.

Short probe pulses would provide good temporal resolution at the expense of suppressing the Mössbauer effect. For probe durations shorter than the oscillation time, the atoms should behave as free particles and receive recoil kicks of 0.5 nK per forward-scattered photon. For our conditions, this energy is negligible compared with the heating from residual absorption. In agreement with this calculation, no difference in the maximum nondestructive probe pulse energy was observed when the pulse duration was varied between 2 and 200 ms. The shortest exposure time was comparable to the radial oscillation period (3 ms). Shorter pulses with the same energy could not be applied because of limitations in probe power but are possible and would give even better temporal resolution.

The ability to take several nondestructive images is useful for the study of the dynamics of a single condensate, such as its formation, decay, and response to external forces (Fig. 3B). If studies are done destructively, each time step is taken with a new sample, and shot-to-shot fluctuations may be limiting.

The angular distribution of the scattered light is anisotropic because of the elongated shape of the cloud. For a dilute sample, the angular distribution is determined by the Fourier transform of the spatial distribution. At low density, the scattering is weak and covers an angle of about $\lambda/4R$. Increasing the density increases only the intensity of the scattered light. However, when the phase shift across the sample approaches $\pi/2$, the cloud behaves as a lens and refracts the incident light with a mean angular deflection larger than $\lambda/4R$ (as estimated above). Further increase of the density will increase the deflection angle.

At a detuning of 1.71 GHz and an estimated resonant optical density of 300, the maximum phase shift is about 0.5, which means that we are still in the diffractive regime but close to the transition where refraction becomes important. Between 10 and 100% of the incident probe light intensity was deflected by the condensate.

By focusing the camera onto the Fourier plane of the first imaging lens, we were able to directly record the angular distribution of scattered light. The BEC phase transition was accompanied by a sudden increase of the scattering angle. The rms scattering angle of the thermal cloud, ≈7 mrad, is the diffraction angle of a cloud with radial diameter 20 μm, in agreement with the size of a 1.5-μK cloud in the magnetic trapping potential (Fig. 4). The angular scattering pattern of the condensate has an rms width of ≈20 mrad, in agreement with the size and shape of the condensate as calculated by the nonlinear Schrödinger equation and the Thomas-Fermi approximation (*19*).

The results presented here demonstrate that dispersive light scattering is an important method for study of BEC. Although we have emphasized qualitative aspects in the present study, quantitative measurements are possible because the signal in dispersive imaging depends only on the phase shift δ; δ is an absolute measure of the line-of-sight integrated atomic density. For small phase shifts, which are obtained at large detunings, the fraction of scattered light in dark-ground imaging is δ^2. A signal linear in δ can be obtained by implementing the phase contrast method.

This work is the starting point for a systematic study of the optical properties of a Bose condensate (*20*). Additional measurements at 100-MHz detuning showed several fringes in dark-ground images as a result of phase shifts $\delta > 2\pi$. We are currently setting up an independent dye laser to characterize the optical properties of the condensate starting from large detunings. It has been predicted that the linewidth of a Bose condensate shows superradiant broadening (*21*). On the other hand, the dispersive signal at far detuning is independent of the linewidth and therefore particularly suited for quantitative measurements. Quantum-statistical effects on the index of refraction have been calculated (*22*) but are only noticeable near the phase transition and vanish at $T = 0$.

We have presented dispersive light scattering as a nondestructive method. Strictly speaking, however, quantum mechanics does not allow nonperturbative measurements. Although dispersive scattering does

Fig. 3. Demonstration of nondestructive imaging. (**A**) Images of the same condensate taken 1 s apart. The axial and radial field curvature were 0.1 and 30 kG/cm², respectively, resulting in an aspect ratio of the trapped cloud of about 20. (**B**) Dynamics of a single condensate. The two pictures were taken 6 s apart during radial decompression of the cloud. The final radial field curvature (right) was 3 kG/cm².

Fig. 4. Angular distribution of the scattered light. The trapping field curvatures are the same as in Fig. 3A. The figure shows the intensity of the scattered light in the Fourier plane of the imaging system, that is, the intensity as a function of the radial and axial scattering angles. The upper image is for a cloud just above BEC, and the lower one is for an almost pure condensate. The central parts of the images are obscured by a 1.0-mm-diameter wire blocking the undeflected probe beam.

not heat up the cloud and destroy the condensate, it will change its phase as a result of frequency shifts by the ac Stark effect. This still allows a nonperturbative measurement of the number of condensed atoms, which is the variable complementary to the phase (so-called quantum nondemolition measurement), and would be the inverse situation compared to related measurements in microwave cavities where the photon number can be determined from the phase shift of Rydberg atoms passing through the cavity (*23*).

REFERENCES AND NOTES

1. A. Griffin, D. W. Snoke, S. Stringari, Eds., *Bose-Einstein Condensation* (Cambridge Univ. Press, Cambridge, 1995).
2. K. Huang, *Statistical Mechanics* (Wiley, New York, ed. 2, 1987).
3. W. E. Lamb Jr. and A. Nordsieck, *Phys. Rev.* **59**, 677 (1941).
4. P. E. Sokol, in (*1*), pp. 51–85.
5. J. L. Lin and J. P. Wolfe, *Phys. Rev. Lett.* **71**, 1222 (1993).
6. M. H. Anderson, J. R. Ensher, M. R. Matthews, C. E. Wieman, E. A. Cornell, *Science* **269**, 198 (1995).
7. K. B. Davis *et al.*, *Phys. Rev. Lett.* **75**, 3969 (1995).
8. T. J. Greytak, in (*1*), pp. 131–159.
9. W. Petrich, M. H. Anderson, J. R. Ensher, E. A. Cornell, *Phys. Rev. Lett.* **74**, 3352 (1995).
10. K. B. Davis *et al.*, *ibid.*, p. 5202.
11. E. Arimondo, W. D. Phillips, F. Strumia, Eds., *Proceedings of the International School of Physics "Enrico Fermi," Course CXVIII* (North-Holland, Amsterdam, 1992).
12. C. C. Bradley, C. A. Sackett, J. J. Tollett, R. G. Hulet, *Phys. Rev. Lett.* **75**, 1687 (1995).
13. Book of abstracts, *Workshop on Collective Effects in Ultracold Atomic Gases*, Les Houches, France, 1–5 April 1996.
14. E. Hecht, *Optics* (Addison-Wesley, Reading, MA, ed. 2, 1989).
15. M.-O. Mewes *et al.*, *Phys. Rev. Lett.*, in press.
16. D. E. Pritchard, K. Helmerson, A. G. Martin, in *Atomic Physics 11*, S. Haroche, J. C. Gay, G. Grynberg, Eds. (World Scientific, Singapore, 1989), pp. 179–197; W. Ketterle and N. J. van Druten, in *Advances in Atomic, Molecular and Optical Physics*, B. Bederson and H. Walther, Eds. (Academic Press, San Diego, in press), vol. 37.
17. It was a coincidence that the ideal detuning for this work was close to the 1.77 GHz ground-state hyperfine splitting in sodium.
18. S. R. de Groot, G. J. Hooyman, C. A. ten Seldam, *Proc. R. Soc. London Ser. A* **203**, 266 (1950).
19. G. Baym and C. J. Pethick, *Phys. Rev. Lett.* **76**, 6 (1996).
20. L. You, M. Lewenstein, R. J. Glauber, J. Cooper, *Phys. Rev. A* **53**, 329 (1996).
21. J. Javanainen, *Phys. Rev. Lett.* **72**, 2375 (1994).
22. O. Morice, Y. Castin, J. Dalibard, *Phys. Rev. A* **51**, 3896 (1995).
23. M. Brune *et al.*, *Phys. Rev. Lett.* **65**, 976 (1990).

24. We are grateful to D. Pritchard for valuable comments on the manuscript and thankfully acknowledge C. Townsend for assistance in the final stages of the experiment. This work was supported by the Office of Naval Research, NSF, Joint Services Electronics Program, and the Sloan Foundation. M.-O.M. and D.M.K. acknowledge financial support from Studienstiftung des Deutschen Volkes and an NSF Graduate Research Fellowship, respectively, and N.J.v.D., from Nederlandse Organisatie voor Wetenschappelijk Onderzoek (NWO) and Netherlands America Commission for Education Exchange (Fulbright fellowship).

29 May 1996; accepted 11 June 1996

Chapter 4

The atom laser

This chapter will be devoted to the concept of the 'atom laser', which has been rudimentarily realized by the references [19] and [9, (4.3)]. Essential to this realization was the demonstration of interference between two condensates [9, (4.3)], and the technique of splitting a coherent matter wave with an 'output coupler' [19]. Whereas the simultaneous interference of a large number of atoms was a demonstration of the so-called 'first-order' coherence of condensates, higher order coherences are also important for conceptions of the laser. First-order coherence establishes the presence of a relative phase, which also ties in with 'spontaneous symmetry breaking'. Second-order coherence was measured by the mean-field energy due to two-body interactions, and third-order coherence was measured by the three-body recombination rate at high density [12, 11]. These measurements show condensates to be clearly 'laser-like' in their coherences, in that density fluctuations are close to a fundamental limit. The results for second and third order coherences can be summed up by saying that the bosons in a condensate are randomly distributed without any bunching or voids, which is just like the optical laser whose photons arrive independently at a detector. Later, the observation of bosonic stimulation as an important feature in condensate formation gave additional support to the identification of a Bose condensate as a coherent matter wave [13]. As in an optical laser, stimulated, or 'amplified' processes are required to obtain a large population of particles in a single quantum state. Although there is no universally accepted definition for lasers, a laser beam is expected not only to be coherent like a classical stable wave, but also bright in terms of flux. Deficiencies in these areas lead one to apply the adjective 'rudimentary' to the present demonstration; these issues and a critical examination of lasers, in general, are discussed by Wiseman in reference [38]. Particularly insightful is Kleppner's discussion in reference [39].

The first implementation of an atom laser emitted pulses of condensed atoms by a repetitious application of rf radiation to the cloud. Each sweep of rf over the atomic hyperfine resonance coupled atoms to a magnetically neutral or expelled state. These untrapped atoms fell due to gravity and

also expanded due to repulsive interactions. The particular atom laser shown in figure (4-1) emits about a hundred thousand atoms per millisecond, and is pulsed at 200 Hz; reference [40] treats the output of a pulsed atom laser theoretically. After the trapped condensate is exhausted of atoms, a new cycle of trapping and cooling begins, and about 30 seconds later the atom laser is returned to its initial state. Note that the reference [19] images the atom laser from above, whereas here it is imaged from the side.

Atom lasers are expected to have select applications as a future generation of atomic beams. The possibilities for using atomic beams include atomic clocks, atom optics, precision measurements of fundamental constants, tests of fundamental symmetries, atomic beam deposition for chip production (atom lithography), and even nanotechnology [41], although it is not clear how (or if) atom lasers can make their impact in each of these areas. Although the flux of an atomic beam is an important quality, so is its temperature. Whereas for an atom laser it is not the low temperature which is paramount, but the coherence of the condensate. Atom laser beams are coherent matter waves that are ideally diffraction limited. With less than a femtomole per second of atomic flux, certain applications requiring the buildup of macroscopic amounts of coherent matter will have to wait for further technical developments. On the other hand, applications requiring the ability to make use of the coherence of an atom laser can begin to proceed immediately. For instance, whereas the usual shot-noise limit for spectroscopy scales with $1/\sqrt{N}$ (N is the number of particles), coherence limited spectroscopy is expected to scale more favorably as $1/N$ [42].

4.1 Interference

Interference between two condensates was a 'smoking gun' for the condensate's quantum nature and the long-range correlations it must possess. In conventional beam sources, every atom comes with its own random phase. For this reason, two separated clouds of uncondensed atoms will not exhibit an interference pattern when overlapped. Two cells each of volume $\hbar^3$ of phase space can interfere coherently with each other, but their interference with other cells carries a random phase. A key point is that condensed sources are mainly contained within a single such cell, whereas uncondensed ones occupy many cells and the interfering amplitudes from a large number average out.

The experiment that allowed an observation of interference between Bose condensates was configured in the following way. Two condensates were formed in a cloverleaf trap with a central barrier of focused green laser light, shown in figure (4-2). These condensates were then released into free space and allowed to overlap. In the overlap region, a slice of atoms was selected by optical pumping, in anticipation of having to enhance the resolution of a finely striated structure (the fringes). Probing the atoms quickly then revealed interference fringes having a range of periods about 15 μm. Varied over many experiments was the power in the green laser, which correspondingly affected the initial

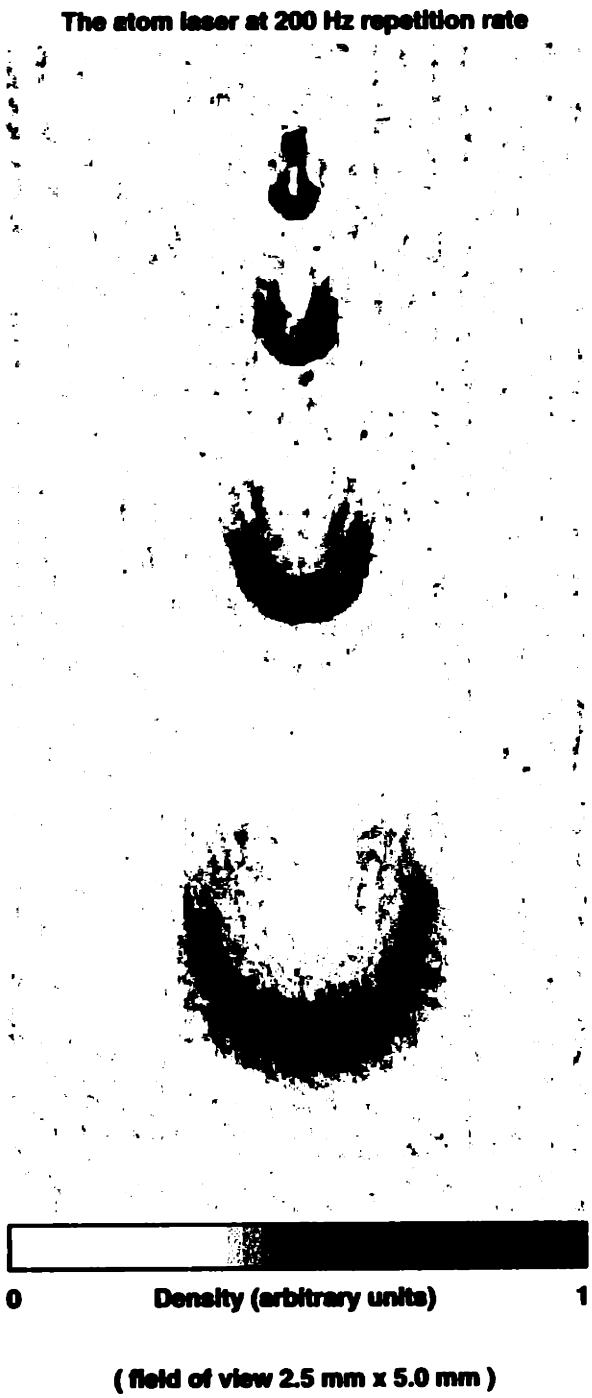

Figure 4-1: The atom laser. Pulses of atoms were created at 200 Hz repetition rate [19] and fell down in the image due to gravity. The pulses also spread as they fell to release their interaction energy.

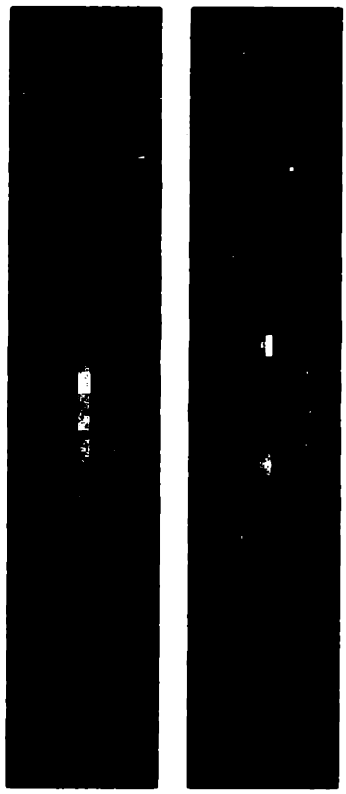

Figure 4-2: One or two long clouds in the cloverleaf trap. On the left is a single cloud, and at right are two clouds separated by a focused argon-ion laser sheet of several mW power. The picture on the right was the initial state for the published interference experiments [9, (4.3)].

separation of the condensates. In rough accordance with de Broglie's relation $\lambda = h/p$, the relative velocities of atoms during imaging led to a particular matter wavelength which was then observed. Since the condensates were always allowed to expand for the same time, 40 ms, as the initial separation became smaller the relative velocity of atoms also became smaller at particular locations in space. See figure (4-3) for examples of interferences between two condensates as a function of their initial separation. Note that straight fringes are characteristic of a pulsed experiment, where here the pulse is the release of trapped condensates. A more complete description of the experiment can be found in the publication [9, (4.3)]. Later, it was remarkable that the observed interference fringes closely matched what can be simulated using the Gross-Pitaevskii equation [43].

To test the interpretation of the fringes as being due to interference, one of the two trapped condensates was destroyed with resonant light to see if the fringes would disappear. Indeed, they did — see figure (4-4), showing that it takes two overlapping clouds to make an interference pattern. The envelope of each half-cloud was the same irrespective of the presence of fringes. Showing the same phenomenon in a different situation also bolsters the interpretation of interference. Thus, interference experiments were also done with halved round clouds, for instance as shown in figure (4-5). These clouds were geometrically more compact than the longer clouds of figure (4-2) and so

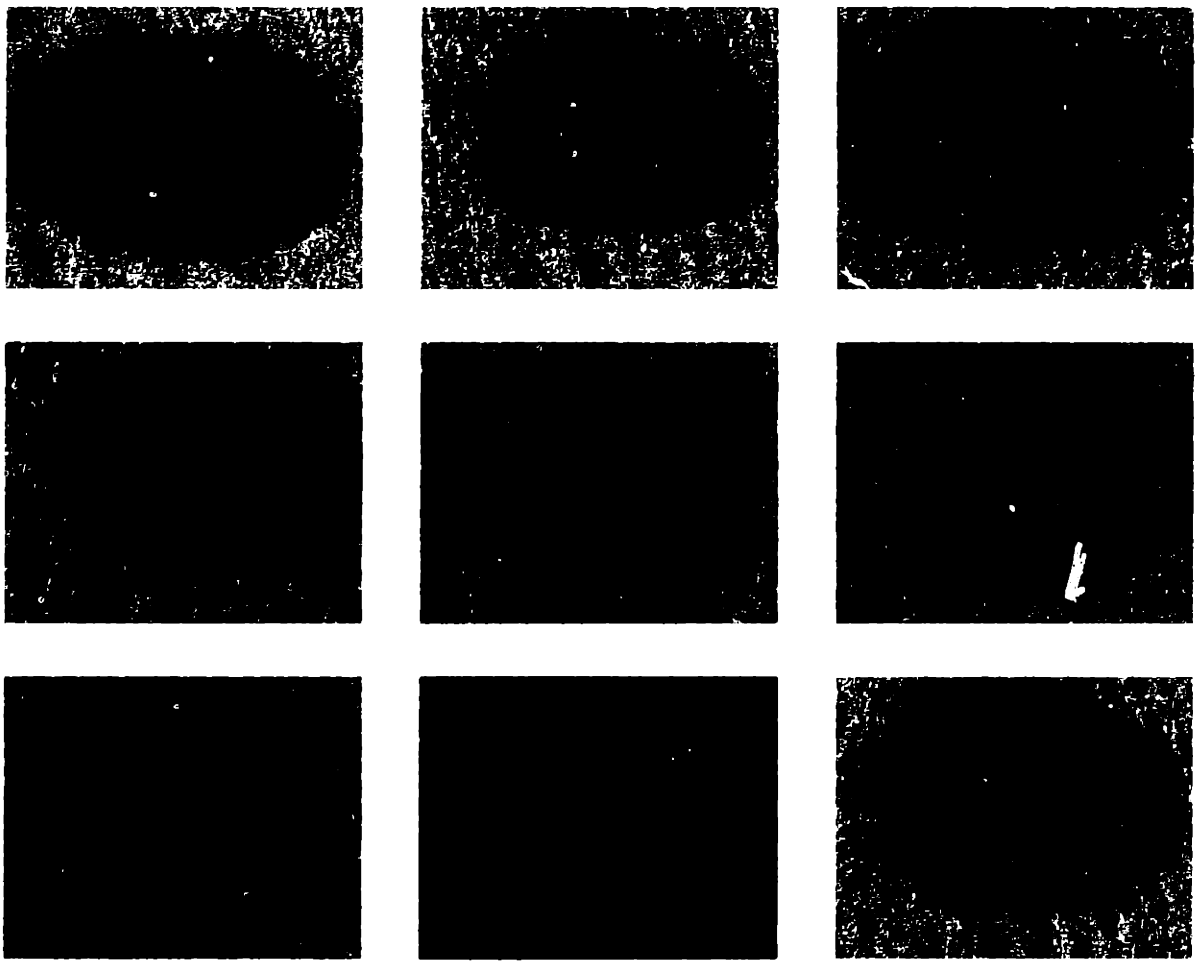

Figure 4-3: A series of interferences between two condensates. The initial separation between condensates was varied by changing the power in argon-ion laser barrier between 1.5 mW (upper left) and 3.5 mW (lower right). The 'cats-eye' feature at the lowest powers indicate that the condensates were initially very close or even touching. (Graphics courtesy of H.-J. Miesner)

Figure 4-4: Whole, double, and half condensates in free expansion. Images are horizontally binned to improve the signal. On the left is a single condensate in free expansion, having started in the trap as in the left half of figure (4-2). In the middle are two condensates expanding into each other, having started in the trap as in the right half of figure (4-2). On the right is a single condensate, with one of the two destroyed by focused resonant light while still in the trap. This shows that it takes two condensates to create an interference pattern.

yielded interference fringes of larger periods close to 25 μm; see figure (4-6). Round clouds were also employed in a study investigating vortices and persistent currents, to be described in chapter 5. The $\sim$ 50% contrast in the round cloud interference fringes of figure (4-6) is not yet understood. Whereas the lower contrast in finer fringes such as those in figure (4-3) could be attributed to imaging resolution, it is more difficult to make the same allowances for the round cloud's fringes, which are larger. Indeed, at 25 μm (40 lp/mm), the modulation transfer function was measured afterwards to be high (approaching 100%), and so the lack of contrast could have originated elsewhere. This result is preliminary, and further study is warranted before definite conclusions can be drawn. Possibilities include the blurred selection of a slice of atoms by optical pumping (flawed 3-d tomographic imaging), an actual lack of coherence of the pattern, or the presence of a significant thermal fraction. A thermal fraction was not detected in the trap, however, and does not seem to contribute significantly to the optical density in figure (4-6).

4.2 Phase

'Spontaneous symmetry breaking' is an important issue in the interference of two condensates, and addresses the existence of a relative quantum phase. More generally, symmetry breaking is ubiquitous and related to a broad range of physical phenomena. For instance, the standard model of particle physics needs it in a fundamental way to resolve the masses of particles via the Higgs field. Symmetry breaking is nature's way of making sure that the ground state of a system is

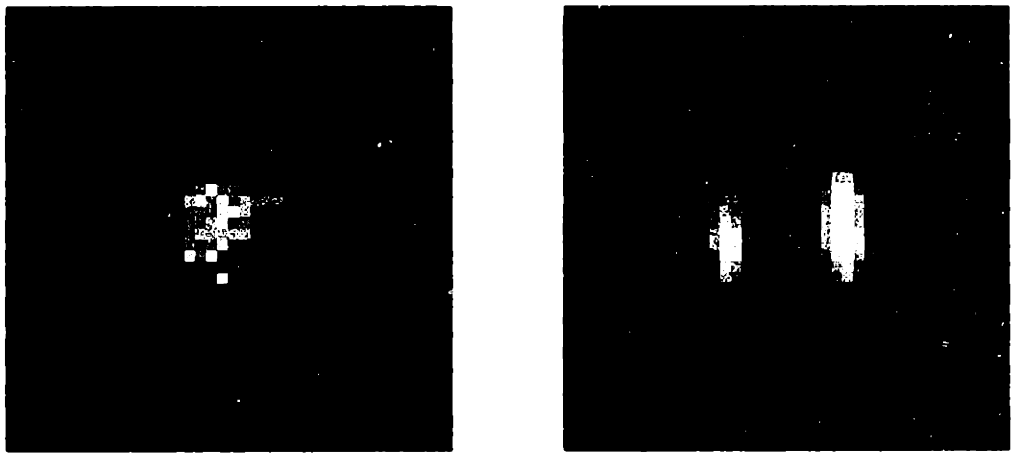

Figure 4-5: A round cloud halved by a focused argon-ion laser sheet in the magnetic trap. The round cloud was made by applying several tens of gauss magnetic bias field to the magnetic trap, weakening the radial confinement until it became comparable to the axial. An argon-ion laser beam sheet was focused into the center of the cloud and repelled atoms due to the optical dipole force, forming two halves.

Figure 4-6: Interference between halves of a round cloud. The two halves of a round cloud in figure (4-5) expand in space and give interference fringes on the order of 25 μm and 50% contrast.

unique. If there is a range of ground states all with the same energy, then any lack of symmetry in the system or its environment could give one of those ground states a preference over the others. Even if not, a particular ground state will become the one realized by the system. This particular ground state will not show the full symmetry of the underlying physical laws. A classic example is a ferromagnetic substance: at zero temperature any orientation for the total magnetization is as good as any other, but because of subtle initial conditions the orientation winds up being in a particular direction. Assuming there are no external magnetic fields, one is free to rotate the ferromagnet and its energy would remain the same. Thus the symmetry has been spontaneously broken and there are 'Goldstone modes' corresponding to excitations of the system in that symmetry variable. Free rotation of the magnetized object in field-free intergalactic space would be an example of this mode. Apply an external field, however, and the low-lying Goldstone modes would correspond to oscillations about the lowest energy orientation.

In the context of Bose condensation, the spontaneously broken symmetry would be the absolute phase $0 \leq \phi \leq 2\pi$ of the system, and the Goldstone modes would correspond to changes in the phase over time. The modes are diffusion of the phase which is predicted to happen at constant density, and excitations (phonons) which also involve variations of the density. Local variations in phase during collective excitations experience a restoring force because they lead to density changes, which increase the mean-field interaction energy above its ground state value. This is because phase gradients are proportional to velocities, which result in the movement of atoms and corresponding variations of the density over time.

In the interference of two condensates released from a trap, the absolute phase of the interference fringes would be due to the relative phases of the two condensates. If the condensates are truly breaking their phase symmetry in a random way, then their relative phase will also be random and so too the position of the central interference fringe. Although it was important to be able to differentiate between a random relative phase and a fixed one, the experimental conditions were not controlled enough. Either the imaging system or parts of the trap itself were not stable at the micron level, which was required to determine the relative phase absolutely. In the study of halves of a round cloud that were made to interfere, the interference fringes were of larger period and it was hoped symmetry breaking could be better addressed. Unfortunately, this system also exhibited fringes that jumped in position from shot to shot, which was most probably due to the jittering laser beam dividing the sample. Several degrees of angular jitter were also observed for these clouds. See figure (4-6).

The image of a condensate (on a ccd camera, for instance) can be taken as analogous to a diagram indicating what one could see in an ordinary atomic interferometer. One difference is that condensates consist of many atoms and atomic interferometers work with only one atom at a time. Rather than considering two condensates as independent entities coming together for the 'first time'

when interfering, they can be considered as two parts of a single superposition state whose history is unknown. The unknown history gives a random phase, and this ties in with the broken symmetry. In an ordinary interferometer, however, the known geometry determines the relative phase, and would correspond to the case of dividing a single condensate in two and interfering the two halves thereafter. The multiparticle aspects of the condensate are not treated by this picture. For instance, if a condensate originally in a definite number state is split, then entanglements between the pair are fundamentally quantum mechanical (as with 'EPR' states), whereas if the condensate was in a coherent state, the split pair will behave classically in the same way that optical laser beams do. Either way, classical or not, the same kinds of interference fringes are predicted [44].

4.3 'Observation of Interference Between Two Bose Condensates'

For this section the following paper is presented:

- 'Observation of Interference Between Two Bose Condensates', by M. R. Andrews, C. G. Townsend, H.-J. Miesner, D. S. Durfee, D. M. Kurn, and W. Ketterle. *Science*, Vol. 275, p. 637, 1997. Reference [9].

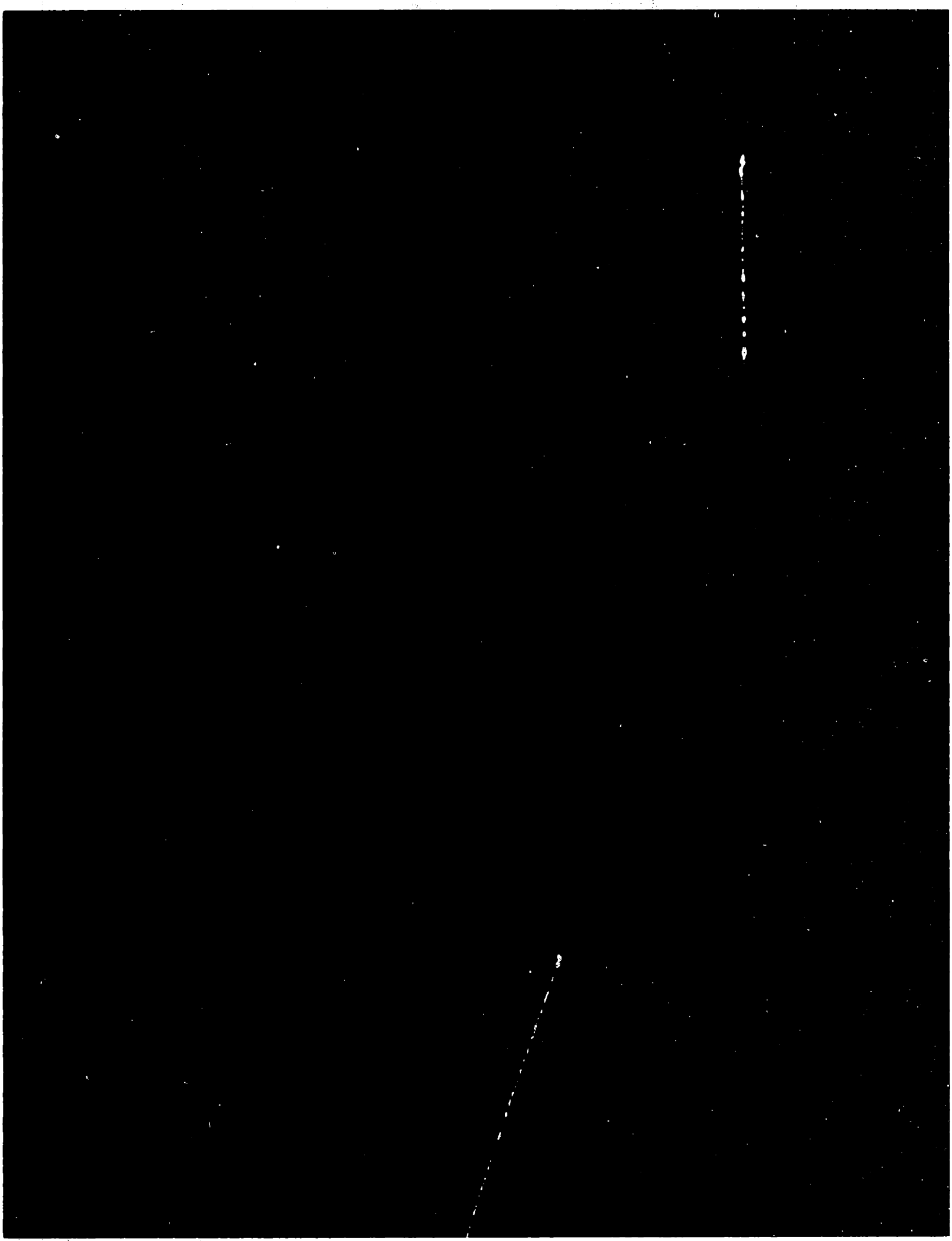

COVER

Matter wave interference of two freely expanding and overlapping Bose-Einstein condensates. The density of atomic sodium (vertical axis, in false color) is shown in an area of 0.1 millimeter by 0.4 millimeter containing about 50,000 atoms. The high-contrast interference fringes demonstrate that Bose-Einstein condensates are "laser-like," made of atoms occupying a single controllable quantum state. See page 637 and the related News story on page 617. [Image: Dallin Durfee]

Observation of Interference Between Two Bose Condensates

M. R. Andrews, C. G. Townsend, H.-J. Miesner, D. S. Durfee, D. M. Kurn, W. Ketterle

Interference between two freely expanding Bose-Einstein condensates has been observed. Two condensates separated by ~40 micrometers were created by evaporatively cooling sodium atoms in a double-well potential formed by magnetic and optical forces. High-contrast matter-wave interference fringes with a period of ~15 micrometers were observed after switching off the potential and letting the condensates expand for 40 milliseconds and overlap. This demonstrates that Bose condensed atoms are "laser-like"; that is, they are coherent and show long-range correlations. These results have direct implications for the atom laser and the Josephson effect for atoms.

The realization of Bose-Einstein condensation (BEC) in dilute atomic gases has created great interest in this new form of matter. One of its striking features is a macroscopic population of the quantum-mechanical ground state of the system at finite temperature. The Bose condensate is characterized by the absence of thermal excitation; its kinetic energy is solely the result of zero-point motion in the trapping potential (in general, modified by the repulsive interaction between atoms). This is the property that has been used to detect and study the Bose condensate in previous experiments. The Bose-Einstein phase transition was observed by the sudden appearance of a "peak" of ultracold atoms, either in images of ballistically expanding clouds (time-of-flight pictures) (*1*–*3*) or as a dense core inside the magnetic trap (*4*, *5*). The anisotropic expansion of the cloud (*1*–*3*) and the appearance of collective excitations at frequencies different from multiples of the trapping frequencies (*6*, *7*) were found to be in quantitative agreement with the predictions of the mean-field theory for a weakly interacting Bose gas (*8*–*11*). However, similar anisotropic expansion and excitation frequencies have been predicted for a dense classical gas in the hydrodynamic regime (*12*, *13*) and are therefore not distinctive features of BEC. Indeed, the nonlinear Schrödinger equation is equivalent to a hydrodynamic equation for superfluid flow, which, in many situations, is very similar to a classical hydrodynamic equation (*9*, *13*, *14*). Previous BEC studies have mainly concerned the "very cold" nature of the Bose condensate but have not revealed properties that directly reflect its coherent nature, such as its phase, order parameter (macroscopic wave function), or long-range order. In superconductors, the phase of the order parameter was directly observed through the Josephson effect, whereas in superfluid helium the observation of the motion of quantized vortices (*15*) provided indirect evidence.

The coherence of a Bose condensate has been the subject of many theoretical studies. Kagan and collaborators predicted that the Bose condensate will form first as a quasi-condensate consisting of very cold atoms but lacking long-range order, which is only established on a much longer time

The authors are in the Department of Physics and Research Laboratory of Electronics, Massachusetts Institute of Technology, Cambridge, MA 02139, USA.

scale (*16*). Stoof predicted that a coherent condensate would form immediately (*17*). Several groups discussed interference experiments and quantum tunneling for condensates (*18–29*). If the condensate is initially in a state of well-defined atom number, its order parameter, which is the macroscopic wave function, vanishes. However, the quantum measurement process should still lead to quantum interference and "create" the phase of the condensate (*20*, *23–25*, *27*, *28*), thus breaking the global gauge invariance that reflects particle number conservation (*30*). This is analogous to Anderson's famous gedanken experiment, testing whether two initially separated buckets of superfluid helium would show a fixed value of the relative phase—and therefore a Josephson current—once they are connected (*31*).

Arguments for and against such a fixed relative phase have been given (*31*, *32*). Even if this phase exists, there has been some doubt as to whether it can be directly measured, because it was predicted to be affected by collisions during ballistic expansion (*12*, *26*) or by phase diffusion resulting from the mean field of Bose condensed atoms (*21*, *25*, *27*, *33*). Additionally, the phase of the condensate plays a crucial role in discussions of an atom laser, a source of coherent matter waves (*34–37*).

The phase of a condensate is the argument of a complex number (the macroscopic wave function) and is not an observable. Only the relative phase between two condensates can be measured. Here, we report on the observation of high-contrast interference between two atomic Bose condensates, which is clear evidence for coherence in such systems.

The experimental setup. Two Bose condensates were produced using a modification of our previous setup (*3*, *7*). Sodium atoms were optically cooled and trapped and were then transferred into a double-well potential. The atoms were further cooled by radio frequency (rf)–induced evaporation (*38*). The condensates were confined in a cloverleaf magnetic trap (*3*), with the trapping potential determined by the axial curvature of the magnetic field $B'' = 94$ G cm^{-2}, the radial gradient $B' = 120$ G cm^{-1}, and the bias field $B_0 = 0.75$ G. The atom clouds were cigar-shaped, with the long axis horizontal. A double-well potential was created by focusing blue-detuned far-off-resonant laser light into the center of the magnetic trap, generating a repulsive optical dipole force. Because of the far detuning of the argon ion laser line at 514 nm relative to the sodium resonance at 589 nm, heating from spontaneous emission was negligible. This laser beam was focused into a light sheet with a cross section of 12 μm by 67 μm ($1/e^2$ radii), with its long axis perpendicular to the long axes of the condensates. The argon ion laser beam propagated nearly collinearly with the vertical probe beam. We aligned the light sheet by imaging the focused argon ion laser beam with the same camera used to image the condensates.

Evaporative cooling was extended well below the transition temperature to obtain condensates without a discernible normal fraction. Condensates containing 5×10^6 sodium atoms in the $F = 1, m_F = -1$ ground state were produced within 30 s. The presence of the laser-light sheet neither changed the number of condensed atoms from our previous work (*3*) nor required a modification of the evaporation path; hence, problems with heating encountered earlier with an optically plugged magnetic trap (*2*) were purely technical. In the present application, the argon ion laser beam was not needed to avoid a loss process, and thus we had complete freedom in the choice of laser power and focal parameters.

The double condensate was directly observed by nondestructive phase-contrast imaging (Fig. 1A). This technique is an extension of our previous work on dispersive imaging (*4*) and greatly improved the signal-to-noise ratio. The probe light frequency was far detuned from a resonant transition (1.77 GHz to the red), and thus absorption was negligible. Images were formed by photons scattered coherently in the forward direction. The phase modulation caused by the condensate was transformed into an intensity modulation at the camera by retarding the transmitted probe beam by a quarter-wave with a phase plate in the Fourier plane. Previously, the transmitted probe beam was blocked by a thin wire (dark-ground imaging).

Interference between the condensates was observed by simultaneously switching off the magnetic trap and the argon ion laser-light sheet. The two expanding condensates overlapped and were observed by absorption imaging. After 40 ms time-of-flight, an optical pumping beam transferred the atoms from the $F = 1$ hyperfine state to the $F = 2$ state. With a 10-μs delay, the atoms were exposed to a short (50 μs) circularly polarized probe beam resonant with the $F = 2 \rightarrow F' = 3$ transition and absorbed ~20 photons each. Under these conditions, the atoms moved ~5 μm horizontally during the exposure.

Absorption imaging usually integrates along the line of sight and therefore has only two-dimensional spatial resolution. Because the depth of field for 15-μm fringes is comparable to the size of an expanded cloud, and because the fringes are in general not parallel to the axis of the probe light, line-of-sight integration would cause considerable blurring. We avoided this problem and achieved three-dimensional resolution by restricting absorption of the probe light to a thin horizontal slice of the cloud. The optical pumping beam was focused into a light sheet of adjustable thickness (typically 100 μm) and a width of a few millimeters; this pumping beam propagated perpendicularly to the probe light and parallel to the long axis of the trap (*39*). As a result, the

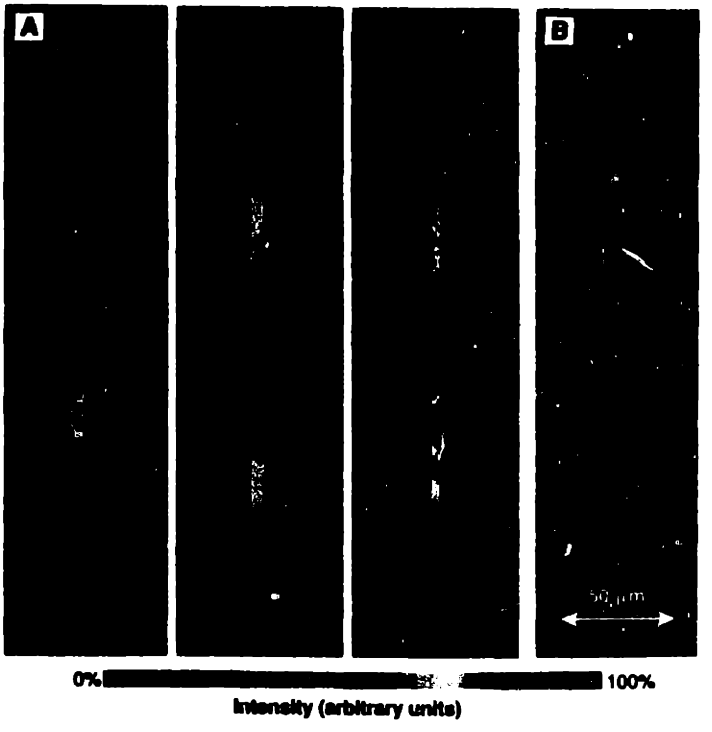

Fig. 1. (A) Phase-contrast images of a single Bose condensate (left) and double Bose condensates, taken in the trap. The distance between the two condensates was varied by changing the power of the argon ion laser-light sheet from 7 to 43 mW. (B) Phase-contrast image of an originally double condensate, with the lower condensate eliminated.

probe light was only absorbed by a thin slice of the cloud where the atoms were optically pumped. Because high spatial resolution was required from only the fraction of atoms residing in the slice, a good signal-to-noise ratio required condensates with millions of atoms.

Interference between two Bose condensates. In general, the pattern of interference fringes differs for continuous and pulsed sources. Two point-like monochromatic continuous sources would produce curved (hyperbolic) interference fringes. In contrast, two point-like pulsed sources show straight interference fringes; if d is the separation between two point-like condensates, then their relative speed at any point in space is d/t, where t is the delay between pulsing on the source (switching off the trap) and observation. The fringe period is the de Broglie wavelength λ associated with the relative motion of atoms with mass m,

$$\lambda = \frac{ht}{md} \qquad (1)$$

where h is Planck's constant. The amplitude and contrast of the interference pattern depends on the overlap between the two condensates.

The interference pattern of two condensates after 40 ms time-of-flight is shown in Fig. 2. A series of measurements with fringe spacings of ~15 μm showed a contrast varying between 20 and 40%. When the imaging system was calibrated with a standard optical test pattern, we found ~40% contrast at the same spatial frequency. Hence, the contrast of the atomic interference was between 50 and 100%. Because the condensates are much larger than the observed fringe spacing, they must have a high degree of spatial coherence.

We observed that the fringe period became smaller for larger powers of the argon ion laser-light sheet (Fig. 3A). Larger power increased the distance between the two condensates (Fig. 1A). From phase-contrast images, we determined the distance d between the density maxima of the two condensates versus argon ion laser power. The fringe period versus maxima separation (Fig. 3B) is in reasonable agreement with the prediction of Eq. 1, although this equation strictly applies only to two point sources. Wallis *et al.* (26) calculated the interference pattern for two extended condensates in a harmonic potential with a Gaussian barrier. They concluded that Eq. 1 remains valid for the central fringes if d is replaced by the geometric mean of the separation of the centers of mass and the distance between the density maxima of the two condensates. This prediction is also shown in Fig. 3B. The agreement is satisfactory given our experimental uncertainties in the determination of the maxima separations (~3 μm) and of the center-of-mass separations (~20%). We conclude that the numerical simulations for extended interacting condensates (26) are consistent with the observed fringe periods.

We performed a series of tests to support our interpretation of matter-wave interference. To demonstrate that the fringe pattern was caused by two condensates, we compared it with the pattern from a single condensate (this is equivalent to performing a double-slit experiment and covering one of the slits). One condensate was illuminated with a focused beam of weak resonant light 20 ms before release, causing it to disappear almost completely as a result of optical pumping to untrapped states and evaporation after heating by photon recoil (Fig. 1B). The resulting time-of-flight image did not exhibit interference, and the profile of a single expanded condensate matched one side of the profile of a double condensate (Fig. 4). The profile of a single expanded condensate showed some coarse structure, which most likely resulted from the nonparabolic shape of the confining potential. We found that the structure became more pronounced when the focus of the argon ion laser had some weak secondary intensity maxima. In addition, the interference between two condensates disappeared when the argon ion laser-light sheet was left on for

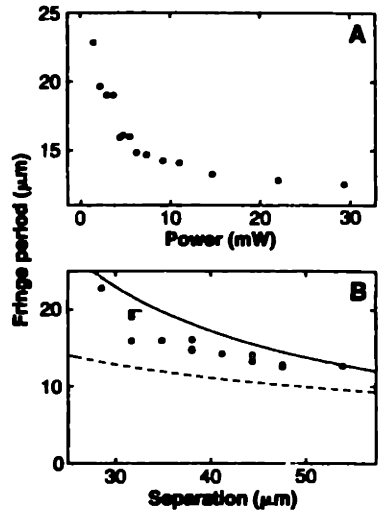

Fig. 3. (A) Fringe period versus power in the argon ion laser-light sheet. (B) Fringe period versus observed spacing between the density maxima of the two condensates. The solid line is the dependence given by Eq. 1, and the dashed line is the theoretical prediction of (26) incorporating a constant center-of-mass separation of 96 μm, neglecting the small variation (±10%) with laser power.

Fig. 2. Interference pattern of two expanding condensates observed after 40 ms time-of-flight, for two different powers of the argon ion laser-light sheet (raw-data images). The fringe periods were 20 and 15 μm, the powers were 3 and 5 mW, and the maximum absorptions were 90 and 50%, respectively, for the left and right images. The fields of view are 1.1 mm horizontally by 0.5 mm vertically. The horizontal widths are compressed fourfold, which enhances the effect of fringe curvature. For the determination of fringe spacing, the dark central fringe on the left was excluded.

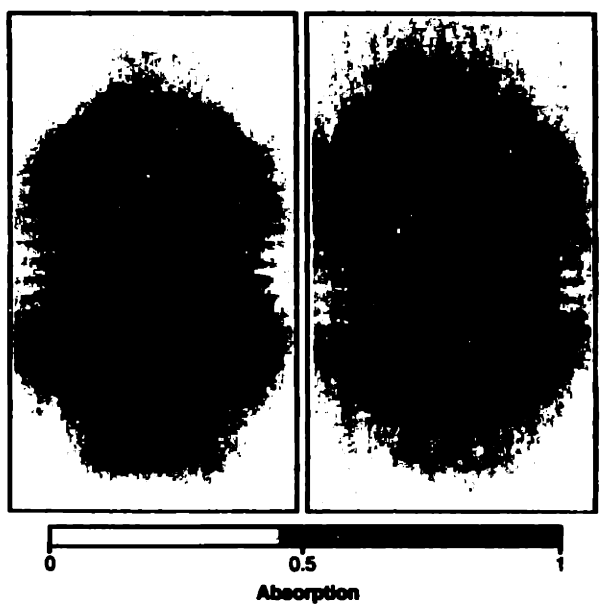

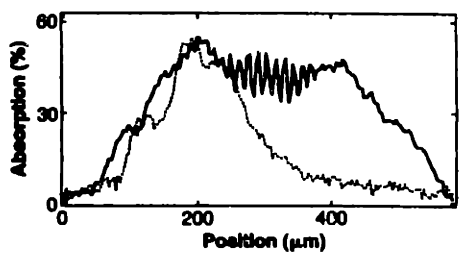

Fig. 4. Comparison between time-of-flight images for a single and double condensate, showing vertical profiles through time-of-flight pictures similar to Fig. 2. The solid line is a profile of two interfering condensates, and the dotted line is the profile of a single condensate, both released from the same double-well potential (argon ion laser power, 14 mW; fringe period, 13 μm; time of flight, 40 ms). The profiles were horizontally integrated over 450 μm. The dashed profile was multiplied by a factor of 1.5 to account for fewer atoms in the single condensate, most likely the result of loss during elimination of the second half.

2 ms after the magnetic trap was switched off. The absorption images showed that the two condensates were pushed apart and did not subsequently overlap.

Another test confirmed that the fringes were not attributable to density waves of two colliding condensates. Because the interference pattern depends on the phases of the condensates, the fringes should be sensitive to perturbations that strongly affect the phase but weakly affect the motion. Applying resonant rf radiation during the expansion of the two condensates caused a reduction of the fringe contrast by up to a factor of 4. The greatest reduction in contrast was found when the rf was swept 25 times between 0 and 300 kHz at 1 kHz. When a single condensate was exposed to the same rf radiation, no clearly discernible differences in the time-of-flight pictures were found. A possible explanation for the reduced fringe contrast is that frequent sweeps through the resonance in slightly inhomogeneous dc and rf magnetic fields created atoms in different superpositions of hyperfine states that only partially interfered.

The visibility of the fringes depended critically on several imaging parameters, as expected for the observation of such a finely striated structure. The fringes became almost invisible when the thickness of the optical pumping sheet was increased to 800 μm, whereas the focus of the imaging system could be varied over a wider range of up to ±1 mm without losing contrast. This implies that the fringes were at a small angle (~20 mrad) with respect to the probe beam.

The interference was remarkably robust. The fringes were very regular, although no attempt was made to control residual magnetic fields during the expansion. The high contrast implies that neither phase diffusion during expansion nor collisions with normal atoms were important. The latter aspect was studied in more detail when the rf evaporation was stopped at higher temperatures. We still observed fringes of identical contrast (40), but with decreasing amplitude because of the smaller number of condensed atoms. At the transition temperature, the fringes and the condensate disappeared.

We now consider whether the two condensates were truly independent. When the power of the argon ion laser was varied, we realized both well-separated and connected condensates. The chemical potential of the Bose condensates was ~4 kHz. The height of the barrier created by the argon ion laser was estimated to be ~2 kHz per milliwatt of power. At 100-mW laser power, the barrier height was 10 μK, resulting in a cloud that was already split well above the phase transition temperature of ~2 μK. The tunneling time of well-separated condensates was estimated to be greater than the age of the universe (19), and thus our experiment should be equivalent to Anderson's gedanken experiment ("What is the relative phase of two buckets of liquid helium?") (31) and also to an interference experiment between two independent lasers (41). Two independent condensates will show high-contrast interference fringes with a phase that varies between experiments (20, 23, 24, 27). In our experiment, however, even a fixed relative phase would have been detected as being random because of mechanical instabilities on a 10-μm scale. Once it becomes possible to distinguish between fixed and random phases, we should be able to investigate how phase coherence is established and lost. One possible experiment would be to adiabatically switch on the argon ion laser after condensation, thus splitting a single condensate, and to study how a definite phase becomes random as a function of time.

For argon ion laser powers below 4 mW, the interference pattern was slightly curved and symmetric about a central fringe that was always dark (Fig. 2). We conjecture that for small separations, the two condensates overlap very early during the expansion and interactions between them are not negligible. When the power of the laser-light sheet was lowered further, the number of fringes decreased, while the central dark feature persisted and eventually lost contrast. For such low powers we were in the regime where the condensates were not fully separated.

The observation of matter-wave interference with a 15-μm period required sources of atoms with a matter wavelength of 30 μm, corresponding to a kinetic energy of 0.5 nK or 1/2600th of the single-photon recoil energy. This energy is much smaller than the mean-field energy of Bose condensates in our trap (~100 nK) and also much less than the zero-point energy (~15 nK). Fortunately, the extremely anisotropic expansion of the condensates released from the cloverleaf trap yields atoms with very long de Broglie wavelengths in the axial direction.

Outlook. The techniques of condensate cutting and three-dimensional absorption imaging described above open up possibilities for further investigations. We have switched off the trap and observed the existence of the relative phase of two condensates. The next logical step is to combine this technique with our recently demonstrated output coupler for a Bose condensate (42). In that case, recording the interference pattern for the first output pulse creates a coherent state of the trapped condensate through the quantum measurement process. Subsequent output pulses could be used to study the time evolution of the phase and the loss of coherence resulting from phase diffusion (21, 27, 33).

By using a thinner barrier (~1 μm) between the two condensates, it should be possible to reliably establish a weak link and study quantum tunneling, or the Josephson effect, for atoms (18, 19, 29). For superconductors, the Josephson effect is the usual way of detecting the phase of the order parameter. For atomic Bose condensates, we observed a relative phase directly. This is an example of the complementary physics that can be explored with Bose condensation in dilute atomic gases. Moreover, we have shown the technical feasibility of manipulating magnetically trapped Bose condensates with far-off-resonant laser beams. Hence, it is possible to perform "microsurgery" of Bose condensates, such as shaping the trapping potential or creating localized excitations (for example, using such a laser beam as a "paddle wheel" to excite rotational motion).

The observation of high-contrast interference fringes is clear evidence for spatial coherence over the extent of the condensates (43). In theoretical treatments, coherence (off-diagonal long-range order) has been used as the defining criterion for BEC (30). Our results also demonstrate that a Bose condensate consists of "laser-like" atoms, or atoms that interfere without any further selection by collimating apertures. This opens up the field of coherent atomic beams. Our recent work on an output coupler for a Bose condensate (42) already contained all the elements of an atom laser (44), because it created multiple pulses that should have a coherence length exceeding the size of a single condensate. Although this has been described as the first realization of an atom laser (45), we felt the demonstration that Bose condensed atoms have a measurable phase was a crucial missing feature. The present work addresses this issue and demonstrates that a Bose condensate with an output coupler is an atom laser.

Note added in proof: We have recently combined the rf output coupler (42) with the observation of interference between two condensates. The output pulse from a split condensate showed high-contrast interference that was very similar to the results discussed above (46). This proves that the rf output coupler preserves the coherence of the condensates.

REFERENCES AND NOTES

1. M. H. Anderson, J. R. Ensher, M. R. Matthews, C. E. Wieman, E. A. Cornell, *Science* **269**, 198 (1995).
2. K. B. Davis *et al.*, *Phys. Rev. Lett.* **75**, 3969 (1995).
3. M.-O. Mewes *et al.*, *ibid.* **77**, 416 (1996).
4. M. R. Andrews *et al.*, *Science* **273**, 84 (1996).
5. C. C. Bradley, C. A. Sackett, R. G. Hulet, in preparation; see also C. C. Bradley *et al.*, *Phys. Rev. Lett.* **75**, 1687 (1995).

6. D. S. Jin, J. R. Ensher, M. R. Matthews, C. E. Wieman, E. A. Cornell, *Phys. Rev. Lett.* **77**, 420 (1996).
7. M.-O. Mewes *et al.*, *ibid.*, p. 988.
8. M. Edwards, P. A. Ruprecht, K. Burnett, R. J. Dodd, C. W. Clark, *ibid.*, p. 1671.
9. S. Stringari, *ibid.*, p. 2350.
10. M. Holland and J. Cooper, *Phys. Rev. A* **53**, R1954 (1996).
11. Y. Castin and R. Dum, *Phys. Rev. Lett.* **77**, 5315 (1996).
12. Y. Kagan, E. L. Surkov, G. V. Shlyapnikov, *Phys. Rev. A* **54**, R1753 (1996).
13. A. Griffin, W.-C. Wu, S. Stringari, in preparation.
14. P. Nozières and D. Pines, *The Theory of Quantum Liquids* (Addison-Wesley, Reading, MA, 1990), vol. 2.
15. P. W. Anderson, *Rev. Mod. Phys.* **38**, 298 (1966).
16. Y. Kagan, in *Bose-Einstein Condensation*, A. Griffin, D. Snoke, S. Stringari, Eds. (Cambridge Univ. Press, Cambridge, 1995), pp. 202–225.
17. H. T. C. Stoof, *ibid.*, pp. 226–245.
18. J. Javanainen, *Phys. Rev. Lett.* **57**, 3164 (1986).
19. F. Dalfovo, L. Pitaevskii, S. Stringari, *Phys. Rev. A* **54**, 4213 (1996).
20. J. Javanainen and S. M. Yoo, *Phys. Rev. Lett.* **76**, 161 (1996).
21. E. M. Wright, D. F. Walls, J. C. Garrison, *ibid.* **77**, 2158 (1996).
22. W. Hoston and L. You, *Phys. Rev. A* **53**, 4254 (1996).
23. M. Naraschewski, H. Wallis, A. Schenzle, J. I. Cirac, *ibid.* **54**, 2185 (1996).
24. J. I. Cirac, C. W. Gardiner, M. Naraschewski, P. Zoller, *ibid.*, p. R3714.
25. T. Wong, M. J. Collett, D. F. Walls, *ibid.*, p. R3718.
26. H. Wallis, A. Röhrl, M. Naraschewski, A. Schenzle, *ibid.*, in press.
27. Y. Castin and J. Dalibard, in preparation.
28. E. M. Wright, T. Wong, M. J. Collett, S. M. Tan, D. F. Walls, in preparation.
29. M. W. Jack, M. J. Collett, D. F. Walls, *Phys. Rev. A* **54**, R4625 (1996).
30. K. Huang, *Statistical Mechanics* (Wiley, New York, ed. 2, 1987).
31. P. W. Anderson, in *The Lesson of Quantum Theory*, J. D. Boer, E. Dal, O. Ulfbeck, Eds. (Elsevier, Amsterdam, 1986), pp. 23–33.
32. A. J. Leggett and F. Sols, *Found. Physics* **21**, 353 (1991).
33. M. Lewenstein and L. You, *Phys. Rev. Lett.* **77**, 3489 (1996).
34. C. J. Bordé, *Phys. Lett. A* **204**, 217 (1995).
35. R. J. C. Spreeuw, T. Pfau, U. Janicke, M. Wilkens, *Europhys. Lett.* **32**, 469 (1996).
36. M. Holland, K. Burnett, C. Gardiner, J. I. Cirac, P. Zoller, *Phys. Rev. A* **54**, R1757 (1996).
37. M. Otshanii, Y. Castin, J. Dalibard, in *Laser Spectroscopy XII*, M. Ignuscio, M. Allegrini, A. Sasso, Eds. (World Scientific, Singapore, 1996), pp. 7–12.
38. W. Ketterle and N. J. van Druten, in *Advances in Atomic, Molecular, and Optical Physics*, B. Bederson and H. Walther, Eds. (Academic Press, San Diego, CA, 1996), vol. 37, pp. 181–236, and references therein.
39. Inhomogeneities in the pumping sheet caused weak striations that were perpendicular to the observed fringes and could therefore be clearly distinguished.
40. The thermal cloud had expanded so much that it contributed negligible background.
41. R. L. Pfleegor and L. Mandel, *Phys. Rev.* **159**, 1084 (1967).
42. M.-O. Mewes *et al.*, *Phys. Rev. Lett.* **78**, 582 (1997).
43. We are not distinguishing here between different aspects of coherence that are expressed by expectation values of products of one, two, or four field operators.
44. E. Cornell, *J. Res. Natl. Inst. Stand. Technol.* **101**, 419 (1996).
45. K. Burnett, *Physics World*, 18 (October 1996).
46. In these experiments, we transferred ~50% of the atoms into the $F = 1$, $m_F = 0$ state, immediately turned off the argon ion laser-light sheet to allow the two out-coupled condensates to overlap, and switched off the magnetic trap 2 ms later to avoid acceleration by quadratic Zeeman shifts.
47. We thank M. Naraschewski and H. Wallis for enlightening discussions; their theoretical simulations (26) were helpful in selecting the final parameters for the experiment. We also thank M.-O. Mewes for essential contributions during the early phase of the experiment, S. Inouye for experimental assistance, and D. Kleppner and D. Pritchard for valuable discussions. Supported by the Office of Naval Research, NSF, Joint Services Electronics Program, and the Packard Foundation. D.M.K. was supported by a NSF Graduate Research Fellowship, C.G.T. by a North Atlantic Treaty Organization (NATO) Science Fellowship, and H.-J.M. by Deutscher Akademischer Austauschdienst (NATO Science Fellowship).

11 December 1996; accepted 19 December 1996

Chapter 5

Dynamics

This chapter is concerned with various dynamical properties of condensates. Understanding these dilute atomic gas properties is important for many reasons. For instance, these properties are important for testing many-body quantum theories. Collective excitations are an important facet of condensate behavior, and have so far been observed and studied in several ways. These studies are essential for a complete understanding of the system, and complement static and thermodynamic equilibrium properties. There has also been work towards the creation and detection of vortices and persistent currents, although no definitive results are in yet. These studies of superfluidity are expected to facilitate a more fundamental, or microscopic, understanding of analogous phenomena in superfluid helium and superconductors. Finite temperature effects and damping are also of intense current interest, and seem to be at the threshold of being understood from first principles.

There is a long history of the study of superfluid excitations, which begins roughly with Kapitza's and others' experimental work on He II in the 1930's and extends into the present day. Landau, Feynman, Bogoliubov, and London were some of the early theorists who tried to explain these phenomena. Landau threw out any relation to Bose condensation, but Bogoliubov and Feynman used Bose statistics in an essential way to understand the system. Thus, the connection can be made with London's explanation of superfluidity in terms of Bose condensation. The low frequency excitations are phonons, which impose stringent constraints on scattering and can give rise to frictionless flow. Prior to the present age of dilute atomic Bose condensates, excitations in He II were directly observed by neutron scattering. Now excitations in trapped atomic condensates are imaged by conventional optical means as density perturbations [8, (5.1)].

The following is a brief sketch of the broad features of excitations. Due to the small size of trapped condensates, the excitation spectrum is discrete. This is in distinction to the spectra of quantum liquids, which are phonon-like at low frequency. In common to both types of systems, however, are characteristic velocities of sound. For localized excitations in trapped condensates the continuum

limit is recovered, and the speed of sound can be directly observed. These localized excitations can also be expressed as superpositions of many discrete modes. At higher frequencies (smaller wavelengths), spectra are more like those of free particles. For dilute gases, the crossover frequency is where the wavelength of the excitation is comparable to the healing length $\xi = (8\pi na)^{-1/2}$ (n, a are density and s-wave scattering length). This is the length scale where the kinetic energy associated with density variations is comparable to the mean-field interaction energy (see Gross-Pitaevskii equation (C.1)). These issues and more will be discussed in the first section of this chapter, which consists of the presentation of a published study that observed localized pulses of sound travel across a condensate [8, (5.1)], and afterwards, an elementary derivation of the speed of sound in a homogeneous system.

Theoretically, damping is still an unresolved issue for excitations, although experimental work has revealed it is always present at attainable temperatures [22, 45, 46, 21]. In addition to damping, shifts of discrete modes have also been observed. Predicted to be undamped, however, are quantized currents in multiply-connected geometries (dissipation is predicted in singly-connected systems [47]). These circulating states are predicted to be metastable, and can be regarded as topologically stabilized by the presence of an empty core imposed by external means. Experimental work in this direction will be the subject of discussion in the second section of the chapter.

5.1 'Propagation of Sound in a Bose Condensate'

The first part of this section will be the presentation of the following paper:

- 'Propagation of Sound in a Bose Condensate', by M. R. Andrews, D. M. Kurn, H.-J. Miesner, D. S. Durfee, C. G. Townsend, S. Inouye, and W. Ketterle. *Physical Review Letters*, Vol. 79, p. 553, 1997. Reference [8].

The second part of this section will be an elementary derivation of the speed of sound in a homogeneous system.

Propagation of Sound in a Bose-Einstein Condensate

M. R. Andrews, D. M. Kurn, H.-J. Miesner, D. S. Durfee, C. G. Townsend, S. Inouye, and W. Ketterle
Department of Physics and Research Laboratory of Electronics, Massachusetts Institute of Technology, Cambridge, Massachusetts 02139
(Received 20 March 1997; revised manuscript received 27 May 1997)

Sound propagation has been studied in a magnetically trapped dilute Bose-Einstein condensate. Localized excitations were induced by suddenly modifying the trapping potential using the optical dipole force of a focused laser beam. The resulting propagation of sound was observed using a novel technique, rapid sequencing of nondestructive phase-contrast images. The speed of sound was determined as a function of density and found to be consistent with Bogoliubov theory. This method may generally be used to observe high-lying modes and perhaps second sound. [S0031-9007(97)03665-X]

PACS numbers: 03.75.Fi, 05.30.Jp, 32.80.Pj, 43.35.+d

The study of quantum liquids has revealed a wealth of physics such as superfluidity, second sound, and quantized vortices. A microscopic picture of these macroscopic quantum phenomena was developed based on elementary excitations and quantum hydrodynamics [1,2]. For a long time such studies were limited to ^{4}He and ^{3}He. The realization of Bose-Einstein condensation in atomic vapors [3–5], however, has provided a new class of macroscopic quantum fluids which are dilute gases. An important issue, which applies both to quantum liquids and quantum gases, is the characterization of the system by its collective excitations. Several experimental [6,7] and theoretical [8,9] papers have studied oscillations in Bose-Einstein condensed gases of trapped atoms. So far, the resonance frequencies and the damping of only the few lowest modes have been investigated. Due to the small size of the trapped clouds, the discrete nature of the spectrum is dominant, in contrast to the continuous spectrum of quantum liquids, which is phononlike at low frequencies. The correspondence between the excitation spectrum of a quantum liquid [2], which consists of zeroth, first, and second sound, and the collective modes of a trapped Bose-Einstein condensate have not yet been delineated.

In this Letter we study zeroth sound in Bose-Einstein condensed samples. After exciting density perturbations much smaller than the size of the condensate, we directly observed the propagation of sound waves, analogous to studies in superfluids, and determined the speed of sound. In this study, we demonstrated a method for locally exciting a condensate using a focused off-resonant laser beam, and a new technique of observing dynamical processes using rapid sequencing of nondestructive phase-contrast images.

Bose-Einstein condensed gases at temperature $T = 0$ are described by the nonlinear Schrödinger equation, which, in the limit of a large number of atoms, yields hydrodynamic equations [1,9]. Density perturbations propagate according to a wave equation for zeroth sound,

$$\partial_t^2 \delta n(r) = \nabla \cdot [c^2(r) \nabla \delta n(r)], \qquad (1)$$

where $\delta n(r)$ is the deviation from the equilibrium density $n(r)$. The local speed of sound $c(r)$ is given by an expression first derived by Bogoliubov [10] and Lee, Huang, and Yang [11]

$$c(r) = \sqrt{n(r)\tilde{U}/m}, \qquad (2)$$

where $\tilde{U} = 4\pi\hbar^2 a/m$ characterizes the (repulsive) interaction of bosons with mass m and scattering length a. In the Thomas-Fermi approximation for a harmonic oscillator potential with frequency ν_0, the wave function of a condensate is nonvanishing over a size [12]

$$d = \sqrt{2n_0\tilde{U}/m} \,/\, \pi\nu_0 = (\sqrt{2}/\pi) c_0/\nu_0, \qquad (3)$$

where c_0 is the speed of sound at peak density n_0. The frequencies of the lowest collective excitations are proportional to c_0/d, and thus, from Eq. (3), do not depend on the speed of sound, being simply proportional to the trapping frequencies. Therefore, previous experiments on collective excitations [6,7] did not yield direct information on the speed of sound.

The experimental setup for creating Bose-Einstein condensates was similar to our previous work [7,13,14]. Briefly, sodium atoms were optically cooled and trapped, and transferred into a magnetic trap where they were further cooled by rf-induced evaporation [15]. Condensates typically containing 5×10^6 sodium atoms in the $F = 1, m_F = -1$ ground state were produced every 30 s. In most cases we studied condensates with no discernible thermal component by extending the evaporative cooling well below the transition temperature. The condensate was confined in a cloverleaf magnetic trap, with the trapping potential determined by the axial curvature of the magnetic field of up to $B'' = 125$ G cm^{-2}, the radial gradient $B' = 120$ G cm^{-1}, and the bias field as low as $B_0 = 1.5$ G. The atom clouds were cigar-shaped, with the long axis horizontal.

The condensate was directly observed by nondestructive phase-contrast imaging [16]. This technique is an extension of our previous work on dispersive imaging [17] and

greatly improved the signal-to-noise ratio. Images were formed by photons scattered coherently in the forward direction. The phase modulation in the probe beam caused by the condensate was transformed into an intensity modulation at the camera by retarding the transmitted probe beam by a quarter-wave. This was done using a glass plate with a small raised spot (500 μm diameter) at its center, placed in the Fourier plane of the imaging system, where the transmitted probe beam is focused. Since the probe light was detuned far off-resonance (1.7 GHz to the red), absorption was very small [17], and the small-angle forward scattering imparted negligible recoil energies to the condensed atoms. Thus our imaging was nondestructive, allowing multiple images of the same condensate. Rapid images were taken by dividing a CCD camera chip into eleven strips, and shifting the accumulated charge after each exposure from the illuminated region of the chip into a covered "storage" region. After eleven exposures taken with a repetition rate of up to 1 kHz, the full chip was read out slowly with low noise.

Localized density pertubations were generated by using the repulsive optical dipole force of a focused blue-detuned far-off-resonant laser beam. Heating from spontaneous emission was negligible due to the far detuning of the argon ion laser line (514 nm) relative to the sodium resonance (589 nm). This laser beam was focused into the center of the trap, and could be switched on and off in less than a millisecond. The $1/e^2$ half-widths were about 12 μm and 100 μm, which created a light shift of $\sim$70 nK per 1 mW of laser power. Localized increases in density (positive perturbations) were created by suddenly switching on the argon ion laser beam after the condensate had formed [see Fig. 1(a)]. The repulsive optical dipole force expelled atoms from the center of the condensate, creating two density peaks which propagated symmetrically outward. Alternatively, we formed a condensate by evaporative cooling in the presence of the argon ion laser light, and then switched the laser off [Fig. 1(b)]. This created localized depletions of density (negative perturbations) which also propagated outward.

Figures 2 and 3 show the propagation of density perturbations observed by sequential phase-contrast imaging of a single condensate. The position of the density maxima varied linearly with time, and the speed of propagation was easily extracted. By changing the power of the argon ion laser, the relative amplitude of the density perturbation was varied between 20 and 100%. Within the accuracy of the measurement, the speed of sound was independent of amplitudes and was the same for positive and negative perturbations.

The density dependence of the speed of sound was studied using adiabatically expanded condensates. The weakest trap was formed when the field curvature was reduced to 20 G/cm^2 and the bias field increased to 4 G. The critical temperatures in the strongest and weakest traps

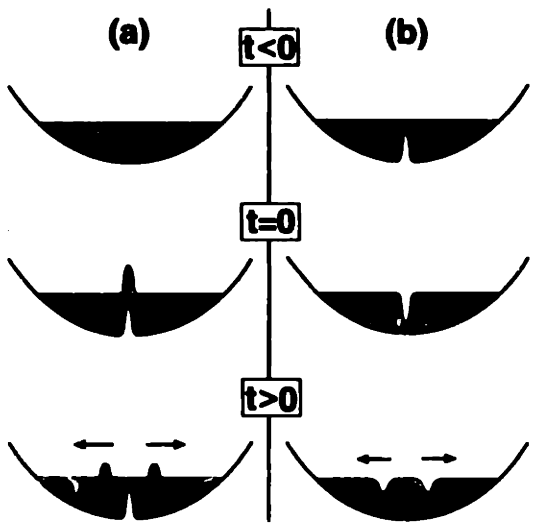

FIG. 1. Excitations of wave packets in a Bose-Einstein condensate. A condensate is confined in the potential of a magnetic trap. At time $t = 0$, a focused, blue-detuned laser beam is suddenly switched on (a) or off (b) and, by the optical dipole force, creates, respectively, two positive or negative pertubations in density which propagate at the speed of sound.

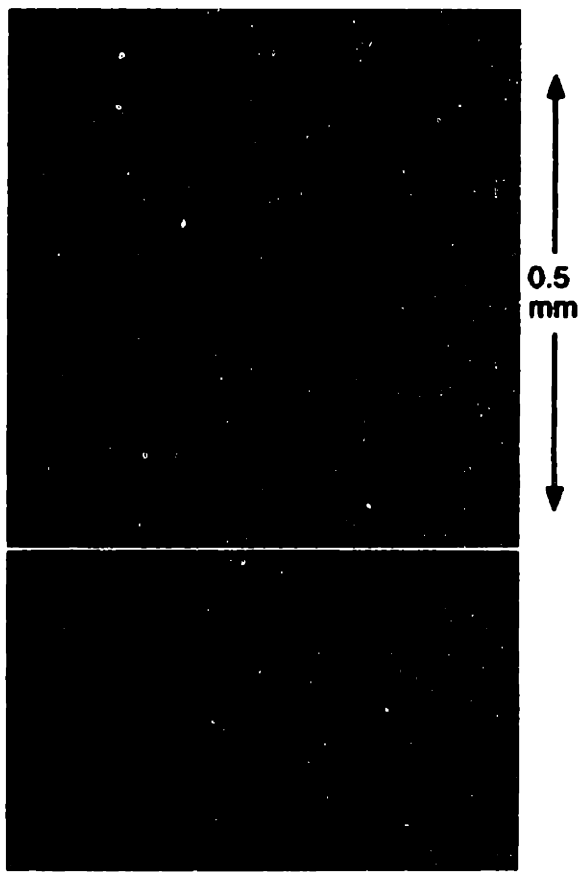

FIG. 2(color). Observation of sound propagation in a condensate by nondestructive rapid phase-contrast imaging. An image was taken every 1.3 ms, beginning 1 ms after switching on the argon ion laser. A power of 7 mW was used, just splitting the condensate into two separated parts. Two pulses traveled outward with the speed of sound. The condensate in the upper sequence was 450 μm long. The lower sequence was taken at lower radial confinement and thus lower peak density. As a result, the pulse propagation was slower.

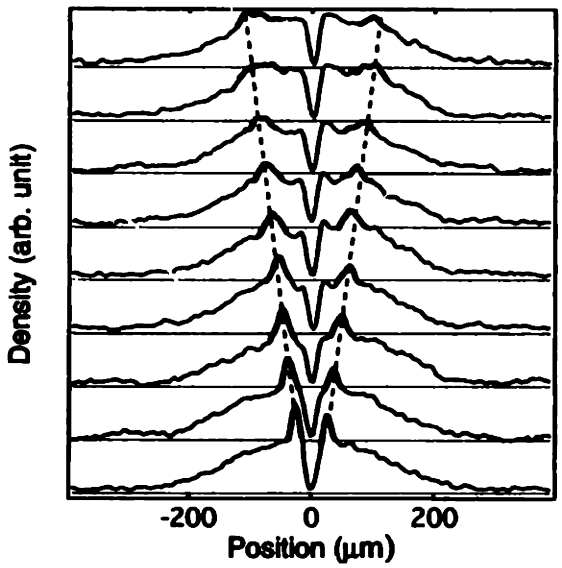

FIG. 3. Vertical profiles through the images in the upper sequence of Fig. 2.

were estimated to be 1.6 and 0.4 μK, respectively. The peak density n_0 was determined using Eqs. (2) and (3):

$$n_0 = (\pi m^2/8\hbar^2 a) d^2 \nu_0^2 . \quad (4)$$

Here d is the measured axial extension of the condensate, and ν_0 is the trap frequency, which was measured in a single shot by exciting a dipole oscillation of the condensate and using rapid image sequences. The scattering length a was recently determined spectroscopically to be 2.75 nm [18]. Condensates up to 450 μm in length were observed (Fig. 2). Alternatively, the density was obtained from the observed phase shift of the probe light and the directly observed size of the condensate. Both measurements agreed to within 20% as long as the condensate was wider than the imaging resolution.

We observed one-dimensional, axial propagation of sound near the center of the cloud, where the axial density varies slowly. However, the local speed of sound varies over the radial cross section of the cloud. One can obtain a one-dimensional wave equation by eliminating the radial degrees of freedom. This is done by assuming a Thomas-Fermi solution for the radial wave function, $\psi(r)$, which adiabatically follows axial density variations, and performing a radial integral of the energy functional. This gives a one-dimensional speed of sound as determined by Eq. (2) for the density at $r = 0$. As is shown in Fig. 4, our experimental results agree well with the theoretical prediction, which has no adjustable parameters. The small discrepancy at higher densities is larger than our statistical error and might indicate that the assumptions of adiabaticity of the radial motion and the neglect of damping and dispersion are not strictly valid.

Indeed, in addition to propagation at a constant speed, we observed spreading of the pulse (Fig. 3). The pulses dispersed typically after traveling half their way to the ends of the condensate, preventing the observation of

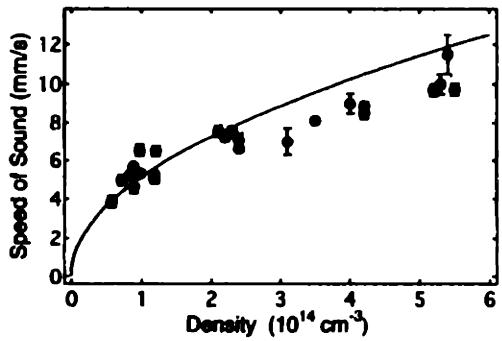

FIG. 4. Speed of sound versus condensate peak density. The solid line is the speed of sound [Eq. (2)] using the maximum cloud density [Eq. (4)] with no adjustable parameter. The error bars show only the statistical error.

a reflection of the pulse or of a decrease in the speed of propagation in the lower-density outer regions of the condensate.

In the language of collective excitations, a localized perturbation is a coherent superposition of many modes [1]. In a homogenous Bose-Einstein condensate, the dispersion relation is linear (phononlike) up to wave vectors comparable to the inverse of the healing length $\xi = (8\pi an)^{-1/2}$, which is approximately 0.2 μm at the peak density of the condensate. Since the extent of the initial perturbation was larger than the healing length, we should have excited predominantly phononlike quasiparticles. The dispersion of the wave packet can be due either to damping or to dephasing of the modes, and we expect the inhomogeneous density distribution of the condensate to play an essential role. After a long time one expects the mode with the smallest damping to dominate. Indeed, in the case of a negative density perturbation, after the propagating pulses died out during the first 25 ms, we observed the lowest collective excitation (the 30 Hz quadrupolelike mode) with a damping time of 300 $\pm$ 120 ms, consistent with our earlier measurement [7].

We also studied sound propagation at various temperatures. By varying the final frequency of the rf sweep during evaporative cooling, we prepared samples with condensate fractions varying from 10% to larger than 60% [19]. The speed of sound decreased with temperature in accordance with Eq. (2) where $n(r)$ accounts for the smaller condensate density. Thus, within the accuracy of measurement we observed no effect of the normal component on the speed of zeroth sound. The dispersion of the pulses was similar over the whole temperature range studied. Further experimental work is necessary to study finite temperature effects in detail.

Above the phase transition we saw no clear evidence of sound wave propagation in the normal cloud. At an estimated density of 10^{14} cm^{-3} and for an elastic scattering cross section of 1.9×10^{-12} cm^2 [18], the mean free path between collisions is $l \approx 35$ μm. Thus the argon ion laser-induced density modulations of spatial extent $\lambda < l$. In contrast to the "hydrodynamic" regime

($\lambda \gg l$), such a density pertubation expands ballistically and the amplitude decreases rapidly, which is consistent with our observation.

Additional information on the pulse propagation can be obtained by using the time-of-flight technique. After creating two Bose-Einstein condensates by evaporative cooling in a double-well potential (see [14] for details), we switched off the argon ion laser beam a variable time (up to 40 ms) before switching off the magnetic trap, and let the cloud expand ballistically. Absorption images taken after 40 ms expansion showed "interference"-like structures with coarse (100 μm) and fine (15 μm) striations [20]. The latter were similar to those observed in the interference of two Bose-Einstein condensates [14], whereas the coarse structures are probably related to collective excitations caused by propagating wave packets.

Focused laser beams can excite collective modes which cannot be excited by simply varying the magnetic trapping potential. Short-wavelength excitations can be studied by using tightly focused beams. To excite a specific high-frequency mode, one could periodically modify the laser power, or even focus several laser beams near the antinodes of the mode.

Another intriguing prospect is the excitation of second sound. Second sound is a collective excitation for which the density of the condensate and the normal component oscillate out of phase; this corresponds to a temperature wave. By focusing near-resonant light into the condensate, one could locally heat the sample by spontaneous scattering and excite such a wave. In our quasi-one-dimensional geometry, the signature of second sound could be a density minimum in the condensate accompanied by a density maximum in the surrounding normal cloud, both propagating together along the axial direction. When we replaced the argon ion laser beam by a beam of near-resonant light, we locally "evaporated" the condensate, but could not discern a localized normal fraction. This was probably due to the ballistic spreading discussed above—the excitation is rapidly damped. Furthermore, the near-resonant light also caused trap loss due to optical pumping to nontrapped states.

In conclusion, we have demonstrated a new method to excite collective excitations in a Bose-Einstein condensed cloud and have determined the speed of sound as a function of condensate density. This method allows for comparison with sound propagation in He II and is promising for the study of higher-lying excitations and perhaps for studying second sound. Furthermore, the method of rapid sequencing of phase-contrast images was used to determine the speed of sound and the frequency and damping of collective modes. This technique allows for single shot measurements of dynamical processes and has two main advantages over previous techniques. The measuring time is greatly reduced, and studies of dynamical properties are possible that might be otherwise obscured by experimental or statistical fluctuations.

We thank C. Kuklewicz for experimental assistance. This work was supported by the Office of Naval Research, NSF, Joint Services Electronics Program (ARO), and the Packard Foundation. D. M. K. would like to acknowledge support from an NSF Graduate Research Fellowship, C. G. T. from a NATO Science Fellowship, and H.-J. M. from Deutscher Akademischer Austauschdienst (NATO Science Fellowship).

[1] P. Nozières and D. Pines, *The Theory of Quantum Liquids* (Addison-Wesley, Redwood City, CA, 1990), Vol. 2.
[2] A. Griffin, *Excitations in a Bose-Einstein-Condensed Liquid* (Cambridge University Press, New York, 1993).
[3] M. H. Anderson *et al.*, Science **269**, 198 (1995).
[4] K. B. Davis *et al.*, Phys. Rev. Lett. **75**, 3969 (1995).
[5] C. C. Bradley, C. A. Sackett, and R. G. Hulet, Phys. Rev. Lett. **78**, 985 (1997); see also: C. C. Bradley, C. A. Sackett, J. J. Tollet, and R. G. Hulet, Phys. Rev. Lett. **75**, 1687 (1995).
[6] D. S. Jin *et al.*, Phys. Rev. Lett. **77**, 420 (1996); D. S. Jin *et al.*, Phys. Rev. Lett. **78**, 764 (1997).
[7] M.-O. Mewes *et al.*, Phys. Rev. Lett. **77**, 988 (1996).
[8] M. Edwards *et al.*, Phys. Rev. Lett. **77**, 1671 (1996); A. L. Fetter, Phys. Rev. A **53**, 4245 (1996); P. A. Ruprecht, M. J. Holland, K. Burnett, and M. Edwards, Phys. Rev. A **51**, 4704 (1995); V. M. Pérez-García *et al.*, Phys. Rev. Lett. **77**, 5320 (1996); K. G. Singh and D. S. Rokshar, Phys. Rev. Lett. **77**, 1667 (1996).
[9] S. Stringari, Phys. Rev. Lett. **77**, 2360 (1996).
[10] N. Bogoliubov, J. Phys. **11**, 23 (1947).
[11] T. D. Lee, K. Huang, and C. N. Yang, Phys. Rev. **106**, 1135 (1957).
[12] G. Baym and C. Pethick, Phys. Rev. Lett. **76**, 6 (1996).
[13] M.-O. Mewes *et al.*, Phys. Rev. Lett. **77**, 416 (1996).
[14] M. R. Andrews *et al.*, Science **275**, 637 (1997).
[15] W. Ketterle and N. J. van Druten, in *Advances in Atomic, Molecular, and Optical Physics*, edited by B. Bederson and H. Walther (Academic Press, San Diego, 1996), Vol. 37, p. 181, and references therein.
[16] E. Hecht, *Optics*, 2nd ed. (Addison-Wesley, Reading, MA, 1989).
[17] M. R. Andrews *et al.*, Science **273**, 84 (1996).
[18] E. Tiesinga *et al.*, J. Res. Natl. Inst. Stand. Technol. **101**, 505 (1996).
[19] The quantitative determination of small thermal fractions was not possible with the far-detuned probe light.
[20] W. Ketterle, invited talks at IQEC, ICAP, LT 21, Summer 1996.

Propagation of Sound in a Bose-Einstein Condensate [Physical Review Letters 79, 553 (1997)]

M.R. Andrews, D.M. Stamper-Kurn, H.-J. Miesner, D.S. Durfee, C.G. Townsend, S. Inouye, and W. Ketterle

We predicted that density perturbations should propagate along the axis of a cigar-shaped Bose-Einstein condensate at a speed $c = (n_0\tilde{U}/m)^{1/2}$ where n_0 is the density at the center of the cloud, $\tilde{U}$ characterizes the repulsive interaction between atoms, and m is their mass. This prediction was based on an incorrect use of an energy functional.

We have since corrected our theoretical approach to reducing three-dimensional sound propagation to a one-dimensional equation. We considered the quantum Lagrangian for a Bose-Einstein condensate [1] confined in a cylindrial tube which is infinite in the z direction. We assumed a Thomas-Fermi solution in the radial direction by using a trial wavefunction of the form

$$\Psi(r,z,t) = \left(1 - \frac{V(r)}{\tilde{U}|\psi_z(z,t)|^2}\right)^{1/2} \psi_z(z,t) \tag{1}$$

where $V(r)$ is the confining potential. $\psi_z(z)$ had the form

$$\psi_z(z,t) = \sqrt{n(z,t)}e^{i\phi(z,t) - i\mu t/\hbar} \tag{2}$$

Equations of motion were determined by minimizing the action S of the system with respect to $n(z,t)$ and $\phi(z,t)$. We thereby obtained $c = (n_0\tilde{U}/2m)^{1/2}$, which differs from our earlier prediction by a factor of $1/\sqrt{2}$, and which agrees with recent results determined by different methods [2-4].

We reanalyzed our experimental data using an improved background subtraction and an improved fit function to measure the condensate length.

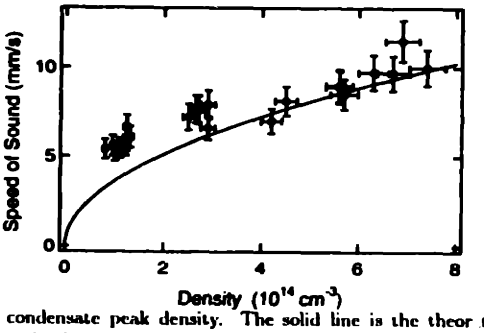

FIG. 1. Speed of sound versus condensate peak density. The solid line is the theoretical prediction with no adjustable parameter. The error bars indicate only the statistical error.

Figure 1 shows the new prediction and the corrected data points. The agreement at high density is good, whereas the discrepancy at low densities is larger than the statistical and estimated systematic errors. Since the lowest densities were achieved by radial decompression, they involve rather small aspect ratios of the condensate ($\lesssim 10$). In this regime a one-dimensional treatment of the sound propagation might not be appropriate.

We are grateful to E. Zaremba, C.J. Pethick, and S. Stringari for insightful discussions.

---

[1] V.M. Pérez-García *et al.*, Phys. Rev. Lett. **77**, 5320 (1996)
[2] E. Zaremba, Report No. cond-mat/9708237.
[3] G.M. Kavoulakis and C.J. Pethick, Report No. cond-mat/9711224.
[4] S. Stringari, private communication.

5.1.1 Speed of sound

The starting point for studying sound in atomic Bose condensates at zero temperature is the Gross-Pitaevskii equation in (C.1) and the hydrodynamic equations that are derived from it in equations (C.2) and (C.3). These equations describe the behavior seen in previous studies of standing waves [46, 21], and more recently, localized pulses of sound [8, (5.1)]. Described are the density of particles in space, ρ, and the velocity field v throughout a Bose condensate. A linear wave equation for the propagation of sound can then be derived by assuming low amplitude excitations. Setting $\rho = (1 + \varepsilon)\rho_0$ for small variations from the unexcited density ρ_0, and keeping velocities v small as well, one arrives at:

$$\rho_0 \frac{\partial \varepsilon}{\partial t} + \rho_0 \nabla v = 0 \tag{5.1}$$

and

$$m \frac{\partial v}{\partial t} + \frac{4\pi\hbar^2 a \rho_0}{m} \nabla \varepsilon = 0 \tag{5.2}$$

neglecting second order terms linear in ε and v. Taking the time derivative of equation (5.1) and the gradient of equation (5.2) gives a common term $\nabla \partial v/\partial t$ in both, and so the two equations can be combined as

$$\frac{\partial^2 \varepsilon}{\partial t^2} - \frac{4\pi\hbar^2 a \rho_0}{m^2} \nabla^2 \varepsilon = 0. \tag{5.3}$$

This equation describes the propagation of disturbances of amplitude ε with the speed

$$c = (4\pi\hbar^2 a \rho_0 / m^2)^{1/2}. \tag{5.4}$$

Pulses of sound propagating at this speed were observed in-situ and in real time [8, (5.1)], adjusted for transverse shape effects in the trap (see the preceding paper and its erratum for more details).

5.2 Persistent currents

There are several strong motivations for wanting to study persistent currents and vortices in dilute Bose condensates; I use these two terms almost interchangeably because they represent very much related phenomena. The first motivation is that such currents would be analogous to superconductivity, and in a sense, would constitute a model system for that more complicated phenomenon. Superconductivity is a field of immense practical importance. Fundamentally, the persistence of motion in the presence of obstacles that could otherwise cause dissipation is interesting to study, and is a macroscopic example of a quantum mechanical stationary state. The same considerations hold for comparisons to superfluidity in helium. Dilute quantum gases offer the possibility for understanding subtle aspects of many-body quantum theory in a simple system.

Another motivation for studying superfluidity in dilute Bose condensates, albeit peripheral to the ones already mentioned, is in expanding upon the relationship between 'rotational shielding' and the Meissner effect in superconductors. In superconductors, phase coherence determines the quantum phase of charged (superconducting) particles as they traverse the sample. On the other hand, the vector potential has the same role, and so there is a competition between the two constraints: magnetic fields smaller than a critical one are expelled from a superconductor, whereas larger ones penetrate in isolated lines called 'magnetic vortices'. Similarly, vortices in superfluids can be loosely considered as the expulsion of rigid-body rotation from the bulk of the fluid. Rigid-body rotation, like magnetic field in superconductors, would destroy the condensate's phase coherence; thus, rotation is effectively relegated to a vortex core so the rest of the fluid can maintain its original coherence. In both systems the imposition of phase coherence under the external perturbation gives rise to a quantization of circulation; see later.

A more 'far-reaching' motivation comes from astrophysics and elementary particle physics. Rututu [48] and Bauerle [49] studied vortex formation in superfluid helium-3, and related it to cosmic string or defect formation in the early universe. The basic idea is that the formation of topological defects during a rapid symmetry breaking stage of the early universe is seen to be analogous to vortex formation after a rapid cooling to the superfluid regime. Rapid cooling in these experiments happened after localized heating by neutrons, and was asserted to mimic processes responsible for initial fluctuations due to a 'Big Bang', the resulting fluctuations in the microwave background radiation, and even (perhaps) to mimic processes leading to the apparent matter-antimatter imbalance. There are other motivations as well, and it is clear that persistent currents, vortices, and superfluidity are related to a wide variety of physics.

5.2.1 Previous work

Superfluidity is a complex of phenomena first observed in the 1930's, where some of the early pioneers were Kapitza [50] and the team of Allen and Misener [51]. As early as 1932, however, others [52, 53, 54] explored remarkable properties of helium's thermal conductivity below the λ-phase transition near 2 K, including its magnitude measured to be at least three million times higher than the fluid's above the transition. Even Onnes, the first to liquefy helium in 1908, must have noticed the sudden cessation of boiling as the substance was cooled well below its point of liquification (but certainly didn't report it, as did the authors of reference [52]) — an early qualitative indication of a large change in the conductivity. Kapitza and others were the first to obtain strong evidence that the viscosity of a component of the fluid nearly vanished, to the extent the apparatuses could detect.

Skipping to modern times, a few selected works are worth pointing out and are particularly relevant to current searches for superfluidity in dilute atomic Bose condensates. Before the advent of Bose condensation in 1995 [2], persistent currents in superfluid helium had been demonstrated by Reppy and Depatie [55] and others. Vinen [56], and later, Zimmerman et al. [57], definitively showed the quantization of circulation for a vortex confined to a wire by the splitting of the wire's transverse vibration modes. On the theoretical side, Pitaevskii [58] discussed vortices in a dilute Bose gas, and showed how the core size should scale with the healing length $\xi \sim (na)^{-1/2}$ (n, a are density and s-wave scattering length). Fetter considered vortex formation in incompressible fluids for several different geometries, namely in rotating containers of arbitrary geometries [59], in a rotating annulus [60], and in deformed rotating cylinders [61]. His work in two-dimensional systems facilitated the complex variables formulation of classical hydrodynamics. There is also the work of Packard et al. [62] and Avenel et al. [63], showing how the quantization of circulation in superfluid helium can be used to realize a detector for the state of absolute rotation. These were clearly results of superfluidity and phase coherence. There have been other contributors too, of course.

After Bose condensation was announced in dilute gases in 1995 [2, 3, 4], there was much publication activity, mostly theoretical in nature. But first some of the experimental works will be mentioned. There were the works coming out of MIT (Ketterle et al.) and JILA (Cornell and Wieman et al.) that studied the low-lying elementary excitations of trapped condensates, including some of the dissipative and temperature dependent properties [21, 46, 45, 22] and [8, (5.1)]. It is the latter properties of dissipation which are of particular interest to this discussion, because so far all excitations have been observed to decay, in contradistinction to exhibiting superfluidity or the absence of dissipation.

On the theoretical side, several authors published on the subject of persistent currents and vortices since 1995. Stringari examined a basic aspect of superfluid rotation, and namely, gave results on the moment of inertia of superfluid compared to rigid-body rotation [64]. Further work of his with others showed more details of vortex structure and formation vs. critical frequency [65, 66].

Marzlin et al. [67] and Bolda and Walls [68] showed how one might create a vortex by a Raman interaction with two lasers, using Laguerre-Gaussian beams which have 'orbital' angular momentum (separate from the spin of the photons). And Dum et al. [69] proposed using adiabatic transfer to create vortices and dark solitons. Rokhsar [47] showed how vortices are generally unstable in trapped samples, specifically in single-connected domains. This realization led to other theoretical works treating vortices in multiply connected domains, in particular the torus, which are expected to show a degree of metastability. Mueller et al. [70] showed how currents in a toroidal geometry might decay due to thermally initiated jumps, where the core traverses the bulk of the fluid and exits the system.

5.2.2 Important issues and ideas

Of prime importance is the difference between rotational and irrotational flow. Rotational flows are characterized by $\nabla \times v \neq 0$, whereas irrotational flows have a vanishing curl of velocity, or $\nabla \times v = 0$. Since velocities in a condensate are proportional to the gradient of the phase (appendix ??), flow must be irrotational since the curl of a gradient is zero. Therefore, a condensate in steady flow is predicted to achieve $\nabla \times v = 0$ by forming linear cores where a nonvanishing $\nabla \times v$ would be concentrated, save for the fact that the cores are devoid of superfluid. This prediction is substantiated by analogous behavior of superfluid helium and superconductors, and the state of motion is called a vortex.

Atoms in a vortex circulate about the core, which forms a line through the system. In quantum mechanics, the angular momentum of particles is quantized in units of $\hbar$. For a classical vortex (such as the one often found in a draining bathtub), the expectation value for angular momentum is an ensemble average of many atoms. But in a dilute condensate that has phase coherence, ensemble averages reduce to expectation values of a single-particle wavefunction. Thus, the net circulation of a condensate is expected to be quantized as a whole and not take on any one of a continuum of expectation values as in the classical case.

The existence of a core can be understood as a consequence of uniform angular momentum density L in a steady flow; on the axis ($r = 0$) the velocities v would have to diverge since $L = mvr$. The core can also be understood quantum mechanically, in that a state with angular momentum must have a node, which is the core.

The structure of the core and excitations associated with it (vortex waves) in an interacting dilute gas condensate were sketched out by Pitaevskii [58]. Arising from this treatment was the healing length $\xi \sim (na)^{-1/2}$, which, as mentioned, is the length scale where the kinetic energy associated with density variations is comparable to the mean-field interaction energy. Or, specifically in the case of the vortex, it is also where the kinetic energy per atom of vortex motion close to the core is comparable to the mean-field interaction energy. The kinetic energy E of vortex motion arises from $L = mvr$ for atoms of mass m having angular momentum $L = \hbar$ and velocity v as a function

of radius r. In equations, $E = mv^2/2$, and so the balance that leads to the core's size ξ is between $\hbar^2/2m\xi^2$ (the kinetic energy) and $4\pi\hbar^2 an/m$ (the mean-field interaction energy).

The topology, or connectedness, of the space is important when considering vortices and persistent currents. In addition, whether or not the system is in a trap matters because this affects the homogeneity of the atomic density; this will be discussed shortly. In a singly connected domain, the fluid must form a core of excluded material in order to achieve a steady current; the position of the core and its dynamics are set by the fluid itself. In a multiply connected domain, the circulation can occur about one of the naturally excluded areas without the need for the fluid to form its own core. In this case, the position of the excluded domain is essentially fixed, and core dynamics are absent; the core can be said to be pinned and the flow is expected to be persistent.

In the next few paragraphs, the formation and stability of vortices and persistent currents will be discussed. For a vortex to form and have some degree of stability it must be thermodynamically advantageous. This has been treated by many authors (e.g., reference [59]). For small frequencies, the low energy of a state without vortices dominates the balance of thermodynamic equilibrium, but for high frequencies the rotating frame becomes more important and vortex formation is favorable. Thus, there is a critical frequency for vortex formation.

To impart rotation to the system, azimuthal anisotropy of the container is necessary. In liquid helium, it has always been the case that microscopic friction of the container's walls was able to bring the fluid into equilibrium with the rotating frame. For trapped atomic gases, however, the 'walls' are typically smooth, being magnetic or optical traps. In this case a deformed trap is called for. One possibility is that the trap may be deformed into an ellipse-like shape, whose orientation is then rotated. Another possibility is to stir up atoms in an isotropic trap with a rotating focused laser beam (optical dipole potential). Each of these possibilities is expected to be equivalent to a rotating frame, and the latter one was investigated experimentally.

There are general aspects of vortex formation worth considering, which is whether or not a persistent current can be formed in an existing condensate at zero temperature, and whether one can be formed as the system is rotated while cooled across the phase transition. Whereas a vortex state or persistent current is metastable or even unstable in the absence of external rotation, it can be the true ground state while driven above the critical frequency. Therefore, it seems reasonable to be able to cool the system into this state when crossing the condensation temperature; in this case condensation should proceed into the circulating ground state.

There are so far several predicted decay modes for vortices. For noninteracting condensates, the core is predicted to fill in with non-circulating atoms and lead to destruction of the vortex [47]. For interacting condensates, vortices are also predicted to be unstable [47]. These results are the subject of current discussion. An alternate understanding of vortex decay for interaction-dominated clouds is the following. Most of the kinetic energy of a vortex lies close to the core, since velocities there

are greatest. But the velocity profile in a vortex is fixed by its structure, whereas the density is variable in an inhomogeneous system. Therefore, a vortex can lower its energy by moving its core to an area of lower density. This would give rise to a classical force proportional to the gradient of the density. Mueller et al. [70] considered another mode of vortex decay in a large toroid with small cross-section. In this work, decay occurs by spontaneous de-pinning of the core, followed by its motion across the fluid and thereafter out of the system. As it was considered, this mechanism of decay is thermally activated and most important near the critical temperature.

5.2.3 Experimental work

In this section some of the experiments directed towards studying vortices will be discussed. This work began in spring 1997 and continued into the summer. In all these experiments on persistent currents and vortices, the mechanisms of formation, the possibilities for decay, and the modes of detection were subject to experimental exploration. No definitive evidence for vortices being created nor detected was obtained. Formation was assumed to be possible by rotating an anisotropic toroidal trap, which was also assumed capable of pinning a vortex to form a persistent current.

A prime concern was detection, and the most obvious mode would have been to image a core directly. Unfortunately, the healing length $\xi = (8\pi na)^{-1/2}$ was quite small, even for the least compressed trap (to be discussed shortly) having a density $n \sim 5 \times 10^{13}$ cm^{-3}; with the scattering length $a \sim 2.75$ *nm* [71], the healing length ξ of about 0.5 μm would be far below the imaging resolution limit near 3 μm and thus difficult to resolve. This is in contrast to previous work where cores were imaged in superfluids, for instance in reference [72]. There are two other detection possibilities. One is to let a cloud with a vortex out of the trap, and allow the core to expand. Classically, one would look for the centrifugal hole in a system where every atom has an identical angular momentum. Quantum mechanically, one would be looking for the node of a wavefunction with angular momentum. Using de Broglie's relation for a non-interacting gas, the core could also be considered to be a central fringe of period $ht/m\xi$ where t is the time-of-flight, h is Planck's constant, and m the mass of the atoms. The expanded core could conceivably be smaller due to the repulsive effects of interactions. The second possibility is that an interferometric method could be used to detect a vortex, involving the interference of two condensates in a manner similar to reference [9, (4.3)]. Should one condensate have a vortex, its phase structure could modify the linear interference pattern in a way shown in figure (5-1).

The particular trap used for vortex work was a round and decompressed version of the cloverleaf-type Ioffe trap [23]. The decompression was attained by applying a high bias field along the long axis of the trap, thereby weakening the radial confinement. The resulting trap was a nearly isotropic harmonic oscillator potential with frequency near 18 Hz. See the left half of figure (5-2)

Two techniques were used to impart rotation to the cloud. The primary one used a combination

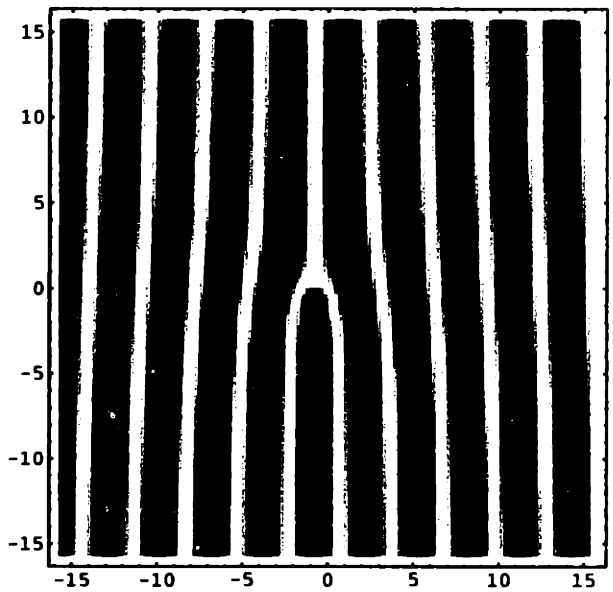

Figure 5-1: An idealized phase slip in a linear interference pattern. Shown is simply $\|e^{i\phi}e^{iz} + e^{-iz}\|^2$ with an arbitrary relative phase to align the singularity with a dark fringe. Note the vortex-like phase factor $e^{i\phi}$ on one of the traveling waves. ϕ is the angle in the plane $0 \leq \phi \leq 2\pi$.

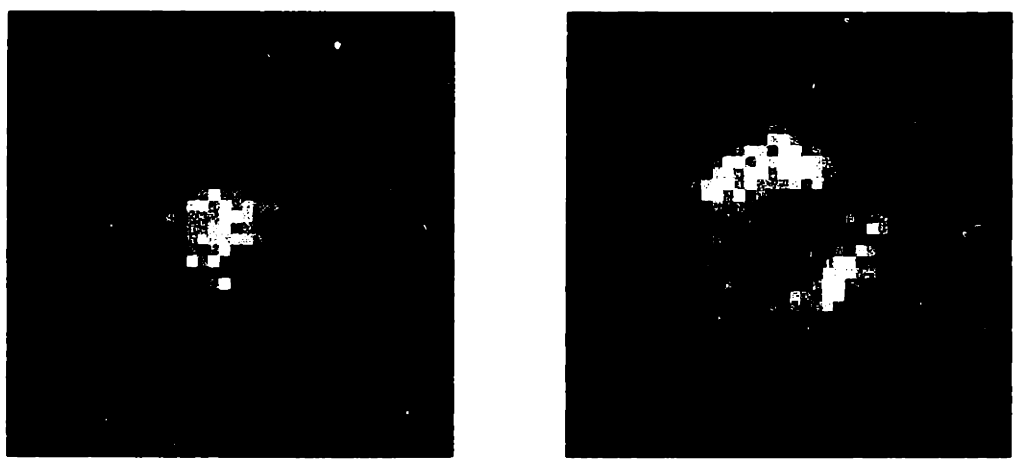

Figure 5-2: A round cloud pierced by a focused argon-ion laser beam in the magnetic trap. The round cloud of about 100 μm diameter was made by applying several tens of gauss magnetic bias field to the magnetic trap, weakening the radial confinement until it became comparable to the axial. An argon-ion laser beam was focused into the center of the cloud and repelled atoms due to the optical dipole force.

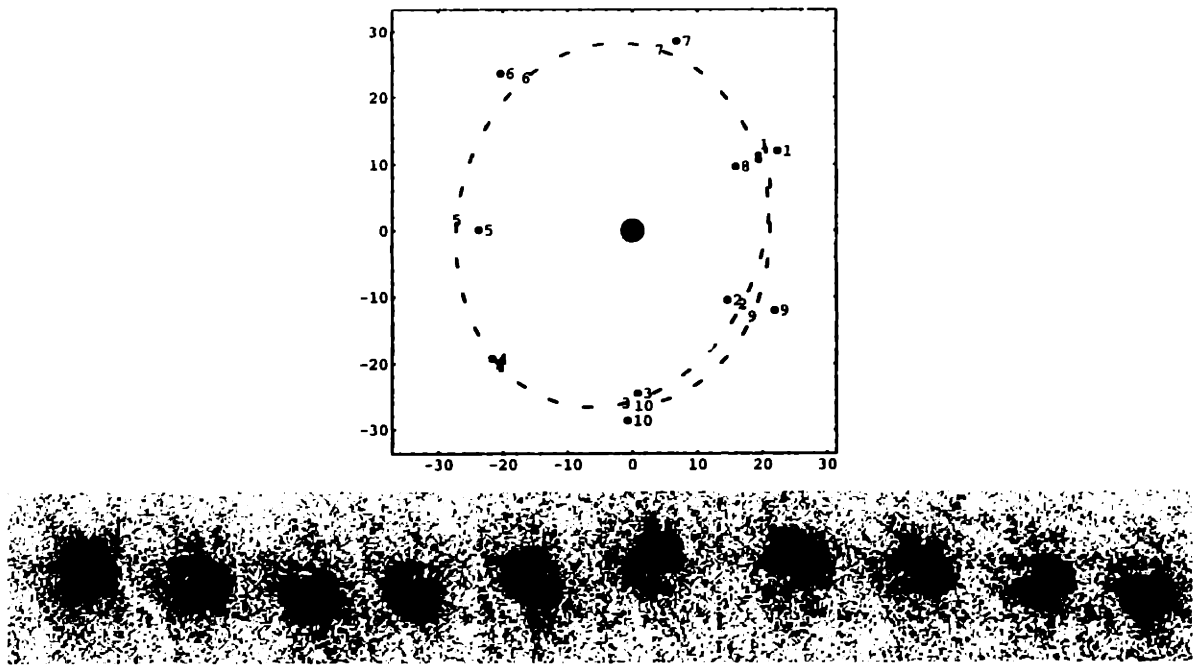

Figure 5-3: 5 Hz driven rotation of a condensate around a focused argon-ion laser beam. Imaging is by the technique of a rapid sequence of phase contrast images [8, (5.1)]. On bottom is a movie of a condensate being driven at 5 Hz rotation. The centrally located argon-ion beam excludes atoms from the center. On top is trace of the center of mass. Labeled numbers correspond to frames in the movie (dots are data and dotted line is fit to a rotation), and axes are in microns. Image is noisy because light level was low to potentially avoid disturbing any vortices.

of oscillating magnetic fields and a blue-detuned optical dipole potential, which was focused green laser light from an argon-ion laser at 514 nm. The green light was focused into a spot about 10 μm wide in the center of the round cloud of atoms; see figure (5-2). The round cloud was then orbitally rotated about the unmoving green light using a combination of phased magnetic fields. The cloud was displaced axially by application of a gradient field, since in that direction the field had curvature. The cloud was displaced radially by application of a bias field, since in this direction the field variation was linear. Displacements were typically a fraction of the cloud radius, up to more than a cloud radius for strong rotation. The cloud was about 100 μm in diameter, and so 1 gauss/cm gradient or 1 gauss bias field were sufficient. See figure (5-3) for an example of a driven condensate.

Particularly important in this configuration was the central green laser beam. It remained in place after the drive, and could serve to anchor a vortex or persistent current. Without it, as already mentioned, a vortex is predicted to be unstable [47]. Various powers of green laser light were applied to the cloud, the highest actually piercing the cloud while the lowest simply reduced the central density.

It is worth making a short theoretical digression of two paragraphs in the midst of discussing the experiment, because Fetter examined this particular toroidal geometry in a semi-classical analysis

assuming an incompressible homogeneous fluid [73]. His work treated fluid between two off-center cylinders, one contained within the other. In this model, the boundary of the cloud in the trap is the outer cylinder, and the green light is the inner cylinder. The amplitude of the rotating drive gives the degree of offset between the centers of the two cylinders. Using the methods of classical hydrodynamics in two-dimensions, he was able to produce expressions for the critical frequency at two limits. One limit was for nearly concentric cylinders, and the other was for the inner cylinder maximally offset and close to the wall of the outer one. The first limit reproduces his earlier results on vortices in an annulus [60], whereas the other limit is particular to this experiment and gives a considerably larger critical frequency. In addition to studying formation of a persistent current in this geometry, he also proposed detecting it by the observation of a force that acts to reduce the gap.

It is expected that this picture of incompressible fluid is applicable when imparted velocities are considerably less than the speed of sound. Any perturbations to density occurring as a result of such small velocities should quickly equilibrate through propagation of sound waves. This approximation, however, can never hold close to the core, because velocities in a vortex increase without bound (up to the core's wall) inversely with radius. The velocity $v = (\hbar/m)\nabla\phi$, where ϕ is the quantum phase angle in a vortex. In a system with cylindrical symmetry, ϕ is also an integral multiple of the azimuthal angle.

No matter what combination was tried of amplitude or frequency of the rotating drive, no evidence for vortices were ever seen. The main detection technique was looking for the centrifugal hole, as mentioned earlier. Perhaps the degree of cylindrical symmetry required for a symmetric expansion into free space is greater than was present in these experimental realizations. While the cloud was trapped but after the drive was stopped, circular motion was observed, consistent with sound propagation; see figure (5-4).

The secondary technique used to impart rotation to the cloud also used a focused green laser beam. Instead of a round beam, an elliptical one was created, which was then rotated. This green light 'sheet' was intense enough to separate the round cloud into two halves, which were seen to rotate as well; see figure (5-5). After a period of rotation, the laser and the magnetic trap were shut off simultaneously. In this setup, vortices are always expected to decay after the drive since there is no pinning. If a vortex had formed in one of the halves, however, it was expected that a singularity in a linear interference pattern would be apparent. Although linear fringes were seen in an undriven cloud, as can be seen in figure (5-6), a cloud released after the drive did not show any fringes. This lack of fringes is still a preliminary result and warrants further study. Possibilities that need testing are the loss of coherence during the drive, excitation of collective modes, transient thermalization of the cloud, or the presence of too many vortices.

Technically, the green laser sheet was produced by diffraction through a roughened rectangular

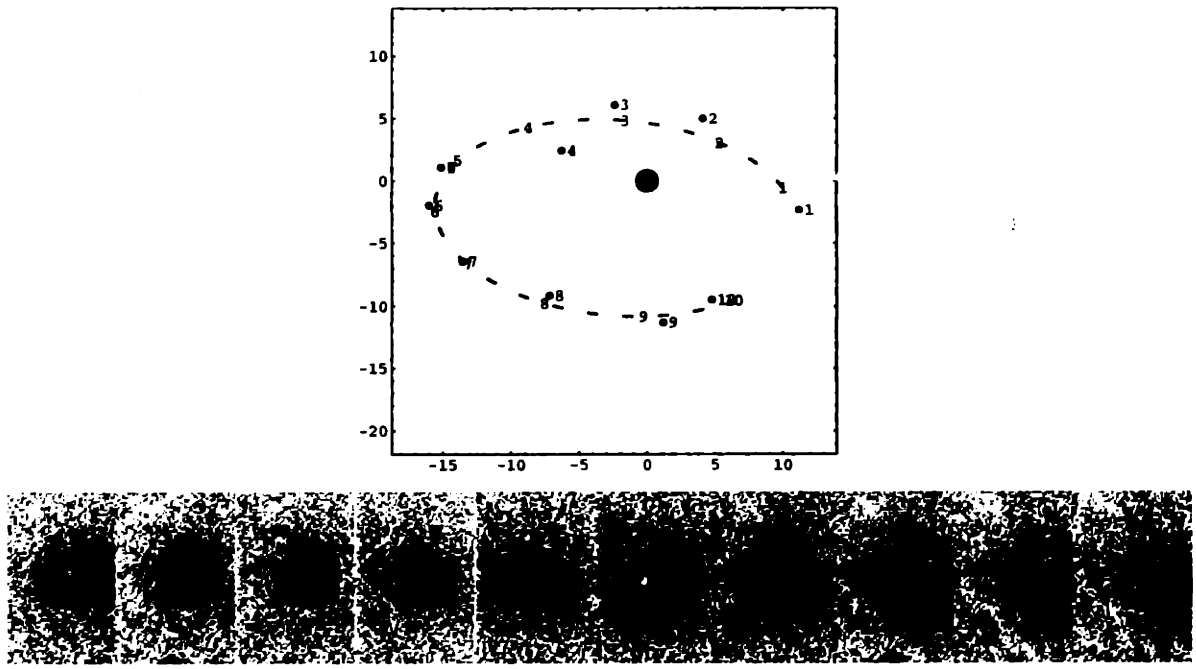

Figure 5-4: Free rotation of a cloud at 15 Hz after drive was stopped. On bottom is a movie of a rotating condensate. The centrally located argon-ion laser beam excludes atoms from the center of the trap. On top is a trace of center of mass, showing evidence for a 'whispering-gallery' type excitation around the laser beam. Labeled numbers correspond to frames in the movie (dots are data and dotted line is fit to a rotation), and axes are in microns. Image is noisy because light level was low to potentially avoid disturbing any vortices.

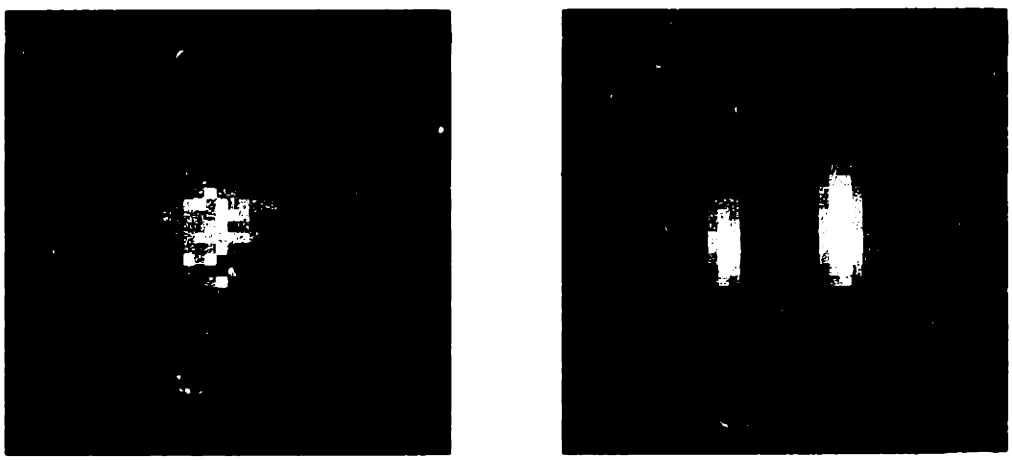

Figure 5-5: A round cloud halved by a focused argon-ion laser sheet in the magnetic trap. The round cloud was made by applying several tens of gauss magnetic bias field to the magnetic trap, weakening the radial confinement until it became comparable to the axial. An anisotropic argon-ion laser beam was focused into the center of the cloud and repelled atoms due to the optical dipole force.

Figure 5-6: Interference between halves of a round cloud. The two halves of a round cloud in figure (5-5) expand in space and give interference fringes on the order of 25 μm and 50% contrast.

aperture (roughened to prevent fringes) immediately before the final focusing lens. Since the extent of a laser beam on a focusing lens determines how tightly it can be focused, the narrow axis of the rectangular mask increased the diffraction limited spot size along that axis. This mask was set on a rotating mount which was driven by a low frequency motor, capable of up to 100 Hz and down to a small fraction of a Hz. Instead of diffracting the beam, a rotating cylindrical lens could have been used. This design, however, would most probably have degraded the alignment during rotation, whereas the diffracted beam's orientation and position was independent of any lens alignments.

5.2.4 Future possibilities

Another technique considered for the creation of vortices or persistent currents was to induce rotational motion directly using a static optical dipole force. This possibility is as yet experimentally unexplored. A pattern such as the one shown in figure (5-7) portrays an azimuthally varying intensity which can be used as a filter on an expanded laser beam. Such a filtered laser beam, if directed at and centered on a condensate, can force atoms to circulate. Depending upon the laser detuning from resonance, the atoms are either azimuthally pushed clockwise towards lower intensity (blue detuning), or pushed counter-clockwise towards higher intensity (red detuning). If the accumulated

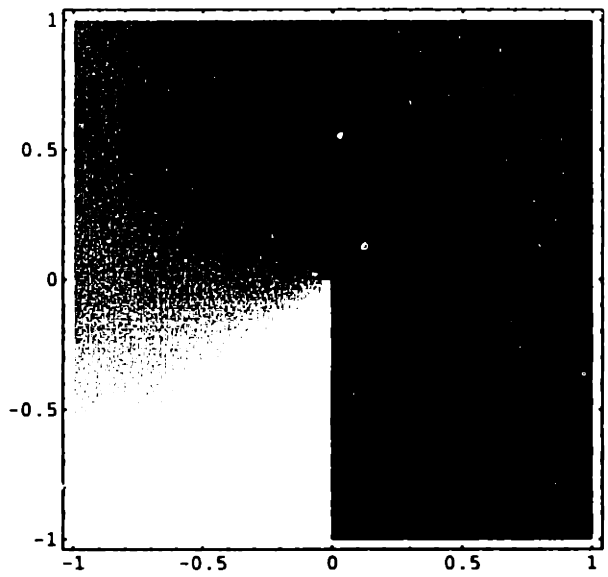

Figure 5-7: Vortex stamp pattern. Exposing a condensate to light passed through a filter such as this might create a vortex, if the fast-moving atoms at the sharp edge are ejected. The functional form is $\phi = \tan^{-1}(y/x) + \pi$ in the left half, and $\phi = \tan^{-1}(y/x)$ on the right. This gives a phase ϕ that wraps around by 2π on any closed path including the center.

phase during exposure in the brightest region is 2π (due to the ac-stark shift), and the black region is totally dark, then a singly charged vortex pattern is imposed on the cloud, save for the boundary region where the brightest and darkest portions overlap. In this region, a compensating force is applied to the cloud, so that there is no net angular momentum imparted; this is because the filter is single-valued while the quantum phase variable is not. If this linear boundary region is sufficiently well focused, however, then the imparted velocities might be so large that atoms are ejected or are dissipated into the normal fraction. In this case, the remaining boundary areas might heal by scattering sound-waves, and a vortex could result. For diffraction limited focusing, the boundary could impart ~ 17 μm/ms velocities, which is greater than the speed of sound (about 3 μm/ms at that density) and thus has a strong particle-like character.

Finally, there will be a short discussion of possibilities for cooling a cloud during rotation. In the round trap, there are several major difficulties. The first is that due to decompression, the density and temperature are quite low. Both of these factors are important for evaporative cooling, since the elastic collision rate rethermalizes the cloud while the most energetic atoms are being removed. The collision rate scales as $n\sqrt{T}$, where n and T are the density and temperature. This makes evaporation quite inefficient since the adiabatic increase in (radial) size by a factor of 10 should decrease $\sqrt{T}$ by roughly the same factor (assuming a box-like potential), but at the same time the density will decrease by a factor of 100, making evaporation (nominally) 1000 times slower. At the same time this is happening, the bias field is being increased by about a factor of 30 (or so) to

decompress the trap. Thus, the same relative fluctuations in that field become 30 times greater in an absolute sense, increasing the ratio of fluctuations in field to the temperature by roughly two orders of magnitude or more. Thus, evaporation is also expected to be erratic since the fluctuations prevent as precise a truncation of the thermal distribution as was possible previously.

Compared to the decompressed Ioffe trap (round trap) considered herein, cooling into the rotating frame seems more promising for the compressed Ioffe trap. The higher density and low bias field result in better evaporation, although the higher density gives a reduced healing length which is even more difficult to image. Critical frequencies are expected to be ten times higher or more because of the higher radial frequency, but at the same time pinning should become technically more difficult since the higher frequency results in a smaller extent of the cloud. The compressed condensate's small radial diameter of roughly 10 μm is scant compared to the focusability of green light. More likely than not, fluctuations in the position of the focused beam would easily interrupt the flow in a circulating cloud. This lack of ability to properly 'pin' is especially unfortunate in light of the predicted instability of vortices in singly connected geometries [47]. In these regards, the 'TOP' trap [74] might be more favorable than the compressed Ioffe trap for implementing the cool-down to a circulating condensate since its aspect ratio is much smaller.

Chapter 6

Feshbach resonances

A 'Feshbach resonance' is when a quasibound molecular state couples resonantly to the free state of colliding atoms, giving an enhanced cross-section for collision. Of particular interest is the dispersive variation of the elastic s-wave scattering length about a Feshbach resonance, mainly because of that scattering length's prominence in the present studies of atomic condensates; see equation (C.1). For a Feshbach resonance in a Bose condensate, the quasibound molecular state must have zero energy in order to couple to low energy condensed colliding atoms. The relative energies of quasibound and free atoms were varied by application of a variable magnetic field. Using this technique the interactions in a Bose condensate can be varied, which complements the ability to change the atomic species or to vary the density.

The reader is encouraged to refer to reference [15, (6.1)], and to a schematic model for Feshbach resonances in figure (6-1). Following presentation of the paper, experimental details that were omitted in the publication are given in section (6.2).

Feshbach resonances offer the possibility to open a new field that will manipulate the interaction properties of quantum gases. The present study begins to look at the effect of changing the scattering length in a Bose condensate, and shows that indeed the interaction energy varies in accordance with theory. As a result, there are many intriguing possibilities. One is to increase the size of the scattering length and study higher order corrections to mean-field theory of a dilute Bose gas. This would be towards the direction of condensed matter systems such as superfluid helium where the interactions are strong. Another possibility is to decrease the scattering length so that the cloud is no longer considered interacting. This would be the regime where zero-point motion in the trap dominates the cloud's behavior.

When a condensate is no longer interacting, zero point motion (quantum diffraction) becomes the dominant source of expansion in free space. Thus, a non-interacting condensate $r \sim 100\ \mu$m wide, as in figure (6-2), could remain under interrogation for many seconds ($t \sim mr^2/\hbar$ for atoms

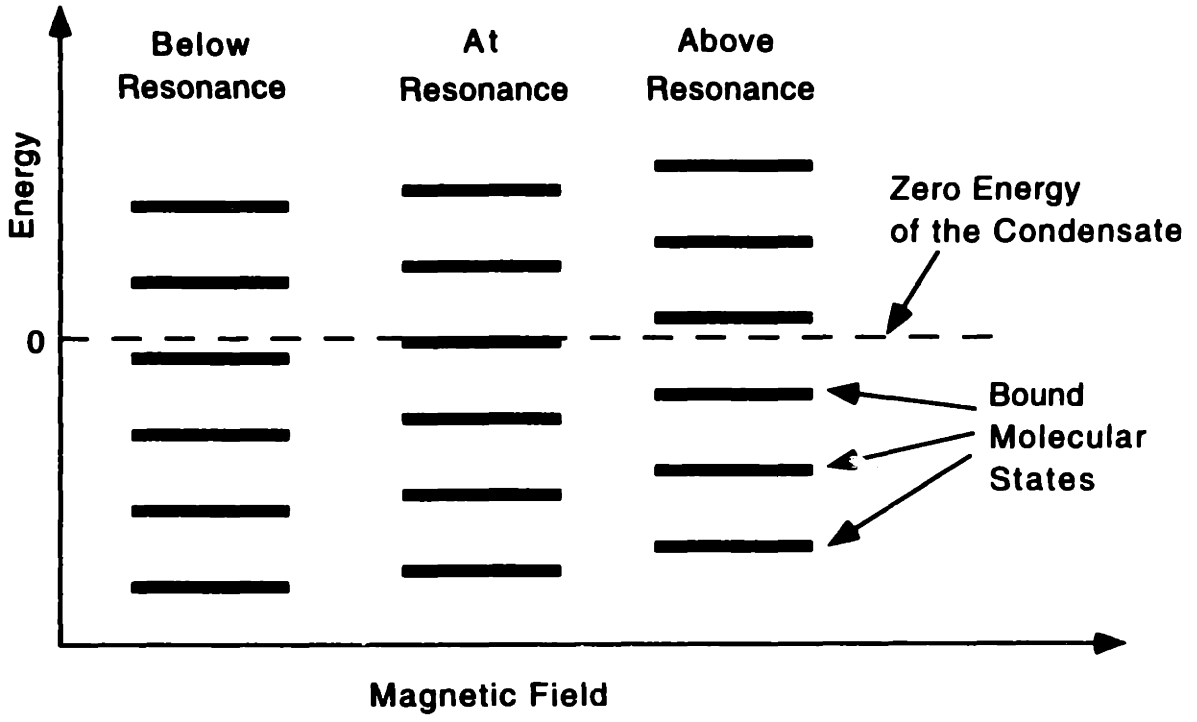

Figure 6-1: A simple model for a Feshbach resonance. As the magnetic field is increased (left to right), quasibound molecular states shift into resonance with atoms colliding at zero energy. Near resonance, the s-wave scattering length varies dispersively and is predicted to attain the full continuum of values. Inasmuch as s-wave scattering can be described as collisions of atoms pictured as hard spheres, Feshbach resonances can be described as collisions of 'hollow spheres'. In this picture of a Feshbach resonance [75], a bound state within the sphere is in resonance with the energy of the colliding atoms.

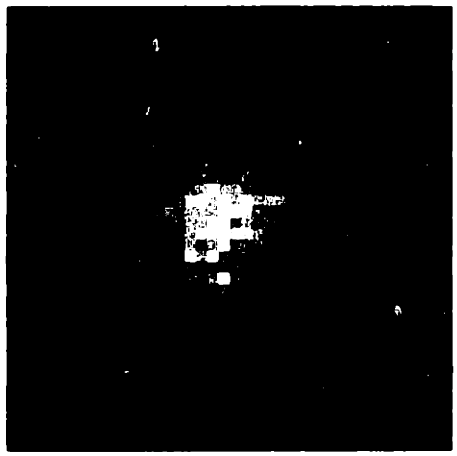

Figure 6-2: A round cloud in a magnetic trap, about 100 μm wide. This is an example of the type of cloud that could be useful to study without interactions.

of mass m) without significant diffraction. But 100 μm is only approaching an earth-bound limit: in the absence of gravity, far weaker traps could be employed and much larger sized condensates ($\sim$ 1 cm) might even be able to completely orbit the earth while diffracting in size by less than a factor of two.

Negative scattering lengths result in attractive interactions, which is qualitatively another regime for condensate dynamics. As observed by Hulet et al. [10], condensates can form with intrinsically attractive interactions because their instability towards collapse is balanced by kinetic pressure (a quantum effect) in the trap. Thus, these condensates have few atoms, and their dynamics are set by the atomic species and are out of the control of the experimenter. On the other hand, Feshbach resonances offer the chance to directly control and study the collapse of unstable condensates, and to study a range of attractive interactions for both large and small numbers of atoms.

One must address the fact that enhanced inelastic decay is also important near a Feshbach resonance. While two atoms are in the quasi-bound state, they are particularly susceptible to collide inelastically with a third atom and leave the trap. In the present studies this has always been an important issue, although it is not yet clear if for particular Feshbach resonances this can be avoided.

6.1 'Observation of Feshbach Resonances in a Bose-Einstein Condensate'

For this section the following paper is presented:

- 'Observation of Feshbach Resonances in a Bose-Einstein Condensate', by S. Inouye, M. R. Andrews, J. Stenger, H.-J. Miesner, D. M. Stamper-Kurn, and W. Ketterle. *Nature*, Vol. 392, p. 151, 1998. Reference [15].

Observation of Feshbach resonances in a Bose–Einstein condensate

S. Inouye*, M. R. Andrews*†, J. Stenger*, H.-J. Miesner*, D. M. Stamper-Kurn* & W. Ketterle*

* Department of Physics and Research Laboratory of Electronics, Massachusetts Institute of Technology, Cambridge, Massachusetts 02139, USA

It has long been predicted that the scattering of ultracold atoms can be altered significantly through a so-called 'Feshbach resonance'. Two such resonances have now been observed in optically trapped Bose–Einstein condensates of sodium atoms by varying an external magnetic field. They gave rise to enhanced inelastic processes and a dispersive variation of the scattering length by a factor of over ten. These resonances open new possibilities for the study and manipulation of Bose–Einstein condensates.

Bose–Einstein condensates of atomic gases offer new opportunities for studying quantum-degenerate fluids[1–5]. All the essential properties of Bose condensed systems—the formation and shape of the condensate, the nature of its collective excitations and statistical fluctuations, and the formation and dynamics of solitons and vortices—are determined by the strength of the atomic interactions. In contrast to the situation for superfluid helium, these interactions are weak, allowing the phenomena to be theoretically described from 'first principles'. Furthermore, in atomic gases the interactions can be altered, for instance by employing different species, changing the atomic density, or, as in the present work, merely by varying a magnetic field.

At low temperatures, the interaction energy in a cloud of atoms is proportional to the density and a single atomic parameter, the scattering length a which depends on the quantum-mechanical phase shift in an elastic collision. It has been predicted that the scattering length can be modified by applying external magnetic[6–10], optical[11,12] or radio-frequency[13] (r.f.) fields. Those modifications are only pronounced in a so-called "Feshbach resonance"[14], when a quasibound molecular state has nearly zero energy and couples resonantly to the free state of the colliding atoms. In a time-dependent picture, the two atoms are transferred to the quasibound state, 'stick' together and then return to an unbound state. Such a resonance strongly affects the scattering length (elastic channel), but also affects inelastic processes such as dipolar relaxation[6,7] and three-body recombination. Feshbach resonances have so far been studied at much higher energies[15] by varying the collision energy, but here we show that they can be 'tuned' to zero energy to be resonant for ultracold atoms. The different magnetic moments of the free and quasibound states allowed us to tune these resonances with magnetic fields, and as a result, minute changes in the magnetic field strongly affected the properties of a macroscopic system.

Above and below a Feshbach resonance, the scattering length a covers the full continuum of positive and negative values. This should allow the realization of condensates over a wide range of interaction strengths. By setting $a \approx 0$, one can create a condensate with essentially non-interacting atoms, and by setting $a < 0$ one can make the system unstable and observe its collapse. Rapid tuning of an external magnetic field around a Feshbach resonance will lead to sudden changes of the scattering length. This opens the way to studies of new dynamical effects such as novel forms of collective oscillations or the sudden collapse of a large condensate when the scattering length is switched from positive to negative[16].

† Present address: Bell Laboratories, Lucent Technologies, Murray Hill, New Jersey 07974, USA.

Theoretical predictions

Calculations for Feshbach resonances in external magnetic fields have been reported for the lower hyperfine states of the atoms Li (ref. 8), K (ref. 10), Na (ref. 8), Rb (ref. 9) and Cs (refs 6, 7). They are typically spaced by several hundred gauss, and for Li and Na occur outside the range where states in the lower hyperfine manifold are weak-field-seeking and can be magnetically trapped. Recent experimental efforts to observe Feshbach resonances have concentrated on ^{87}Rb (ref. 17) and on ^{85}Rb (ref. 18 and C. E. Wieman, personal communication) where Feshbach resonances have been predicted at relatively low magnetic fields[9]. However, our recently demonstrated all-optical confinement of a Bose condensate[19] opened the possibility of observing Feshbach resonances for strong-field-seeking states which cannot be trapped in a d.c. magnetic trap. The optical trapping potential is unaffected by magnetic fields and is independent of the hyperfine ground state. We report here the observation of two Feshbach resonances of sodium in a strong-field-seeking state.

Several Feshbach resonances in sodium are caused by quasibound hyperfine states of the second highest vibrational level, $v = 14$, of the triplet potential of the sodium dimer. The lowest magnetic field value B_0 for a strong Feshbach resonance in sodium was predicted to lie in the range $760 < B_0 < 925$ G (B. J. Verhaar and F. A. van Abeelen, personal communication). It occurs in collisions between atoms in the lowest hyperfine state $|m_s = -1/2, m_I = +3/2\rangle$, which correlates with the $|F = 1, m_F = +1\rangle$ state at low fields (S, I and F are the usual quantum numbers for the electronic, nuclear and total spin, respectively). This Feshbach resonance is due to a quasibound molecular state $|S = 1, m_s = +1, I = 1, m_I = +1\rangle$. A much weaker resonance due to a $|S = 1, m_s = +1, I = 3, m_I = +1\rangle$ state (which is almost degenerate with the other quasibound state) was predicted to occur 50 to 75 G below.

Near a Feshbach resonance, the scattering length a should vary dispersively as a function of magnetic field B (ref. 8):

$$a = \bar{a}\left(1 - \frac{\Delta}{B - B_0}\right) \quad (1)$$

where Δ parametrizes the width of the resonance at $B = B_0$, and $\bar{a}$ is the scattering length outside the resonance. For sodium, $\bar{a}$ was found spectroscopically to be 2.75 nm at zero field, and increases to the triplet scattering length of 4.5 nm (ref. 20) at high magnetic fields. The widths Δ for the strong and weak resonance were predicted to be 1 G and 0.01 G, respectively (B. J. Verhaar and F. A van Abeelen, personal communication).

Experimental set-up

Bose–Einstein condensates in the $|F = 1, m_F = -1\rangle$ state were produced as in our previous work by laser cooling, followed by evaporative cooling in a magnetic trap[21]. The condensates were transferred into an optical dipole trap formed at the focus of an infrared laser beam[19]. Atoms were then spin-flipped with nearly 100% efficiency to the $|F = 1, m_F = +1\rangle$ state with an adiabatic r.f. sweep while applying a 1 G bias field. Without large modifications of our magnetic trapping coils, we could provide bias fields of up to ~1,200 G, but only by using coils producing axial curvature[21], which for high-field-seeking states generated a repulsive axial potential. At the highest magnetic fields, this repulsion was stronger than the axial confinement provided by the optical trap. To prevent the atoms from escaping, two 'end-caps' of far-off-resonant blue-detuned laser light were placed at the ends of the condensate, creating a repulsive potential, and confining the atoms axially (Fig. 1a). For this, green light at 514 nm from an argon-ion laser was focused into two sheets about 200 μm apart. The focus of the optical trap was placed near the minimum of the bias field in order to minimize the effect of the destabilizing magnetic field curvature. The axial trapping potential at high fields was approximately "W"-shaped (Fig. 1b), and had a minimum near one of the end-caps as observed by phase-contrast imaging[22] (Fig. 1c, d).

The calibration factor between the current (up to ~400 A) in the coils and the magnetic bias field was determined with an accuracy of 2% by inducing r.f. transitions within the $|F = 1\rangle$ ground-state hyperfine manifold at about 40 G. Additionally, an optical resonance was found around 1,000 G, where the Zeeman shift equalled the probe light detuning of about 1.7 GHz and led to a sign-reversal of the phase-contrast signal. These two calibrations agreed within their uncertainties.

The condensate was observed in the trap directly using phase-contrast imaging[22] or by using time-of-flight absorption imaging[1,2,21]. In the latter case, the optical trap was suddenly switched off, and the magnetic bias field was shut off 1–2 ms later to ensure that the high-field value of the scattering length was responsible for the acceleration of the atoms. After ballistic expansion of the condensate (either 12 or 20 ms), the atoms were optically pumped into the $|F = 2\rangle$ ground state and probed using resonant light driving the cycling transition. The disk-like expansion of the cloud and the radial parabolic density profile were clear evidence for the presence of a Bose condensed cloud.

Locating the resonances

When the magnetic field is swept across a Feshbach resonance one would expect to lose a condensate due to an enhanced rate of inelastic collisions (caused either by the collapse in the region of negative scattering length or by an enhanced rate coefficient for inelastic collisions). This allowed us to implement a simple procedure to locate the resonances: we first extended the field ramp until the atoms were lost and then used successively narrower field intervals to localize the loss. This procedure converged much faster than a point-by-point search. As we could take many non-destructive phase-contrast images during the magnetic field ramp, the sharp onset of trap loss at the resonance was easily monitored (Fig. 1c, d).

The most robust performance was obtained by operating the optical dipole trap at 10 mW laser power focused to a beam waist of 6 μm, resulting in tight confinement of the condensate and therefore rather short lifetimes owing to three-body recombination[19]. This required that the magnetic field be ramped up in two stages: a fast ramp at a rate of ~100 G ms^{-1} to a value slightly below that expected for a Feshbach resonance, followed by a slow ramp at a rate between 0.05 and 0.3 G ms^{-1} to allow for detailed observation. Near 907 G, we observed a dramatic loss of atoms, as shown in Figs 1c and 2a. This field value was reproducible to better than 0.5 G and had a calibration uncertainty of ±20 G.

To distinguish between an actual resonance and a threshold for trap loss, we also approached the resonance from above. Fields above the Feshbach resonance were reached by ramping at a fast rate of 200 G ms^{-1}, thus minimizing the time spent near the resonance and the accompanying losses. The number of atoms above the resonance was typically three times smaller than below. Approaching the resonance from above, a similarly sharp loss phenomenon was observed about 1 G higher in field than from below (Fig. 2a), which roughly agrees with the predicted width of the resonance. A second resonance was observed 54 ± 1 G below the first one, with the observed onset of trap loss at least a factor of ten sharper than for the first. As the upper resonance was only reached by passing through the lower one, some losses of atoms were unavoidable; for example, when the lower resonance was crossed at 2 G ms^{-1},

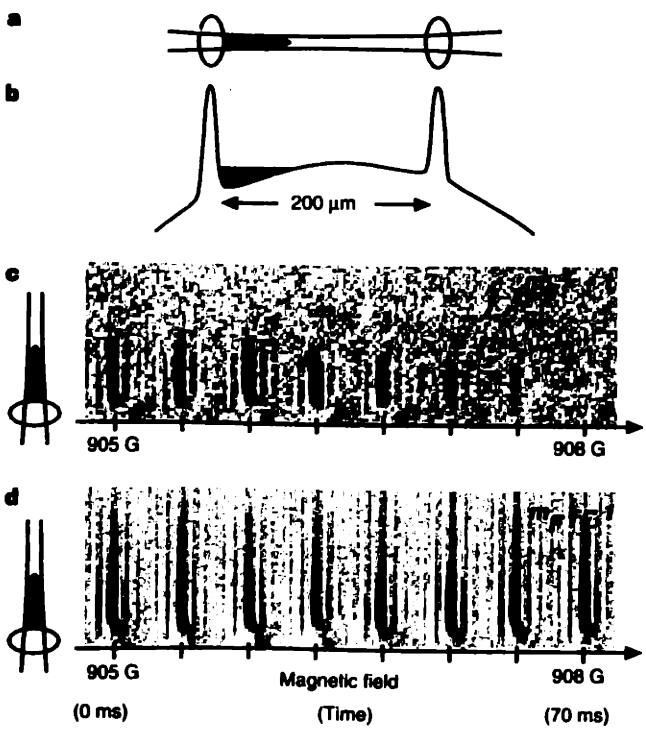

Figure 1 Observation of the Feshbach resonance at 907 G using phase-contrast imaging in an optical trap. A rapid sequence (100 Hz) of non-destructive, *in situ* phase-contrast images of a trapped cloud (which appears black) is shown. As the magnetic field was increased, the cloud suddenly disappeared for atoms in the $|m_F = +1\rangle$ state (see images in **c**), whereas nothing happened for a cloud in the $|m_F = -1\rangle$ state (images in **d**). The height of the images is 140 μm. A diagram of the optical trap is shown in **a**. It consisted of one red-detuned laser beam providing radial confinement, and two blue-detuned laser beams acting as end-caps (shown as ovals). The minimum of the magnetic field was slightly offset from the centre of the optical trap. As a result, the condensate (shaded area) was pushed by the magnetic field curvature towards one of the end-caps. The axial profile of the total potential is shown in **b**.

about 80% of the atoms were lost. This, coupled with the stability and finite programming speed of the power supplies, limited the ramp rates to those given above.

The observation of twin resonances separated by 54 ± 1 G, with the weaker one at lower field, exactly matches the theoretically predicted pattern and thus strongly confirms our interpretation. No resonance phenomena were observed in the $|m_F = -1\rangle$ state at any field up to 1,000 G, in agreement with theory which predicted resonances for this state only at much higher fields.

Changing the scattering length

The trap loss measurements easily located the Feshbach resonances. To measure the variation of the scattering length around these resonances, we determined the interaction energy of a trapped condensate. This was done by suddenly switching off the trap, allowing the stored interaction energy to be converted into the kinetic energy of a freely expanding condensate and measuring it by time-of-flight absorption imaging[1,2,21]. The interaction energy is proportional to the scattering length and the average density of the condensate $\langle n \rangle$:

$$E_i/N = \frac{2\pi\hbar^2}{m} a \langle n \rangle \qquad (2)$$

where N is the number of condensed atoms of mass m. For a large condensate the kinetic energy in the trap is negligible (Thomas–Fermi limit), and E_i is equal to the kinetic energy E_K of the freely expanding condensate $E_K/N = mv_{rms}^2/2$, where v_{rms} is the root-mean-square velocity of the atoms. For a three-dimensional harmonic oscillator potential one finds $\langle n \rangle \propto N(Na)^{-3/5}$ (ref. 23) (We note that, for a general power-law potential $\Sigma_i c_i x_i^{p_i}$, one obtains $\langle n \rangle \propto N(Na)^{k-1}$, where $k = 1/(1 + \Sigma_i 1/p_i)$). Thus, the value of the scattering length scales as:

$$a \propto \frac{v_{rms}^5}{N} \qquad (3)$$

Both v_{rms} and N can be directly evaluated from absorption images of freely expanding condensates. For a cigar-shaped condensate the free expansion is predominantly radial, and so the contribution of the axial dimension to v_{rms} could be neglected. The quantity v_{rms}^5/N (equation (3)), normalized to unity outside the resonance, should be identical to $a/\bar{a}$ (equation (1)). This quantity was measured around the resonance at 907 G and is shown in Fig. 2b together with the theoretical prediction of a resonance with width $\Delta = 1$ G. The data clearly displays the predicted dispersive shape and shows evidence for a variation in the scattering length by more than a factor of ten.

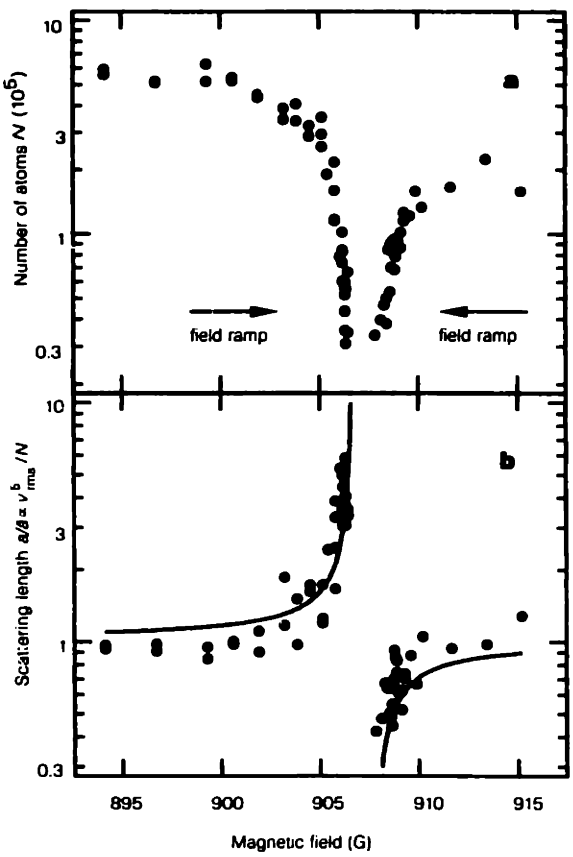

Figure 2 Observation of the Feshbach resonance at 907 G using time-of-flight absorption imaging. **a**, Number of atoms in the condensate versus magnetic field. Field values above the resonance were reached by quickly crossing the resonance from below and then slowly approaching from above. **b**, The normalized scattering length $a/\bar{a} \propto v_{rms}^5/N$ calculated from the released energy, together with the predicted shape (equation (1), solid line). The values of the magnetic field in the upper scan relative to the lower one have an uncertainty of <0.5 G.

We now discuss the assumptions for equation (3) and show that it is approximately valid for our conditions. (1) We assumed that the condensate remains in equilibrium during the magnetic field ramp. This is the case if the adiabatic condition $\dot{a}/a \ll \omega_i$ holds for the temporal change of the scattering length[16], and a similar condition for the loss of atoms (the ω_i are the trapping frequencies). For the condensate's fast radial dynamics ($\omega_r \approx 2\pi \times 1.5$ kHz) this condition is fulfilled, whereas for the slower axial motion ($\omega_z \approx 2\pi \times 0.1$ kHz) it breaks down close to or within the resonance. In this case the density would approach the two-dimensional scaling $N(Na)^{-1/2}$, but the values for $a/\bar{a}$ (Fig. 2b) would differ by at most 50%. (2) The second assumption was a three-dimensional harmonic trap. If the axial potential has linear contributions, the density scales instead like $N(Na)^{-2/3}$ resulting in at most a 50% change for $a/\bar{a}$. (3) We assumed that contributions of collective excitations to the released energy were small. Axial striations were observed in free expansion for both $|m_F = +1\rangle$ and $|m_F = -1\rangle$ atoms (probably created by the changing potential during the fast magnetic field ramp). However, the small scatter of points outside the resonance in Fig. 2b, which do not show any evidence of oscillations, suggests that the contribution of excitations to the released energy is negligible. (4) We assumed a sudden switch-off of the trap and ballistic expansion. The inhomogeneous bias field during the first 1–2 ms of free expansion accelerated the axial expansion, but had a negligible effect on the expansion of the condensate in the radial direction, which was evaluated for Fig. 2b.

None of the corrections (1)–(4) discussed above affect our conclusion that the scattering length varies dispersively near a Feshbach resonance. More accurate experiments should be done with a homogeneous bias field. In addition, an optical trap with larger volume and lower density would preclude the need to ramp the field quickly because three-body recombination would be reduced.

The trap losses observed around the Feshbach resonances merit further study as they might impose practical limits on the possibilities for varying the scattering length. An increase of the dipolar relaxation rate near Feshbach resonances has been predicted[6,7], but for atoms in the lowest hyperfine state no such inelastic binary collisions are possible. Therefore, the observed trap loss is probably due to three-body collisions. In this case the loss rate is characterized by the coefficient K_3, defined as $\dot{N}/N = -K_3\langle n^2 \rangle$. So far, there is no theoretical work on K_3 near a Feshbach resonance. An analysis based on Fig. 2 shows that K_3 increased on both sides of the resonance, because the loss rate increased while the density decreased or stayed constant. In any case, the fact that we observed Feshbach resonances at high atomic densities ($\sim 10^{15}$ cm^{-3}) strongly enhanced this loss process, which can be avoided with a condensate at lower density in a modified optical trap. Control of the bias field with a precision better than $\sim 10^{-4}$ will be necessary to achieve negative or extremely large values of the scattering length in a stable way.

A tunable condensate

We have observed two Feshbach resonances for Bose–Einstein condensates of sodium through the abrupt loss of atoms, and obtained strong evidence for a dispersive variation of the scattering length by a factor of more than ten. 'Tuning' of the scattering length should become an important tool for 'designing' atomic quantum gases with novel properties; for example, to create ideal Bose–Einstein condensates with nearly zero scattering length, and to obtain a detailed picture of the collapse of a condensate with negative scattering length, which is so far not fully understood. Tuning the scattering length can also be used to vary interactions between different species[24] and thus control the phase diagram of multi-component condensates, possibly switching from interpenetrating superfluids to phase separation[25]. Feshbach resonances may also be important in atom optics, for modifying the atomic interactions in an atom laser, or more generally, for controlling nonlinear coefficients in atom optics with coherent beams of atoms. □

Received 18 February; accepted 19 February 1998.

1. Anderson, M. H., Ensher, J. R., Matthews, M. R., Wieman, C. E. & Cornell, E. A. Observation of Bose-Einstein condensation in a dilute atomic vapor. *Science* **269**, 198–201 (1995).
2. Davis, K. B. *et al.* Bose-Einstein condensation in a gas of sodium atoms. *Phys. Rev. Lett.* **75**, 3969–3973 (1995).
3. Bradley, C. C., Sackett, C. A. & Hulet, R. G. Bose-Einstein condensation of lithium: Observation of limited condensate number. *Phys. Rev. Lett.* **78**, 985–989 (1997).
4. Georgia Southern University BEC home page, http://amo.phy.gasou.edu/bec.html.
5. Bradley, C. C., Sackett, C. A., Tollett, J. J. & Hulet, R. G. Evidence of Bose-Einstein condensation in an atomic gas with attractive interactions. *Phys. Rev. Lett.* **75**, 1687–1690 (1995).
6. Tiesinga, E., Moerdijk, A. J., Verhaar, B. J. & Stoof, H. T. C. Conditions for Bose-Einstein condensation in magnetically trapped atomic cesium. *Phys. Rev. A* **46**, R1167–R1170 (1992).
7. Tiesinga, E., Verhaar, B. J. & Stoof, H. T. C. Threshold and resonance phenomena in ultracold ground-state collisions. *Phys. Rev. A* **47**, 4114–4122 (1993).
8. Moerdijk, A. J., Verhaar, B. J. & Axelsson, A. Resonances in ultracold collisions of ^{6}Li, ^{7}Li and ^{23}Na. *Phys. Rev. A* **51**, 4852–4861 (1995).
9. Vogels, J. M. *et al.* Prediction of Feshbach resonances in collisions of ultracold rubidium atoms. *Phys. Rev. A* **56**, R1067–R1070 (1997).
10. Boesten, H. M. J. M., Vogels, J. M., Tempelaars, J. G. C. & Verhaar, B. J. Properties of cold collisions of ^{39}K atoms and of ^{41}K atoms in relation to Bose-Einstein condensation. *Phys. Rev. A* **54**, R3726–R3729 (1996).
11. Fedichev, P. O., Kagan, Yu., Shlyapnikov, G. V. & Walraven, J. T. M. Influence of nearly resonant light on the scattering length in low-temperature atomic gases. *Phys. Rev. Lett.* **77**, 2913–2916 (1996).
12. Bohn, J. L. & Julienne, P. S. Prospects for influencing the scattering lengths with far-off-resonant light. *Phys. Rev. A* **56**, 1486–1491 (1997).
13. Moerdijk, A. J., Verhaar, B. J. & Nagtegaal, T. M. Collisions of dressed ground-state atoms. *Phys. Rev. A* **53**, 4343–4351 (1996).
14. Feshbach, H. A unified theory of nuclear reactions. II. *Ann. Phys.* **19**, 287–313 (1962).
15. Bryant, H. C. *et al.* Observation of resonances near 11 eV in the photodetachment cross-section of the H^- ion. *Phys. Rev. Lett.* **38**, 228–230 (1977).
16. Kagan, Yu., Surkov, E. L. & Shlyapnikov, G. V. Evolution and global collapse of trapped Bose condensates under variations of the scattering length. *Phys. Rev. Lett.* **79**, 2604–2607 (1997).
17. Newbury, N. R., Myatt, C. J. & Wieman, C. E. s-wave elastic collisions between cold ground-state ^{87}Rb atom. *Phys. Rev. A* **51**, R2680–R2683 (1995).
18. Courteille, P. & Heinzen, D. Paper presented at *SPIE Photonics West*, 24–30 Jan., San Jose, California (1998).
19. Stemper-Kurn, D. M. *et al.* Optical confinement of a Bose-Einstein condensate. *Phys. Rev. Lett.* (in the press).
20. Tiesinga, E. *et al.* A spectroscopic determination of scattering lengths for sodium atom collisions. *J. Res. Natl Inst. Stand. Technol.* **101**, 505–520 (1996).
21. Mewes, M.-O. *et al.* Bose-Einstein condensation in a tightly confining d.c. magnetic trap. *Phys. Rev. Lett.* **77**, 416–419 (1996).
22. Andrews, M. R. *et al.* Propagation of sound in a Bose–Einstein condensate. *Phys. Rev. Lett.* **79**, 553–556 (1997).
23. Baym, G. & Pethick, C. J. Ground-state properties of magnetically trapped Bose-condensed rubidium gas. *Phys. Rev. Lett.* **76**, 6–9 (1996).
24. van Abeelen, F. A., Verhaar, B. J. & Moerdijk, A. J. Sympathetic cooling of ^{6}Li atoms. *Phys. Rev. A* **55**, 4377–4381 (1997).
25. Ho, T.-L. & Shenoy, V. B. Binary mixtures of Bose condensates of alkali atoms. *Phys. Rev. Lett.* **77**, 3276–3279 (1996).

Acknowledgements. We thank J. M. Vogels for discussions, A. P. Chikkatur for experimental assistance, and B. J. Verhaar and F. A. van Abeelen for providing updated theoretical predictions. We also thank D. Kleppner, D. E. Pritchard and R. A. Rubenstein for a critical reading of the manuscript. This work was supported by the Office of Naval Research, NSF, Joint Services Electronics Program (ARO), and the David and Lucile Packard Foundation. J.S. acknowledges support from the Alexander von Humboldt-Foundation, and D.M.S.-K. was supported by the JSEP graduate fellowship program.

Correspondence and requests for materials should be addressed to W.K.

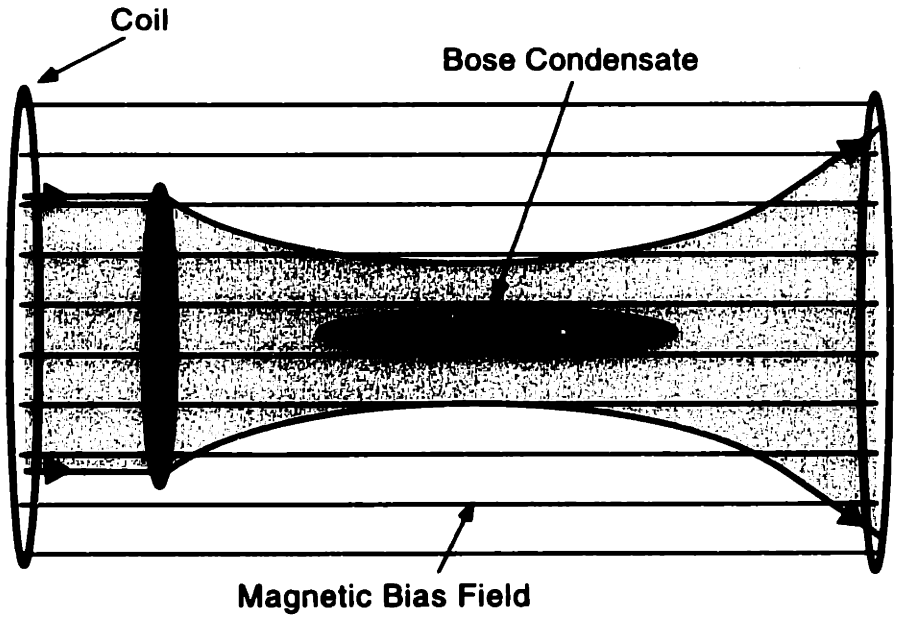

Figure 6-3: Schematic of experimental setup. A focused infrared laser beam traps atoms with the optical dipole force, and a magnetic bias field is applied to the atoms. Atoms in the optical trap are insensitive to magnetic field, although the curvature of the field tended to pull atoms out of the optical trap axially. Not shown are two 'endcaps' of focused argon-ion laser light at either end of the trapped condensate.

6.2 Experimental details

The infrared trap was crucial for this work because of the need for high magnetic fields, particularly because at high fields the $|F = 1\rangle$ states are strong-field seeking and can not be magnetically trapped. An additional concern was that high fields within a Ioffe-type magnetic trap would severely perturb the potential because the radial curvature varies inversely with the bias. The optical trap has no such limitation, although any residual curvature of the magnetic field can still apply forces to the atoms. See figure (2-4) for a schematic of the optical trap, and figure (6-3) for another schematic showing the application of a magnetic bias field within the optical trap. In particular, the residual curvature of the applied field was actually strong enough to defeat the optical trap's axial confinement, and thus 'endcaps' of green laser light were needed to hold the atoms in that direction. To minimize these magnetic forces, the optical trap was positioned at the center of the bias field's curvature where the forces are smallest.

An accurate determination of the field at a Feshbach resonance informs atomic theorists about properties of sodium and its homonuclear molecular states. Therefore, an accurate calibration of that field was essential. For this purpose, rf spectroscopy was performed within the $|F = 1\rangle$ ground state hyperfine manifold and the Breit-Rabi formula was used for interpretation. In general, there are different frequencies for the $|F = 1, m_F = -1\rangle$ to $|F = 1, m_F = 0\rangle$ and the $|F = 1, m_F = 0\rangle$ to $|F = 1, m_F = +1\rangle$ transitions, which depend upon the magnetic field. In particular, at about 40 G

an adiabatic rf sweep over about 200 KHz near 30 MHz was able to completely transfer $|m_F = -1\rangle$ atoms to $|m_F = 0\rangle$, as opposed to transferring them through $|m_F = 0\rangle$ to $|m_F = 1\rangle$, because the difference in transition frequencies is about 1 MHz. By measuring the transfer of atoms from $|F = 1, m_F = -1\rangle$ to $|F = 1, m_F = 0\rangle$ as a function of frequency, a calibration was arrived at that could be extrapolated to over 1000 G with an uncertainty of about 2%.

Optical spectroscopy validated the field calibration obtained with rf spectroscopy. At about 998 G an optical resonance was seen in the phase contrast signal for atoms in the optical trap. Images of trapped condensates gave a positive signal at fields below resonance ('white') and an inverted one above ('black'). The probe light used for this purpose had a particular polarization and frequency that was in resonance with the $|F = 2, m_F = -2\rangle$ to $|F = 3, m_F = -3\rangle$ transition at zero field. By diagonalizing the hyperfine hamiltonian in equation (3.31), it was deduced that (also) at about 998 G the probe light would be in resonance with the $|F = 1, m_F = +1\rangle$ to $|F = 0, m_F = 0\rangle$ transition. This explains the observed optical resonance in phase contrast. Additionally, the Zeeman shift of this optical resonance (−1.5 MHz/G) was just as expected. Thus, the rf spectroscopy and optical spectroscopy agreed within their uncertainties, and agreed over a large extrapolation of magnetic field.

Appendix A

Natural units

For convenience in doing quick calculations, units other than the meter-kilogram-second system are used. Microns and milliseconds and substituted for meters and seconds. Making these choices, one still has the freedom to choose a unit of mass. What is choosen instead is to numerically equate energy with frequency by setting $\hbar = 1/2\pi$. $\hbar/m$, using as m the mass of sodium, is 2.763×10^{-9} m^2/s, or $2.763\ \mu$m^2/ms. Thus, the mass of sodium is $m \approx 1/17.4$ cmu in these units, and the unit of mass, called 'cmu' for condensate mass unit, is about 6.644×10^{-25} kg. The utility of this system is that calculations involve numbers in a moderate range. See the following tables for examples.

The milligauss is chosen as an alternate unit for magnetic field. In these units the Bohr magneton is 1.399 kHz/mG. This choice fixes the units for all of electrodynamics, although as always the subtle differences with cgs units remain. One finds that $\mu_0 = 8.15 \times 10^{-5}$ and $\epsilon_0 = 1.36 \times 10^{-10}$. The electron charge in these units is 2.44×10^{-5}. For calculating fields from macroscopic coils, however, the units in chapter 2 are more appropriate where $\mu_0 = 4\pi/10$ gauss $\cdot$ cm/ampere.

Incidentally, an alternate way to do electromagnetism is to get rid of the engineering constants ϵ_0, μ_0, and other odd units for the fields and charge. It's based on the fine structure constant,

$$\alpha = \frac{e^2}{4\pi\epsilon_0\hbar c} \approx \frac{1}{137}. \tag{A.1}$$

mks	*natural*
meter	micron, or 'μm' (defined)
second	millisecond, or 'ms' (defined)
kilogram	cmu = 6.644×10^{-25} kg
gauss	milligauss, or 'mG' (defined)

Table A.1: Natural condensate units.

quantity	*value*
$\hbar$	$1/2\pi$ kHz (defined)
μ_B	1.399 kHz/mG
ϵ_0	1.36×10^{-10}
μ_0	8.15×10^{-5}

Table A.2: Physical constants

quantity	*value*
$\hbar/m$	$2.763\ \mu\text{m}^2/\text{ms}$
m	1/17.4 cmu
a	2.75 nm
$\mu = 4\pi\hbar^2 an/m$	$n/65.7$ kHz
$c = \sqrt{4\pi\hbar^2 an/m^2}$	$\sqrt{n/3.77}\ \mu\text{m/ms}$

Table A.3: Numerical constants for sodium

What one does is re-write Maxwell's equations

$$\nabla \cdot E = \frac{\rho}{\epsilon_0} \tag{A.2}$$

$$\nabla \cdot B = 0 \tag{A.3}$$

$$\nabla \times E = -\frac{\partial B}{\partial t} \tag{A.4}$$

$$\nabla \times B = \mu_0 \left(J + \epsilon_0 \frac{\partial E}{\partial t} \right) \tag{A.5}$$

by redefining the fields and charges. Since charge is quantized in units of e, one uses $\rho = e\rho'$ and $J = eJ'$ for the charge and current densities. It then becomes natural to use $E' = eE$ (in units of force) and $B' = eB$ (units of force/velocity) for the fields. Maxwell's equations in this context become:

$$\nabla \cdot E' = (4\pi\alpha\hbar c)\,\rho' \tag{A.6}$$

$$\nabla \cdot B' = 0 \tag{A.7}$$

$$\nabla \times E' = -\frac{\partial B'}{\partial t} \tag{A.8}$$

$$\nabla \times c^2 B' = (4\pi\alpha\hbar c)\,J' + \frac{\partial E'}{\partial t}. \tag{A.9}$$

This leaves only constants of 'physics' (not engineering) α, $\hbar$ and c, and all the units are in distance, mass, and time.

Appendix B

Bose condensation

Statistically, the indistinguishability of neighboring atoms forces a large fraction of them into the ground state of the system through considerations of entropy. This does not apply to Fermions, which obey the Pauli exclusion principle and must occupy distinct states. As pointed out in ref. [76], one finds for the fictional case of indistinguishable bosonic pennies (1¢ pieces) that the probability for finding a set of n of them all heads-up is $1/(n+1)$ rather that $1/2^n$ for distinguishable ones; the difference is immense. The list of states in the former case is just the list of numbers 0 through n, signifying how many pennies are heads up. Whereas in the latter case, each penny can independently be heads up or down. Analogously, there is expected to be a vast difference, and indeed there is, between a cold classical gas and a Bose condensed quantum gas. Like the indistinguishable pennies, bosons have an enhanced chance for being in the same state and thus a condensate forms.

The criterion for Bose condensation is to have a high enough phase space density $n\Lambda^3$ [25], where n is the number density and Λ is the thermal de Broglie wavelength as already pointed out in equation (2.1) and equation (2.2). In that criterion for the phase transition, there is a function $\zeta_{3/2}$ that comes into play. $\zeta_{3/2}$ can be numerically computed with the Euler-Maclaurin sum expansion formula [77], which in this case is

$$\zeta_{3/2} = \sum_{s=1}^{\infty} \frac{1}{s^{3/2}} \approx \sum_{s=1}^{n-1} \frac{1}{s^{3/2}} + \frac{2}{n^{1/2}} + \frac{1}{2n^{3/2}} + \frac{1}{8n^{5/2}}. \tag{B.1}$$

To bound the error to η, choose $n > (2.6\eta)^{2/7}$. For $\eta = 10^{-6}$, one chooses $n - 1 = 39$ terms, achieving the actual error of about a part per billion. $n - 1 = 9$ terms gives $\zeta_{3/2} = 2.612375$, which is coincidentally correct in every displayed decimal place (part per million accuracy). This technique is to be compared with direct summation, requiring orders of magnitude more terms for the same level of accuracy.

The chemical potential plays a major role in the thermodynamics of condensation. In the grand

canonical ensemble, one allows a system to be in both diffusive and energetic equilibrium with a reservoir [26]. One finds the occupancy of any quantum level of energy ϵ in a system of bosons to be

$$f(\epsilon, \tau) = \frac{1}{\exp[(\epsilon - \mu)/\tau] - 1}, \tag{B.2}$$

where the temperature is $\tau = k_B T$ (energy units), and the chemical potential is μ. ϵ and μ are defined up to the same arbitrary constant, which can include the ground state energy. One way to derive this distribution is to assume the highest possible entropy and that the bosons are indistinguishable with no limit on state occupancies [26]. In contrast, fermions are governed by the exclusion principle and there would instead be a +1 in the denominator of equation (B.2). Another way of deriving these distributions is by using the principle of detailed balance [78]. Bosons have an N-times enhanced chance for scattering into states already occupied by N particles, whereas fermions are prohibited from scattering into occupied states. This effect was observed in the formation of a condensate [13].

To calculate the chemical potential one needs to look further into the thermodynamics of the system. Substituting a value for μ into equation (B.2) and then summing over all states must give the correct number of particles. On the other hand, there are also a set of equivalent thermodynamic definitions for μ. One definition is the derivative of the total energy (U) versus number (N):

$$\mu = \left(\frac{\partial U}{\partial N}\right)_S, \tag{B.3}$$

holding the entropy S constant. This definition can be transformed using the fact that the temperature is defined as

$$\frac{1}{\tau} = \left(\frac{\partial S}{\partial U}\right)_N. \tag{B.4}$$

Thus, the ratio of chemical potential to temperature, which appears in equation (B.2), is

$$\frac{\mu}{\tau} = \left(\frac{\partial S}{\partial U}\right)_N \times \left(\frac{\partial U}{\partial N}\right)_S = -\left(\frac{\partial S}{\partial N}\right)_U \tag{B.5}$$

using the reciprocity theorem for partial derivatives.

From the definition in equation (B.5) one concludes that the chemical potential for any gas in the classical regime is negative: if one adds a particle to the gas while keeping the energy constant, the entropy increases. Fermions behave similarly, except below a certain temperature the chemical potential becomes positive because of the 'Fermi sea'. Bosons, on the other hand, have a chemical potential infinitesimally close to zero below the condensation temperature, causing a buildup of particles in the ground state. The argument put forward by the authors of ref. [79] shows why the chemical potential behaves this way near zero temperature. See figure (B-1) to figure (B-5) for their essential points regarding bosons.

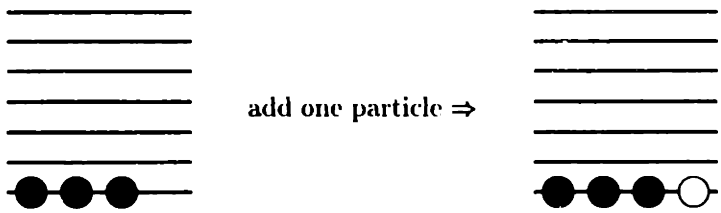

Figure B-1: System of three bosons at zero energy, before and after adding a particle at constant energy (ground state has zero energy). The horizontal lines represent harmonic oscillator energy levels $(0, 1, 2, 3, 4, 5, 6)\,\hbar\omega$, and circles represent particles in those quantum states. The blank circle is the fourth particle added at total constant energy. Number of microstates before (one) and after (one) is the same, and so entropy does not increase and the chemical potential is zero.

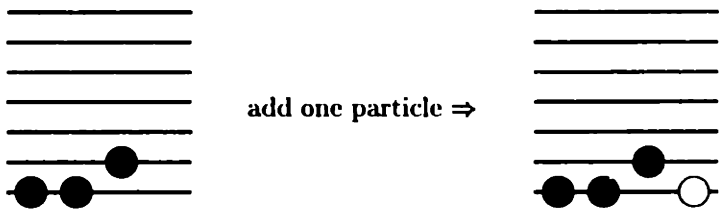

Figure B-2: System of three bosons at energy $\hbar\omega$, before and after adding a fourth particle at constant energy. Number of microstates before (one) and after (one) is the same, and so entropy does not increase and chemical potential is zero.

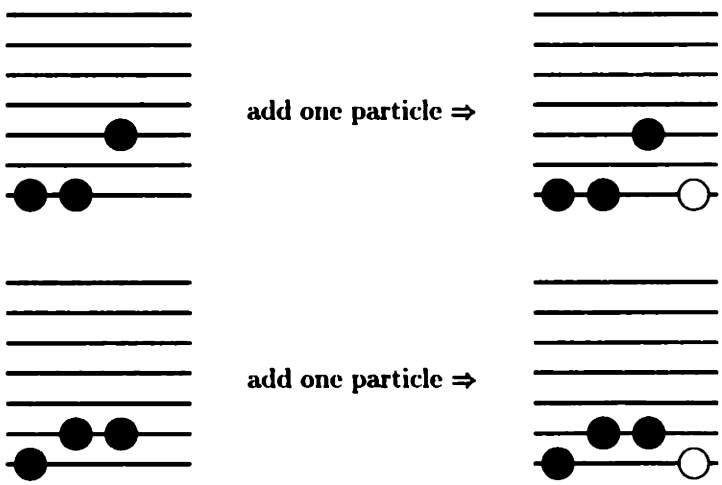

Figure B-3: System of three bosons at energy $2\hbar\omega$, before and after adding a fourth particle at constant energy. Number of microstates before (two) and after (two) is the same, and so entropy does not increase and chemical potential is zero.

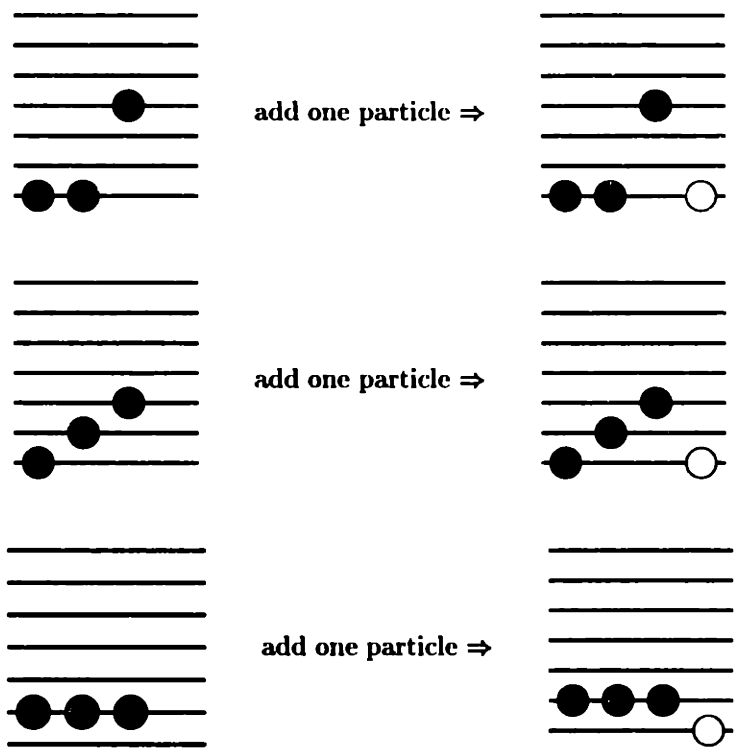

Figure B-4: System of three bosons at energy $3\hbar\omega$, before and after adding a fourth particle at constant energy. Number of microstates before (three) and after (three) is the same, and so entropy does not increase and chemical potential is zero.

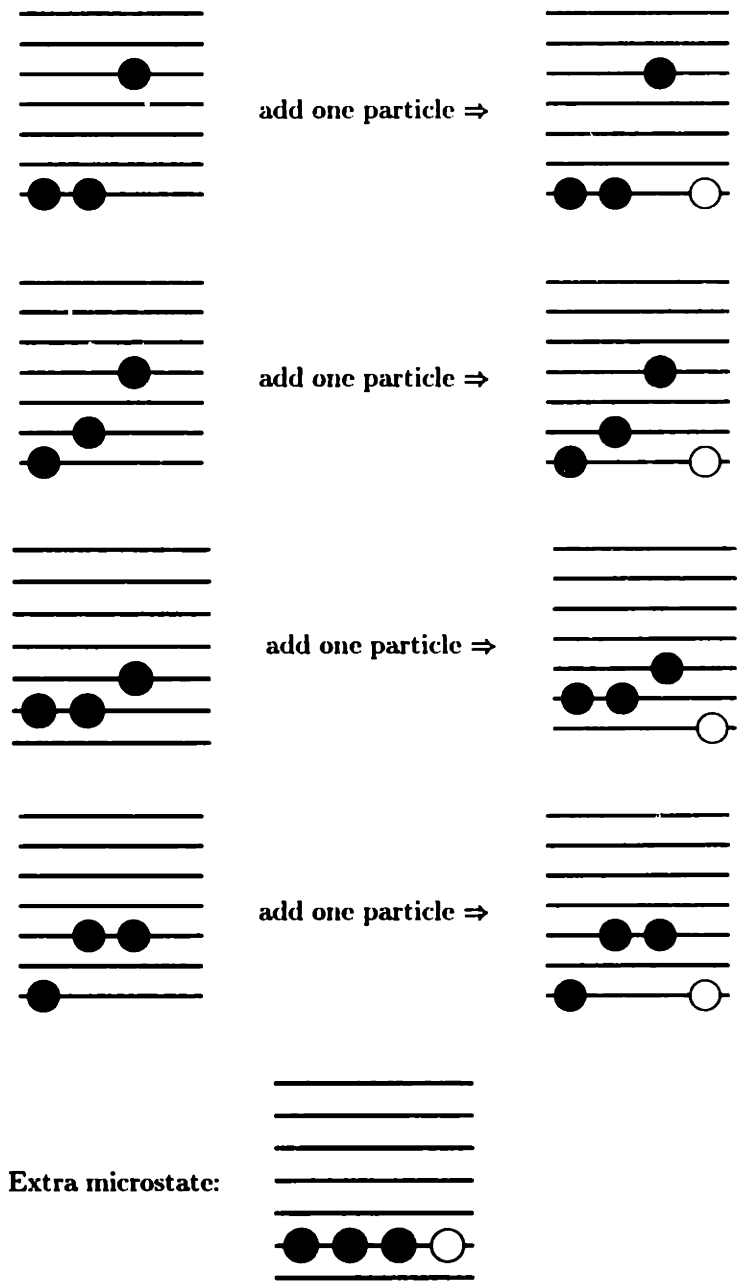

Figure B-5: System of three bosons at energy $4\hbar\omega$, before and after adding a fourth particle at constant energy. Four particles with total energy $4\hbar\omega$ have a fifth microstate, $\{1111\}_4$, which has no correspondence with states of three particles. Number of microstates before (four) and after (five) is *not* the same, and so entropy increases. Since the entropy increases, by equation (B.5) the chemical potential must be negative.

Appendix C

The interacting condensate

This appendix will sketch out some of the features of the wave equation that describes condensates at zero temperature. This wave equation is just the Schrödinger equation with a nonlinear term due to the interactions. The interaction energy is proportional to the density and a single atomic parameter, the s-wave scattering length a, giving what's called the Gross-Pitaevskii equation for $\Psi(r,t)$:

$$\left(\frac{-\hbar^2}{2m}\nabla^2 + V(r) + \frac{4\pi\hbar^2 a}{m}|\Psi(r,t)|^2\right)\Psi(r,t) = i\hbar\frac{\partial\Psi(r,t)}{\partial t}. \tag{C.1}$$

The wavefunction Ψ is normalized so that $|\Psi|^2$ is the number density n. It's convenient to frame these equations as Stringari did [80], separating the wavefunction into density and phase parts as $\Psi = \sqrt{n}e^{i\varphi}$. Whenever one images a condensate, what is seen is the density n since the measurement process detects $|\Psi|^2$ and the absolute phase ϕ is unobservable. This density/phase expression for Ψ also gives a simple interpretation to the gradient of the phase as a velocity $v = \hbar\nabla\phi/m$. Using the density n and velocity v instead of Ψ, the dynamics of the condensate are equivalent to a rather classical system's in the following way:

$$\frac{\partial}{\partial t}n + \nabla(vn) = 0 \tag{C.2}$$

$$m\frac{\partial}{\partial t}v + \nabla\left(\delta\mu + \frac{1}{2}mv^2\right) = 0 \tag{C.3}$$

Equation (C.2) is a continuity equation and taken with equation (C.3) they both describe hydrodynamic behavior. $\delta\mu$ is the local difference from the chemical potential μ of the system itself and is defined as

$$\delta\mu = V_{\text{ext}} + \frac{4\pi\hbar^2 a}{m}n - \frac{\hbar^2}{2m\sqrt{n}}\nabla^2\sqrt{n} - \mu. \tag{C.4}$$

The chemical potential μ is taken to be positive since repulsion between atoms raises the ground state energy.

The interactions in an atomic Bose condensate are determined by the scattering length a in equation (C.1). This equation is a good approximation to the actual dynamics when the density is low enough to satisfy $na^3 \ll 1$, which is practically always true for sodium's scattering length of 2.75 nm [71]. Maximum atomic densities have been about 5×10^{15} cm^{-3}, making na^3 at most about 10^{-4}.

Usually the kinetic energy pressure $\hbar^2 \nabla^2 \sqrt{n}/2m\sqrt{n}$ is negligible in the bulk of the condensate, meaning that the density is a rather slowly varying function over space. This is the case. the so-called 'Thomas-Fermi' approximation, when the interaction energy $4\pi\hbar^2 an/m$ is much larger than the kinetic energy and the particles spread out over many trap states. Near the surface of the condensate the density goes to zero sharply and the kinetic energy pressure is always important [81].

These hydrodynamic equations give rise to propagation effects which are colloquially called 'sound'. The speed of sound c satisfies a simple relation with the chemical potential $\mu = mc^2$ (looks like Einstein's famous equation), and is just the speed Bogoliubov and others [82] derived years back. For instance, pulses of sound are observed travelling across a condensate with a speed adjusted for finite-size effects. See chapter 5.

Since the kinetic energy in the ground state is negligible within the Thomas-Fermi approximation, the density distribution is the result of a balance between interatomic repulsion and the forces of confinement in the trap. The (repulsive) interaction energy at the center of the cloud is equal to the potential energy at its boundary. This balance results in particles within the cloud experiencing no net forces. For a three-dimensional harmonic trap, the density is a parabolic function of the coordinates. Also, the boundary of the cloud is an ellipsoid with radii r_1, r_2, and r_3 (volume $4\pi r_1 r_2 r_3/3$), where $r_i\omega_i = r_j\omega_j$ gives the aspect ratios in terms of the trapping frequencies ω_i. Examples of several different geometries of confining potentials are shown in figure (2-3), where magnetic field curvatures and gradients are being varied and optical dipole forces are present as well.

Bibliography

[1] A. Griffin, D. W. Snoke, and S. Stringari, editors. *Bose-Einstein Condensation.* Cambridge University Press, Cambridge, UK, 1995.

[2] M. H. Anderson, J. R. Ensher, M. R. Matthews, C. E. Wieman, and E. A. Cornell. Observation of Bose-Einstein condensation in a dilute atomic vapor. *Science*, 269:201, 1995.

[3] K. B. Davis, M.-O. Mewes, M. R. Andrews, N. J. van Druten, D. S. Durfee, D. M. Kurn, and W. Ketterle. Bose-Einstein condensation in a gas of sodium atoms. *Phys. Rev. Lett.*, 75:3969, 1995.

[4] C. C. Bradley, C. A. Sackett, J. J. Tollett, and R. G. Hulet. Evidence of Bose-Einstein condensation in an atomic gas with attractive interactions. *Phys. Rev. Lett.*, 75:1687, 1995.

[5] M. R. Andrews, D. S. Durfee, S. Inouye, D. M. Stamper-Kurn, H. J. Miesner, and W. Ketterle. Studies of Bose-Einstein condensates. *J. Low Temp. Phys.*, 110:153, 1998.

[6] D. S. Jin, J. R. Ensher, M. R. Matthews, C. E. Wieman, and E. A. Cornell. Quantitative studies of Bose-Einstein condensation in a dilute atomic vapor. *Czech. J. Phys.*, 46:3070, 1996. Suppl. S6.

[7] N. J. van Druten, C. G. Townsend, M. R. Andrews, D. S. Durfee, D. M. Kurn, M.-O. Mewes, and W. Ketterle. Bose-Einstein condensates — a new form of quantum matter. *Czech. J. Phys.*, 46:3077, 1996. Suppl. S6.

[8] M. R. Andrews, D. M. Kurn, H.-J. Miesner, D. S. Durfee, C. G. Townsend, S. Inouye, and W. Ketterle. Propagation of sound in a Bose condensate. *Phys. Rev. Lett.*, 79:553, 1997. see erratum.

[9] M. R. Andrews, C. G. Townsend, H.-J. Miesner, D. S. Durfee, D. M. Kurn, and W. Ketterle. Observation of interference between two Bose condensates. *Science*, 275:637, 1997.

[10] Bradley C. C., Sackett C. A., and Hulet R. G. Bose-Einstein condensation of lithium: Obervation of limited condensate number. *Phys. Rev. Lett.*, 78:985, 1997.

[11] E. A. Burt, R. W. Ghrist, C. J. Myatt, M. J. Holland, E. A. Cornell, and C. E. Wieman. Coherence, correlations, and collisions: What one learns about Bose-Einstein condensates from their decay. *Phys. Rev. Lett.*, 79:337, 1997.

[12] W. Ketterle and H.-J. Miesner. Coherence properties of Bose-Einstein condensates and atom lasers. *Phys. Rev. A*, 56:3291, 1997.

[13] H.-J. Miesner, D. M. Stamper-Kurn, M. R. Andrews, D. S. Durfee, S. Inouye, and W. Ketterle. Bosonic stimulation in the formation of a Bose-Einstein condensate. *Science*, 279:1005, 1998.

[14] K. B. Davis, M.-O. Mewes, M. A. Joffe, M. R. Andrews, and W. Ketterle. Evaporative cooling of sodium atoms. *Phys. Rev. Lett.*, 74:5202, 1995.

[15] S. Inouye, M. R. Andrews, J. Stenger, H.-J. Miesner, D. M. Stamper-Kurn, and W. Ketterle. Observation of Feshbach resonances in a Bose-Einstein condensate. *Nature*, 392:151, 1998.

[16] M. R. Andrews, M.-O. Mewes, N. J. van Druten, D. S. Durfee, D. M. Kurn, and W. Ketterle. Direct, nondestructive observation of a Bose condensate. *Science*, 273:84, 1996.

[17] Ken Davis. *Evaporative Cooling of Sodium Atoms.* PhD thesis, Massachusetts Institute of Technology, 1995.

[18] M. A. Joffe. *Trapping and cooling atoms at high densities.* PhD thesis, Massachusetts Institute of Technology, 1993.

[19] M.-O. Mewes, M. R. Andrews, D. M. Kurn, D. S. Durfee, C. G. Townsend, and W. Ketterle. Output coupler for Bose condensed atoms. *Phys. Rev. Lett.*, 78:582, 1997.

[20] Marc-Oliver Mewes. *Bose-Einstein Condensation of Sodium Atoms.* PhD thesis, Massachusetts Institute of Technology, 1997.

[21] M.-O. Mewes, M. R. Andrews, N. J. van Druten, D. M. Kurn, D. S. Durfee, C. G. Townsend, and W. Ketterle. Collective excitations of a Bose-Einstein condensate in a magnetic trap. *Phys. Rev. Lett.*, 77:988, 1996.

[22] D. M. Stamper-Kurn, H.-J. Miesner, S. Inouye, M. R. Andrews, and W. Ketterle. Excitations of a Bose-Einstein condensate at non-zero temperature: A study of zero, first, and second sound. 1998. submitted cond/mat-9801262.

[23] M.-O. Mewes, M. R. Andrews, N. J. van Druten, D. M. Kurn, D. S. Durfee, and W. Ketterle. Bose-Einstein condensation in a tightly confining dc magnetic trap. *Phys. Rev. Lett.*, 77:416, 1996.

[24] Stamper-Kurn D. M., Andrews M. R., Chikkatur A. P., Inouye S., Miesner H.-J., Stenger J., and Ketterle W. Optical confinement of a Bose-Einstein condensate. *Phys. Rev. Lett.*, 80:2027, 1998.

[25] K. Huang. *Statistical Mechanics.* John Wiley & Sons, Inc., New York, 2nd edition, 1987.

[26] C. Kittel and H. Kroemer. *Thermal Physics.* W. H. Freeman and Co., New York, 2nd edition, 1987.

[27] W. Ketterle, K. B. Davis, M. A. Joffe, A. Martin, and D. E. Pritchard. High-densities of cold atoms in a dark spontaneous-force optical trap. *Phys. Rev. Lett.*, 70:2253, 1993.

[28] T. Bergeman, G. Erez, and H. J. Metcalf. Magnetostatic trapping fields for neutral atoms. *Phys. Rev. A*, 35:1535, 1987.

[29] B. J. Hughey. *Cavity modified atom-photon interaction.* PhD thesis, Massachusetts Institute of Technology, 1989.

[30] L. Allen and J. H. Eberly. *Optical resonance and two-level atoms.* Dover Publications, New York, 1975.

[31] E. Hecht. *Optics.* Addison-Wesley, Reading, MA, 2nd edition, 1989.

[32] H. D. Politzer. Bose-stimulated scattering off a cold atom trap. *Phys. Rev. A*, 55:1140, 1997.

[33] Otger Jan Luiten. *Lyman-α spectroscopy of magnetically trapped atomic hydrogen.* PhD thesis, Universiteit van Amsterdam, 1993.

[34] Irwan Dani Setija. *Optical cooling of magnetically trapped atomic hydrogen.* PhD thesis, Universiteit van Amsterdam, 1995.

[35] O. J. Luiten, H. G. C. Werij, I. D. Setija, M. W. Reynolds, T. W. Hijmans, and J. T. M. Walraven. Lyman-α spectroscopy of magnetically trapped atomic hydrogen. *Phys. Rev. Lett.*, 70:544, 1993.

[36] P. J. Ungar, D. S. Weiss, E. Riis, and S. Chu. Optical molasses and multilevel atoms: theory. *J. Opt. Soc. Am. B*, 6:2058, 1989.

[37] E. Arimondo and P. Violino M. Ignuscio. Experimental determinations of the hyperfine structure in the alkali atoms. *Rev. Mod. Phys.*, 49:31, 1977.

[38] H. M. Wiseman. What is an atom laser? *Phys. Rev. A*, 56:2068, 1997.

[39] D. Kleppner. A beginner's guide to the atom laser. *Physics Today*, page 11, August 1997.

[40] H. Steck, M. Naraschewski, and H. Wallis. Output of a pulsed atom laser. *Phys. Rev. Lett.*, 80:1, 1998.

[41] W. Ketterle. The atom laser. http://amo.mit.edu/~bec/atomlasr/atomlasr.html.

[42] P. Bouyer and M. A. Kasevich. Heisenberg-limited spectroscopy with degenerate Bose gases. *Phys. Rev. A*, 53:R1083, 1997.

[43] A. Rohrl, M. Naraschewski, A. Schenzle, and H. Wallis. Transition from phase locking to the interference of independent Bose condensates: Theory vs. experiment. *Phys. Rev. Lett.*, 78:4143, 1997.

[44] Y. Castin and J. Dalibard. Relative phase of two Bose-Einstein condensates. *Phys. Rev. A*, 55:4330, 1997.

[45] D. S. Jin, M. R. Matthews, J. R. Ensher, C. E. Wieman, and E. A. Cornell. Temperature-dependent damping and frequency shifts in collective excitations of a dilute Bose-Einstein condensate. *Phys. Rev. Lett.*, 78(5):764, 1997.

[46] D. S. Jin, J. R. Ensher, M. R. Matthews, C. E. Wieman, and E. A. Cornell. Collective excitations of a Bose-Einstein condensate in a dilute gas, 1996.

[47] D. S. Rokhsar. Vortex stability and persistent currents in trapped Bose gases. *Phys. Rev. Lett.*, 79:2164, 1997.

[48] V. M. H. Ruutu, V. B. Eltsov, , A. J. Gill, T. W. B. Kibble, M. Krusius, Y. G. Makhlin, B. Placais, G. E. Volovik, and W. Xu. Vortex formation in neutron-irradiated superfluid he-3 as an analogue of cosmological defect formation. *Nature*, 382:334, 1996.

[49] C. Bauerle, Y. M. Bunkov, S. N. Fisher, H. Godfrin, and G. R. Pickett. Laboratory simulation of cosmic string formation in the early universe using superfluid he-3. *Nature*, 382:332, 1996.

[50] P. Kapitza. Viscosity of liquid helium below the λ-point. *Nature*, 141:74, 1938.

[51] J. F. Allen and A. D. Misener. *Nature*, 141:75, 1938.

[52] J. C. McLennan, H. D. Smith, and J. O. Wilhelm. *Phil. Mag.*, 14:161, 1932.

[53] W. H. Keesom and Miss A. P. Keesom. *Physica*, 3:359, 1936.

[54] Allen, Peierls, and Uddin. *Nature*, 140:62, 1937.

[55] J. D. Reppy and D. Depatie. Persistent currents in superfluid helium. *Phys. Rev. Lett.*, 12:187, 1964.

[56] W. F. Vinen. The detection of single quanta of circulation in liquid helium II. *Proc. Roy Soc. (London)*, A260:218, 1961.

[57] P. W. Karn, D. R. Starks, and Jr. W. Zimmermann. Observation of quantization of circulation in rotating superfluid he-4. *Phys. Rev. B*, 21:1797, 1980.

[58] L. P. Pitaevskii. Vortex lines in an imperfect Bose gas. *Sov. Phys. JETP*, 13:451, 1961.

[59] Alexander Fetter. Equilibrium distribution of rectilinear vortices in a rotating container. *Phys. Rev.*, 152:183, 1966.

[60] Alexander Fetter. Low-lying superfluid states in a rotating annulus. *Phys. Rev.*, 153:285, 1967.

[61] Alexander Fetter. Vortex nucleation in deformed rotating cylinders. *J. Low Temp. Phys.*, 16(5):533, 1974.

[62] K. Schwab, N. Bruckner, and R. R. Packard. Detection of the earth's rotation using superfluid phase coherence. *Nature*, 386:585, 1997.

[63] O. Avenel, P. Hakonen, and E. Varoquaux. Detection of the rotation of the earth with a superfluid gyrometer. *Phys. Rev. Lett.*, page 3602, 1997.

[64] S. Stringari. Moment of inertia and superfluidity of a trapped Bose gas. *Phys. Rev. Lett.*, 76:1405, 1996.

[65] F. Dalfovo and S. Stringari. Bosons in anisotropic traps: Ground state and vortices. *Phys. Rev. A*, 53:2477, 1996.

[66] F. Dalfovo, L. Pitaevskii, and S. Stringari. The condensate wave function of a trapped atomic gas. *Journal of Research of the National Institute of Standards and Technology*, 10:537, 1996.

[67] K.-P. Marzlin, W. Zhang, and E. M. Wright. Vortex coupler for atomic Bose-Einstein condensates. *Phys. Rev. Lett.*, 79:4728, 1997.

[68] E. L. Bolda and D. F. Walls. creation of vortices in a Bose-Einstein condensate by a Raman technique, 1997. cond/mat 9708189.

[69] R. Dum, J. I. Cirac, M. Lewenstein, and P. Zoller. Creation of dark solitons and vortices in Bose-Einstein condensates. *Phys. Rev. Lett.*, 80:2972, 1998.

[70] E. J. Mueller, P. M. Goldbart, and Y. Lyanda-Geller. Multiply connected Bose-Einstein-condensed alkali-metal gases: Current-carrying states and their decay. *Phys. Rev. A*, 57:R1505, 1998.

[71] Tiesinga E., Williams C. J., Julienne P. S., Jones K. M., Lett P. D., and Phillips W. D. A spectroscopic determination of scattering lengths for sodium atom collisions. *J. Res. Natl. Inst. Stand. Technol.*, 101:505, 1996.

[72] E. J. Yarmchuck and R. E. Packard. Photographic studies of quantized vortex lines. *J. Low Temp. Phys.*, 46:479, 1982.

[73] A. Fetter. Model for creation and detection of persistent currents in a dilute trapped Bose condensate, 1997. Talk given in Perth.

[74] W. Petrich, M. H. Anderson, J. R. Ensher, and E. A. Cornell. Stable, tightly confining magnetic trap for evaporative cooling of neutral atoms. *Phys. Rev. Lett.*, 74:3352, 1995.

[75] J. M. Vogels, 1998. Private communication.

[76] H. C. von Baeyer. *The Sciences*, 5:11, 1997.

[77] P. B. Kahn. *Mathematical methods for scientists and engineers.* John Wiley & Sons, Inc., New York, 1990.

[78] D. I. Blokhintsev. *Quantum Mechanics.* D. Reidel, Dordrecht, Holland, 1964.

[79] G. Cook and R. H. Dickerson. Understanding the chemical potential. *Am. J. Phys.*, 63:737, 1995.

[80] S. Stringari. Collective excitations of a trapped Bose-condensed gas. *Phys. Rev. Lett.*, 77:2360, 1996.

[81] F. Dalfovo, L. Pitaevskii, and S. Stringari. Order parameter at the boundary of a trapped Bose gas. *Phys. Rev. A*, 54:4213, 1996.

[82] N. Bogoliubov. *J. Phys.*, 11:23, 1947.